Some recent intermediate-and high-energy proton–nucleus research

G. J. Igo*

Department of Physics, University of California, Los Angeles, California 90024

A review of several new or very active areas of research in the field of intermediate-and high-energy proton–nucleus research is presented. Theoretical advances used in treating the data are described. The areas covered include: $p-{}^4$He elastic scattering and polarization; elastic and inelastic scattering, $A \geq 4$; the neutron pickup reaction; and particle production and elastic scattering near 180°.

CONTENTS

I. Introduction 523
II. Theoretical Models 524
A. Glauber theory 524
B. Optical potential model of Kerman, McManus, and Thaler 526
C. Other treatments including relativistic corrections in the Hamiltonian 527
D. Extraction of nearly model-independent nuclear matter densities from proton scattering 527
III. Proton Elastic Scattering from ^{4}He 528
A. Dependence of the elastic scattering cross section on bombarding energy 528
B. Polarization in p-^{4}He elastic scattering 536
C. Some recent results of phenomenological analyses of p-^{4}He elastic scattering 538
IV. Elastic and Inelastic Scattering, $A \geq 4$ 540
A. Measurements of the neutron mass distributions in calcium isotopes 541
B. Model-independent analysis of calcium elastic scattering data 542
C. Attempts to extract nuclear correlation structure information from (p,p) and (p,p') scattering near 1 GeV 543
V. Neutron Pickup Reaction 547
VI. Particle Production and Elastic Scattering Near 180° 551
A. Inclusive production of $z=1$ particles 552
B. Large-angle elastic scattering 554
VII. Conclusions and Expected Trends 556
A. p-^{4}He scattering 556
B. Elastic and inelastic scattering $A \geq 4$ 556
C. Neutron pickup reaction 557
D. Particle production and elastic scattering near 180° 557
Acknowledgments 557
References 557

I. INTRODUCTION

At the High-Energy Physics and Nuclear Structure Conference in Santa Fe, New Mexico, a survey of recent nucleon–nucleus research was presented (Igo, 1976). For the purpose of proton–nucleus research, the intermediate-energy range can be conveniently defined by physical features of the n-n interaction (lower limit, onset of pion production, and the rise in the pp total cross section; upper limit, disappearance of isobar resonances). Some of these topics have been selected for this review and are described here in more detail along with newer developments. For recent reviews focused on other aspects of this field, the reader is referred to articles by Saudinos and Wilkin (1974), Weber (1975), and Ciofi degli Atti (1975).

In the review article by Saudinos and Wilkin, one finds a description of the experimental facilities used in the past few years; a tabulation of the data sets, complete through 1973; and a concise summary of theoretical conclusions up to that date regarding the data. Weber (1975) has reviewed other aspects of the medium-energy field. He has discussed data on complex nuclei taken between 150 MeV and 1 GeV using hadronic (pion, nucleon) projectiles. Emphasis is placed on inelastic scattering as a tool to extract nuclear structure information. Ciefo degli Atti (1975) has reviewed the evidence: (a) for two-body, short-range correlations in ^{4}He from p-^{4}He elastic scattering at 1 GeV; (b) for deformation of ^{12}C obtained from elastic scattering of electrons, and elastic and inelastic scattering of protons from ^{12}C; and (c) for differences between the neutron and proton mass distributions in ^{208}Pb from p-^{208}Pb elastic scattering at 1 GeV. A comparison is given in the article by Ciofi delgi Atti (1975) of the predictions of two frequently used theoretical models, the Glauber model (Glauber, 1959) and the model of Kerman, McManus, and Thaler (Kerman *et al.*, 1959) as developed for proton scattering by Feshbach and his collaborators (Feshbach, 1969; Feshbach and Hufner, 1970; Feshbach *et al.*, 1971; Lambert and Feshbach, 1973, 1973; Ullo and Feshbach, 1974; Boridy and Feshbach, 1974). The conclusion reached is that high-energy proton scattering by selected nuclei, which represent three important regions of the periodic table (few-body system, light nuclei, and heavy nuclei), can be interpreted satisfactorily at small momentum transfers q ($q^2 \leq 6.25$ fm^{-2}) in terms of either model provided the scattering angle is less than 20° in the center-of-mass system.

In recent experiments on proton–nucleus scattering at intermediate energies, the cross sections pertaining to elastic scattering, and to inelastic scattering to the low-lying states, have been the most thoroughly studied. The (p,d) reaction on ^{12}C has also been studied. New data on the backward production of $z=1,2$ particles with high momentum and on backward elastic scattering are available. The new data in these categories are the principal subjects of this review. An important example is the appearance of accurate data on the scattering of protons by light elements, particularly helium-4 and deuterium, taken over a broad spectrum of total energy squared s, and a broad range of momentum transfer squared t. These data reveal salient features which illustrate the general correctness of theoretical descriptions based on multiple-scattering models (Glauber,

*Work supported in part by the U. S. Department of Energy.

1959; Kerman *et al.*, 1959). Moreover, the s dependence of the p-^{4}He data in the t region between 0.05–0.8 (GeV/c)^2 is unexpectedly rich in detail. In related work, large-angle p-^{4}He elastic scattering has been measured over an extended range of s (Goldstein *et al.*, 1969; Votta *et al.*, 1974; Comparat *et al.*, 1975; Berger *et al.*, 1975).

The new experimental results have been accompanied by theoretical activity. For example, in three recent investigations (Gurvitz *et al.*, 1975a and 1975b; Chen, 1974) it is proposed that, at backward angles, the scattering amplitudes involve one large momentum transfer to a target nucleon. This would be interesting because the theoretical description of back-angle scattering could provide data on large momentum components in the nuclear wave function. At intermediate angles, because of the t dependence of the nucleon–nucleon interaction, the incident proton is expected to interact sequentially with several target nucleons. Elastic scattering in this region is thought to be sensitive to nucleon–nucleon correlations, of long range if associated with collective phenomena and of short range if associated with close nucleon–nucleon encounters within the nucleus. We are reminded that in electron scattering, correlation phenomena are seen only through their effects on the one-body density distribution. Since it is in principle always possible to replicate the manifestations of correlation phenomena by altering the single-particle distribution sufficiently, the information content in proton-nucleus scattering on correlations will be difficult to obtain. Of course, altered single-particle distributions are subject to the restraint that they must reproduce the electron scattering results. Another possible obstacle to extracting correlations is that the nuclear structure information is not always clearly separated from the influence of the reaction mechanism.

II. THEORETICAL MODELS

The basis of the two widely used approaches, discussed in Sec. I, for the high-energy proton–nucleus interaction is reviewed in this section. In contrast to the case of electron scattering, the Born approximation does not apply at intermediate energies even for light elements.

A. The Glauber theory

As is well known, the basic assumption and approximations underlying Glauber's model are:

(1) *the restriction to small scattering* θ: Glauber (1959) shows that $\theta^2 kd \ll 1$ where d is either the range of the nucleon–nucleon force or of the order of $\hbar v/V$, whichever is smaller. Here k is the wave number of the incident nucleon, and v and V are the velocity of the projectile, and the depth of the nucleon-nucleon interaction, respectively.

(2) *the high-energy condition*: Two inequalities must be satisfied, $V/T_k \ll 1$ and $ka \gg 1$, where T_k is the kinetic energy of the incident particle (Glauber, 1959), and a is the range. These conditions are satisfied at 1 GeV. Recently (Harrington, 1975) it has been suggested that the Glauber model is valid even when $V/T_k \sim 1$, as long as $ka \gg 1$. This is important in the treatment of the short-range forces.

(3) *the dynamical approximation*: This means that the potentials describing the interaction between the incident particle and the nucleons of the target do not overlap; consequently phase shifts from the scattering by various nucleons may be added to obtain the nuclear phase shift.

(4) *the frozen nucleus approximation*: At high energies the proton traverses the nucleus in such a short time that it is a good approximation to assume the nucleons do not rearrange themselves until the probe has left. It is not necessary to make the frozen nucleus approximation (Wallace, 1975; Wong and Young, 1975).

If the frozen nucleus approximation as well as approximations (1)–(3) are adopted, it is straightforward to calculate the transition amplitude $F(\underline{q}, \underline{r}_1, \ldots \underline{r}_A)$. The physical amplitude F_{f0} for elastic scattering, nuclear excitation, or rearrangement is calculated by averaging this amplitude over the nucleon distribution using the nuclear wave functions in the initial and final states, $|0\rangle$ and $|f\rangle$,

$$F_{f0}(\underline{q}) = \langle f | F(\underline{q}, \underline{r}_1, \ldots \underline{r}_A) | 0 \rangle . \tag{1}$$

In the Glauber model, the scattering amplitude is described in the impact-parameter representation

$$F_{f0}(\underline{q}) = \frac{k}{2\pi i} \langle f | \int e^{i\underline{q}\cdot\underline{r}} \Gamma(\underline{b}, \underline{s}_1, \ldots \underline{s}_A) d^2b \, | 0 \rangle , \tag{2}$$

where $\underline{s}_n$ is the transverse component of the vector position of a nucleon $\underline{r}_n$ in the nucleus, and $\underline{b}$ is the impact parameter. The profile function $\Gamma(\underline{b}, \underline{s}_1, \ldots \underline{s}_A)$ is defined in terms of the phase-shift function $\chi(\underline{b}, \underline{s}_1, \ldots \underline{s}_A)$. Invoking the dynamical approximation (c), the phase is the sum of the phase shifts contributed by the individual nucleons

$$\chi(\underline{b}, \underline{s}_1, \ldots \underline{s}_A) = \sum_i^A \chi_i(\underline{b} - \underline{s}_i) . \tag{3a}$$

The phase $\chi(\underline{b}, \underline{s}_1, \ldots \underline{s}_A)$ can be expressed in terms of the nucleon–nucleon profile function through the relation

$$\Gamma(\underline{b}) = 1 - \exp[i\chi(\underline{b})] . \tag{3b}$$

The scattering amplitude of the incident particle by one of the nucleons, if it were isolated from the others, would be

$$f(\underline{q}) = \frac{ik}{2\pi} \int e^{i\underline{q}\cdot\underline{b}} \Gamma(\underline{b}) d^2b . \tag{3c}$$

This is generalized to the case of more than one nucleon by taking account of the transverse component of the ith nucleon's position s_i.

In Eqs. (1) and (2), $|0\rangle$ and $|f\rangle$ are intrinsic initial and final nuclear wave functions depending on $A-1$ coordinates. Sometimes it is more convenient to work with A coordinates. If this is the case, a delta function has to be introduced:

$$F_{f0}(\underline{q}) = \frac{ik}{2\pi} \int e^{i\underline{q}\cdot\underline{b}} d^2b \left\{ \int \psi_f(\underline{\xi}_1 \cdots \underline{\xi}_A) \left[1 - \prod_{j=1}^{A} (1 - \Gamma(\underline{b} - \underline{s}_j)) \right] \times \delta\left(\sum_{i=1}^{A} \underline{\xi}_1 \right) \psi_0(\underline{\xi}_1 \cdots \underline{\xi}_A) \Pi_k d\underline{\xi}_k \right\} . \tag{4}$$

For light nuclei ($A \leq 4$), the model wave functions can be

written in terms of the intrinsic coordinates due to the spatial symmetry. For heavier nuclei, the nuclear wave functions are usually represented by the shell model, or by approximate many-body wave functions which depend on a nonintrinsic (external) coordinate $\underline{r}_i$. The relation between $\underline{\xi}_i$ and $\underline{r}_i$ may be $\underline{\xi}_i = \underline{r}_i - \underline{R}, \underline{R} = 1/A \sum_i^A \underline{r}_i$. Removal of the center-of-mass coordinate from the nonintrinsic matrix element cannot be accomplished uniquely unless one is dealing with harmonic-oscillator orbitals. When other types of shell-model wave functions are used, theoretical calculations concerning light nuclei may contain some ambiguities at high momentum transfer.

By introducing the concept of an optical phase shift and correlation functions of various orders, the scattering amplitude is shown by Ciofi degli Atti (1975) to have a very useful form. As an example, in elastic scattering the intrinsic A-body density

$$\rho_A(\underline{\xi}_1 \cdots \underline{\xi}_A) = |\psi(\underline{\xi}_1 \cdots \underline{\xi}_A)|^2 \delta\left(\sum_i^A \underline{\xi}_i\right) \tag{5a}$$

and various n-body ground-state densities can be defined as

$$\rho_n(\underline{\xi}_1 \cdots \underline{\xi}_n) \equiv \int \rho_{n+1}(\underline{\xi}_1 \cdots \underline{\xi}_{n+1}) d\underline{\xi}_{n+1}, \quad n = 1, \ldots A-1. \tag{5b}$$

With the single-particle density function $\rho_1(\xi_1)$ defined as

$$\rho(\underline{\xi}) \equiv \rho_1(\underline{\xi}_1), \tag{5c}$$

the intrinsic A-body density can be represented as

$$\rho_A(\underline{\xi}_1 \cdots \underline{\xi}_A) = \prod_{j=1}^{A} \rho(\underline{\xi}_j) + \sum_{l<\pi} \prod_{k \neq l, m}^{A-2} \rho(\underline{\xi}_k)\{\rho_2(\underline{\xi}_l, \underline{\xi}_m) - \rho(\underline{\xi}_l)\rho(\underline{\xi}_m)\} + \text{higher-order correlations}. \tag{6}$$

The bracketed term is the two-body correlation function. Taking into account the translational invariance [the delta function in Eq. (4)], and because of the Pauli principle, the correlation functions will generally be nonzero. If hard-core effects are taken into account, there are other contributions. Thus in a correct, translational-invariant approach there is no "independent" particle model.

In the optical-model limit for elastic scattering, the nucleus is represented by a one-body potential giving the same phase shift as the many-body model

$$F_{00}(\underline{q}) = \frac{ik}{2\pi} \int e^{i\underline{q}\cdot\underline{b}}\{1 - \exp[i\chi_{\text{opt}}(b)]\} d^2b. \tag{7}$$

For $A \gg 1$, we obtain the optical limit phase function

$$\exp[i\chi_{\text{opt}}(\underline{b})] = \exp\left\{-A \int d\underline{\xi}\rho(\underline{\xi})\Gamma(\underline{b} - \underline{s}) + \frac{A^2}{2} \int d\underline{\xi}_1 d\underline{\xi}_2 \times [(A-1)\rho_2(\underline{\xi}_1, \underline{\xi}_2) - A\rho(\underline{\xi}_1)\rho(\underline{\xi}_2)]\Gamma(\underline{b} - \underline{s}_1)\Gamma(\underline{b} - \underline{s}_2) + \text{higher-order correlations}\right\}. \tag{8}$$

Pauli correlations and all types of dynamic correlations present in the wave function ψ_0 will appear in the correlation terms. In principle, all order of correlations would have to be determined. However, because of the dynamical approximation discussed in Sec. II.A, formula (8) does not contain some important correlation effects.

In recent papers, corrections to the Glauber model have been investigated (Wallace, 1975; Wong and Young, 1975). Wallace (1975) presents a high-energy expansion of the Watson multiple-scattering series (Watson, 1953), which reproduces the Glauber approximation as the leading (asymptotic) term and which produces systematic corrections to the particular combination of eikonal and frozen nucleus approximations inherent in Glauber theory. For elastic scattering, the method is free from the approximation of setting the longitudinal momentum transfer to zero. Close attention is paid to Fermi-motion effects and two-body recoil kinematic effects by consideration of the deviations from eikonal propagation between scatterings. A significant finding of the analysis is that there is substantial cancellation between leading order corrections to the Glauber approximation arising from noneikonal, kinematic, and Fermi-motion effects. Thus the high-energy expansion can be convergent at rather low momenta where the interactions are highly overlapping. One conclusion is that straightforward improvements of the Glauber model based on removing one of the approximations can be less accurate rather than more accurate. It is shown that the eikonal perturbation theory in the form used does give a reliable extension of the angular validity. This is illustrated in Fig. 1 for proton-^{4}He elastic scattering at 1

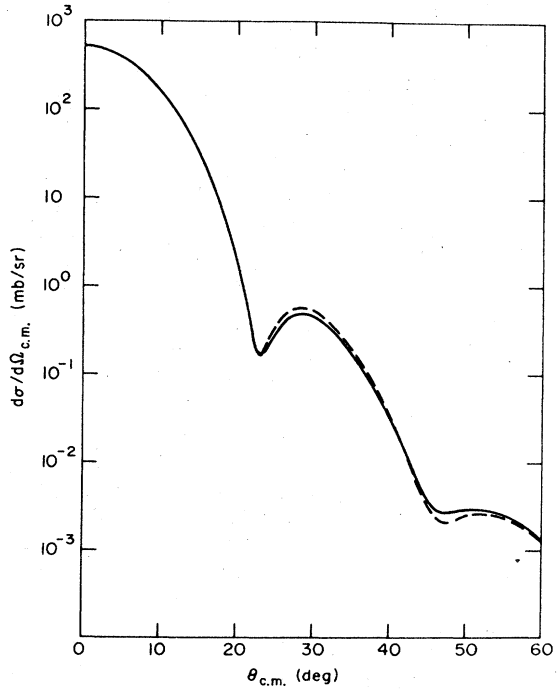

FIG. 1. Elastic scattering of 1.05-GeV protons by ^{4}He (Wallace, 1975). The Glauber approximation (dashed line) is compared to the high-energy expansion result (solid line). The solid line incorporates effects of eikonal, Fermi motion, and kinematic corrections.

GeV, where the Glauber and the high-energy expansion models are compared using a Gaussian model for ^{4}He. The correction is 15% at the double scattering maximum, and less than 31% in the range, $\theta \leq 60°$. Gillespie, Gustafson, and Lombard (1974) have examined these corrections to the eikonal amplitudes by calculating proton scattering on ^{16}O and ^{4}He between 0.1 and 1 GeV. They find rapid convergence to the exact results above 500 MeV out to 40°. The high-energy expansion (Wallace, 1975) at 1 GeV is expected to be accurate in the forward hemisphere.

In the above discussion of the Glauber model, the nuclear amplitudes have been taken as scalars. The Glauber model can also handle spin and isospin degrees of freedom, but so far these have been treated perturbatively (Auger *et al.*, 1976; Young and Wong, 1977a; Wallace, 1977).

B. Optical potential model of Kerman, McManus, and Thaler

The optical potential model of Kerman, McManus, and Thaler (KMT) (1959) has been developed by Feshbach and co-workers (see Sec. I). It can be used to interpret data at all angles and contains the effects of overlapping potentials. The one-body equation $(E - T_k - V_{opt})\phi = 0$ is solved in this approach. Here E is the total center-of-mass energy; T_k is the kinetic operator; and the optical potential V_{opt} is defined in terms of the total energy E, the effective potential $V_{\alpha\beta}$, and the energy of the intermediate nuclear state ϵ_α appearing in the propagator G_α,

$$V_{opt} = V_{00} + \sum_{\alpha=0} V_{0\alpha} G_\alpha V_{\alpha 0} + \sum_{\substack{\alpha\neq 0 \\ \beta\neq 0}} V_{0\alpha} G_\alpha V_{\alpha\beta} G_\beta + \cdots , \quad (9)$$

where

$$G_\alpha = (E^{(+)} - \epsilon_\alpha - T_k - V_{\alpha\alpha})^{-1} , \quad (10)$$

and

$$V_{\alpha\beta} = (A-1)\langle \alpha | \tau | \beta \rangle . \quad (11)$$

The t matrix for nucleon–nucleon scattering inside the nucleus is

$$\tau = v + v[a/(E^{(+)} - H_n - T_k)]\tau . \quad (12)$$

It is different from the free nucleon–nucleon t matrix, which is also expressed in terms of the nucleon–nucleon potential v, but differs because of the presence of the nuclear Hamiltonian H_n in the denominator and the projection operator A onto antisymmetric states of the target. Feshbach and co-workers replace the optical series to a certain order by a set of differential equations coupled by potentials which are proportional to the two-body correlation function [Eq. (6)] and higher-order ones. The lowest-order term in the potential depends only on the one-particle density and the nucleus is in the ground state between scatterings. The second term is proportional to the two-body correlation function, leading to a contribution to the potential where the nucleus may through a correlation not remain in the ground state between scatterings. The third term is proportional to triple scattering, etc. This formalism has been extended to include the first three terms of the expression (Feshbach, 1969); we will restrict the discussion here to the first two terms in the potential. The procedure then can be outlined as follows (Ciofi degli Atti, 1975). It is assumed the scattering matrix element is factorable because the momentum of the struck particle is much larger than the momentum of the bound particle and therefore

$$V_{\alpha 0} = \langle \underline{k}'\alpha | \tau | 0\underline{k} \rangle \cong \langle \underline{k}' | \tau | \underline{k} \rangle \langle \alpha | e^{i(\frac{A-1}{A}\underline{k} - \underline{k}')\cdot\underline{\xi}} | 0 \rangle = \tau(\underline{q}) F_{\alpha 0}(\underline{q}) . \quad (13)$$

In the propagation, only average excitation energies and matrix elements are considered, which is equivalent to the frozen nucleus approximation discussed in connection with the Glauber theory: $V_{\alpha\alpha} = \overline{V}$, $\epsilon_\alpha = \overline{\epsilon}$. With the use of closure over nuclear states, the second term in Eq. (9) becomes

$$\frac{1}{E - \epsilon - V - T_k} \sum_\alpha V_{0\alpha} V_{\alpha 0} = \frac{1}{E - \overline{\epsilon} - \overline{V} - T_k} (A-1)^2 \tau(\underline{q}_1)\tau(\underline{q}_2) C(\underline{q}_1, \underline{q}_2) . \quad (14)$$

Here $C(\underline{q}_1, \underline{q}_2)$ is

$$C(\underline{q}_1, \underline{q}_2) = \int \exp[i(\underline{q}_1 \cdot \underline{\xi}_1 + \underline{q}_2 \cdot \underline{\xi}_2)] \times [(A-1)\rho_2(\underline{\xi}_1, \underline{\xi}_2) - A\rho(\underline{\xi}_1)\rho(\underline{\xi}_2)] d\underline{\xi}_1 d\underline{\xi}_2 , \quad (15)$$

with $\underline{q}_1 = \underline{k} - \underline{k}''$, $\underline{q}_2 = \underline{k}'' - \underline{k}'$. The optical potential is

$$V_{opt}(\underline{q}) = (A-1) f(\underline{q}) F_{00}(\underline{q}) + (A-1)^2 \int d\underline{k}'' d\underline{k}''' G(\underline{k}'', \underline{k}''') f(\underline{q}_1) f(\underline{q}_2) C(\underline{q}_1, \underline{q}_2) , \quad (16)$$

where G is

$$G(\underline{k}, \underline{k}') = \langle \underline{k} | \frac{1}{E - \overline{\epsilon} - T_k - \overline{V}} | \underline{k}' \rangle . \quad (17)$$

Next, the basic assumption of this formulation is invoked. An eikonal solution of the propagator with $\overline{V}$ = constant leads to a diagonal form for G

$$G(k, k') = G(\underline{k})\delta(\underline{k} - \underline{k}') . \quad (18)$$

Then a function $U_2(\underline{q})$ is defined which satisfies the following relation

$$\int d\underline{k} f(\underline{q}_1) C(\underline{q}_1, \underline{q}_2) f(\underline{q}_2) \sim \int d\underline{k} U_2(\underline{q}_1) U_2(\underline{q}_2) G(\underline{k}) . \quad (19)$$

Under this condition, the optical series can be replaced by a set of coupled equations

$$(E - T_k - V_{00})\Phi_0 = (A-1) U_2 \Phi_1 , \quad (20a)$$

$$(E - \overline{E} - T_k - \overline{V})\Phi_1 = (A-1) U_2 \Phi_0 , \quad (20b)$$

where Φ_0 describes the elastic channel, and Φ_1 describes the average effects of the inelastic channels on the elastic channel; U_2 couples the elastic and inelastic channels and is proportional to the two-body correlation function of Eq. (6). To solve the coupled equations, the nucleon–nucleon scattering amplitude, the transition form factor $F_{\alpha 0}$, Eq. (13), and the correlation function, Eq. (15), must be specified. Equation (20) is solved by proper choices of $\overline{E}$ and $\overline{V}$.

C. Other treatments including the use of relativistic formulations of the optical-model potential

In the Glauber- and KMT-model approaches described in Secs.II.A and II.B, respectively, the nuclear potential is dependent on the parameters describing the nuclear charge form factor and the nucleon–nucleon t matrix. The effects of other properties of the nuclear wave function (correlations) can be fed in explicitly. Although the fits obtained qualitatively reproduce the data, there are many discrepancies.

In an attempt to obtain quantitative agreement with the data, several authors (Clark *et al.*, 1973; Arnold *et al.*, 1976a; Ray and Coker, 1976; Rule and Hahn, 1975a, 1975b, 1975c) have developed relativistic, phenomenological optical potentials, i.e., potentials not based explicitly on the nucleon–nucleon t matrix. A justification for using phenomenological potentials is that the nucleon-nucleon interaction is not well known. An early analysis (Palevsky *et al.*, 1967) of this kind was employed to describe the elastic scattering of 1 GeV protons from light nuclei, using the Klein–Gordon equation. Clark (1973) and Arnold (1976) use the Klein–Gordon or Dirac equation with a charge distribution determined from electron scattering. The basis for the theoretical optical-model potential used in some of their work is described by Goldberger and Watson (1964). In its simplest form, it relates the optical potential to the nucleon-nucleon forward scattering amplitude and the matter density of the nucleus:

$$V_{\rm opt}(r) = -A[\sigma_t p(1+\alpha)\rho(r)]/2E\,, \tag{21}$$

where A is the number of nucleons in the target, α is the ratio of real to imaginary parts of the nucleon–nucleon scattering magnitude, σ_t is the average nucleon–nucleus total cross section, and p and E are the projectile momentum and energy in the nucleon–nucleus center-of-mass system. It should be noted that the potential appearing in Eq. (21) is the first approximation to the KMT optical potential [see Eq. (13)]. For $\rho(r)$, they have used the nuclear charge density function. The potential of Eq. (21) is inserted as the fourth component of a four vector in either the Dirac or Klein–Gordon equation or, alternatively, as a pure scalar quantity. In a parallel development, a purely phenomenological potential defined by $V(r) = (V + iW)f(r)$, where V and W are real and imaginary strength parameters, has been used.

In other recent work, Ray and Coker (1976) have employed the Schrödinger equation with corrections for relativistic kinematics. Rule and Hahn (1975a, 1975b, 1975c) have employed a coupled-channel calculation, where the effect of coupling between elastic and inelastic channels is approximated by replacing the inelastic channels by one level whose excitation is treated as an adjustable parameter. When best fits to elastic scattering are obtained, the level position is found to be at 48 ±15 MeV.

D. Extraction of nearly model-independent nuclear matter densities from proton scattering

The most detailed information on nuclear charge distributions have been derived from electron scattering. Friederich and Lenz (1972), Friar and Negele (1972), and Sick (1974) have studied the problem of extracting this information with a model-independent analysis (MIA). Using this technique, meaningful error bars can be assigned to nuclear parameters. The magnitude of the effect of enlarging the range of momentum transfer, or, alternatively, of increasing the experimental precision, can be expressed quantitatively.

Lombard and Wilkin (1975) point out that measurements of elastic proton nuclear scattering generally extend to large values of the momentum transfer q and are measured with higher statistical precision than in elastic electron–nucleus scattering. Therefore Lombard and Wilkin have extended the MIA technique to proton data. To investigate this question, they generated pseudodata for elastic scattering at 1 GeV from the Glauber model (1959). To do this they used a simplistic nucleon–nucleon amplitude: purely imaginary, spin–isospin-independent, and of zero range. The proton–nucleus amplitude then may be written simply as (Saudinos and Wilkin, 1974)

$$F(q) = ik \int_0^\infty \Gamma(b) J_0(qb) b\, db\,. \tag{22}$$

Here the Bessel function of zero order $J_0(qb)$ appears in the expression. In the absence of nucleon correlations, the profile function $\Gamma(b)$ is related to the nucleon density $\rho(r)$ and the nucleon–nucleon total cross section σ_t by

$$\Gamma(b) = 1 - \exp\left\{-\frac{\sigma_t}{2}\int_{-\infty}^{\infty}\rho(b,z)dz\right\}. \tag{23}$$

In the spirit of the MIA, $\Gamma(b)$ is expanded on a fairly general basis and kept "as free from prejudice as is possible" according to the authors. In this work, $\Gamma(b)$ is expanded in terms of a sum of step functions, $S(b)$. In a recent application by Brissaud and Brussel (1976a) to ^{40}Ca data, a sum of Gaussian functions is used. This paper will be discussed in Sec.IV.A.

Following the argument of Lombard and Wilkin (1975), $\Gamma(b)$ is written as

$$\Gamma(b) = \sum_{i=1}^{N} a_i S(b - b_i) S(b_{i+1} - b) \tag{24}$$

from which Eq. (22) may be rewritten as

$$F(q) = \frac{i\hbar}{q}\sum_{i=1}^{N} a_i\{b_{i+1}J_1(qb_{i+1}) - b_i J_1(qb_i)\}. \tag{25}$$

This form is fit to the computer generated data. Next, if spherical symmetry applies, Eq. (23) can be inverted to obtain the density distribution. If measurements are carried out to some momentum transfer $q_{\rm max}$, the structure in the impact parameter space with width of the order of $d = \text{const}/q_{\rm max}$ can be examined. The constant has been found in electron scattering analysis (Sick, 1974) to be numerically equal to π. This determines the lower limit on the bin size in Eq. (24). Since most of the data with large momentum transfers are in the 0.6–1.1 GeV range, the effects of spin and the real part of the scattering amplitude have to be considered. It is for this reason that the authors confine themselves to pseudoexperimental data generated using a simplified Glauber model. The information content of elastic scattering

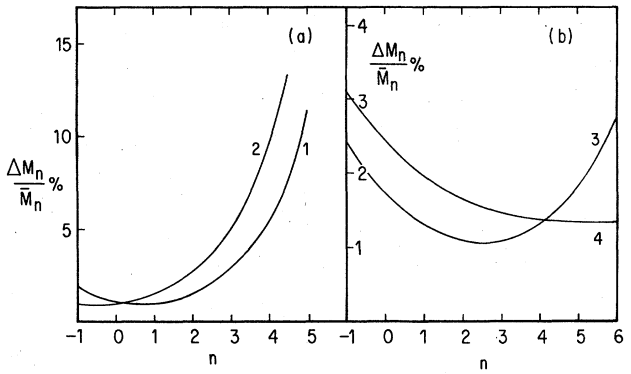

FIG. 2. The fractional error in the moment function m defined in text (Lombard and Wilkin, 1975). It is obtained by fitting pseudodata with no dependence on spin or isospin. (a) Proton scattering (curve 1) and electron scattering (curve 2) from ^{16}O. The statistical error is 1% and q_{max} is 2fm^{-1}. (b) Proton scattering from ^{208}Pb. Curve 3: the statistical error is 0.1% and q_{max} is 2fm^{-1}. Curve 4: q_{max} is increased from 2fm^{-1} to 4fm^{-1}, and the statistical error is 1%.

data is best expressed in terms of a moment function

$$M_n = \langle r^n \rangle^{1/n} . \tag{26}$$

In the limit of small σ_t(~0.1 fm^2), the results may be identified with electron scattering from light nuclei. In Fig. 2, the fractional error $\Delta M_n/M_n$ for $\sigma_t = 4.3$ fm^2 (protons incident) and for electrons incident on ^{208}Pb and ^{16}O are compared. For ^{208}Pd the validity of the analysis for electron scattering is not completely justified; this introduces some uncertainty into the conclusion reached. For purposes of comparison, the statistical error is taken to be the same in both electron and proton cases, and the maximum momentum transfers are taken to be the same.

In Fig. 2(a), the general features are made clear. The curves for electrons and protons cross, favoring the small moments in electron scattering measurements. Protons produce the best precision for the higher moments. For ^{16}O, the point of intersection has moved down toward smaller n. Figure 2(b) shows the effect of reducing the uncertainty of the data points (proton scattering) from 10^{-2} to 10^{-3}. The surface of the mass density distribution is determined more precisely. Increasing q_{max} from 2 to 4 fm^{-1} with uncertainties in the data points fixed at 10^{-2} [Fig. 2(b)], probes with higher precision inside the surface of the nucleus. As mentioned at the outset, we can expect the proton data to cover a broad range of q for a given overall accuracy. This feature will enhance the information obtainable from proton measurements.

III. PROTON ELASTIC SCATTERING FROM ^{4}He

Elastic scattering of high-energy protons from helium-4 at forward angles has been studied relatively thoroughly recently. The general features of the angular distributions are well described by the multiple-scattering models described in Sec. II. These features include a region at $-t < 0.25$ (GeV/c)^2 which is primarily single scattering, a region near 0.25 (GeV/c)^2 where single and double scattering amplitudes interfere destructively; a secondary maximum, followed by another region of interference between double and triple scattering; and finally a region near 1.45 (GeV/c)^2 where triple scattering is predominant. It is no surprise that there is no evidence of a rise in the region where quadruple scattering would be expected. To describe the features of $d\sigma/dt$ more quantitatively, energy-dependent data are useful. Evidence has been obtained from these data that the spin-dependent part of the nucleon-nucleon amplitude plays a significant role in describing the variation in the depth of the first minimum with energy as does α, the ratio of the real to imaginary parts of the nucleon-nucleon scattering amplitudes. The effects of short-range correlations have been investigated rather carefully and are found to produce results on $d\sigma/dt$ and on the polarization $P(t)$ which are too small to obtain quantitative information at the present stage of development of the subject. The combination of $d\sigma/dt$ and $P(t)$ data, especially at 1 GeV, teaches us that by now it is almost certain that the variation in the depth of the first minimum amplitudes are better understood. There appears to be a necessity to add an amplitude in double scattering involving a $\Delta(1232)$. The q dependence of α must also be taken into account. Polarization data in p-^{4}He scattering gives previously unknown information about the relative phases of the spin-dependent and spin-independent parts of the N–N amplitudes. There is no evidence that the helium-4 wave function needs to be more detailed than is already known from the form factor studies of 4-helium with electron scattering. The experimental evidence bearing on these features is discussed in this section. Phenomenological calculations (see Sec. C) for p-^{4}He scattering provide quantitatively good fits. As at lower energies, systematic phenomenological studies of the energy dependence provide very useful information, for example, on the variation of the real part of the potential with energy.

A. Dependence of the elastic scattering cross section on bombarding energy

Stimulated by the BNL data at 1 GeV obtained in 1967 (Palevsky *et al.*, 1967), theoretical investigations have been made using the KMT model (Kerman *et al.*, 1959), the Glauber model (1959), and phenomenological optical potentials. A measurement in 1974 by Baker *et al.* (1974a) did not show the deep minimum seen in the BNL data. Measurements at 650 MeV and 350 MeV suggested an interesting variation of the depth of the minimum near and below 1 GeV. The single-arm magnetic spectrometers used in these experiments have been described by Saudinos and Wilkin (1974). In view of the need to resolve the conflicting results on the depth of the first minimum at 1 GeV and to provide more data on the energy dependence, experiments have been reported recently (Geaga *et al.*, 1977a; Nasser *et al.*, 1977; Verbeck *et al.*, 1975; Fain *et al.*, 1976) which employ independent techniques, differing from the single-arm magnetic spectrometer method used at BNL and Saclay. The Saclay spectrometer is shown in Fig. 3.

In the work reported in Geaga (1977a), a 7.0 GeV/c alpha particle beam at the Bevatron has been used to

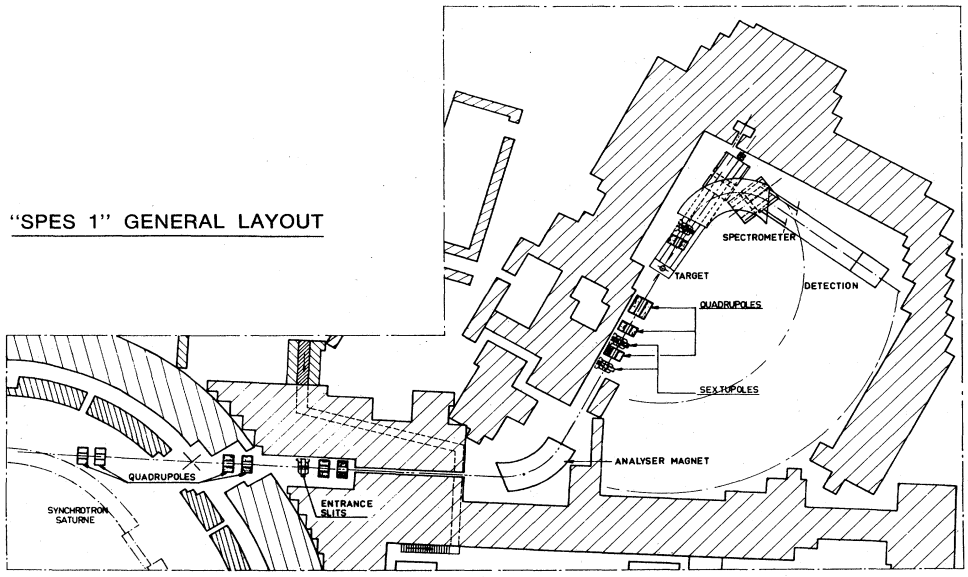

FIG. 3. Overall layout of the SPES 1 facility at Saturne, a one- arm, high-resolution spectrometer used to study p-^{4}He elastic scattering.

study p-^{4}He elastic scattering in a two-arm geometry. This is equivalent to protons incident on helium at 1.05 GeV bombarding energy. The two-arm geometry is illustrated in Fig. 4. Since there are no bound, excited states of the alpha particle, all but coherent scattering processes are excluded simply by the detection of an alpha particle in the magnetic spectrometer. Coherent pion production events can be distinguished from elastic scattering since the momentum resolution of the spectrometer is sufficient. At 3.9 GeV, elastic events are separated by at least 2% (σ) in momentum from events where coherent pion production is kinematically possible. The resolution of the spectrometer, defined by one standard deviation, σ, is 0.8%. This is sufficient to exclude the bulk of the coherent three- (or more-)-body final-state interactions.

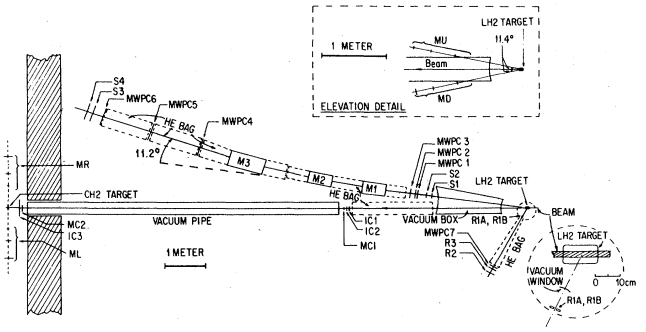

FIG. 4. Two-arm geometry used to study p-^{4}He elastic scattering with alpha particles incident: plastic scintillators S1–S4, bending magnets M1-3, and multiple-wire proportional counters MWPC 1-6 are used in the spectrometer arm. Plastic scintillators R1-R3 and MWPC 7 are used in the proton recoil detector. The beam is measured with ion chambers IC1-3, triple scintillation counter telescopes MR and ML, and with multiple-wire ion chambers MC1-2. The beam and scattered particles pass through vacuum (vacuum pipe, vacuum box) or helium gas (He bag). The liquid-hydrogen target (LH_2 target) thickness is monitored (see insert) by triple scintillation counter telescopes MU and MR.

An accurate determination of the center-of-mass scattering angle cannot be made by measuring the alpha particle's direction (angular resolution, $\sigma = 0.1°$) due to the magnification of σ in the transformation to the center of mass. (This feature of the Jacobian is also advantageous since it greatly increases the acceptance of the spectrometer, when evaluated in the center-of-mass system.) The limitation in the angular accuracy of determining the beam particle's direction imposed by the divergence of the incident beam ($\sigma = 0.2°$) adds to the uncertainty. The scattering angle was therefore determined by measuring the recoil proton's direction θ. The quantity $[d\theta_{cm}/d\theta]$ in this case is near unity. (θ_{cm} and θ are, respectively, the proton scattering angle in the center-of-mass and laboratory systems).

Particular attention was paid to the absolute determination of the scattering angle and the absolute scale of the cross section. The absolute angular measurement was especially important to remeasure since the Saclay data, taken in two runs separated by a period of a year, have an uncertainty in absolute angular scale (±0.25°) due to a shift in the beam direction during the year (Aslanides, 1975). The uncertainty in the BNL measurement is comparable. In fact, it is possible to obtain excellent agreement of the two data sets from Palevsky (1967) and Baker (1974a), except in the region of the minimum, by shifting them, relative to one another. This is illustrated in Fig. 5. The BNL and Saclay data have been shifted relative to one another by 0.5°, which is comparable to the combined angular uncertainty of the two data sets.

The data of Geaga *et al.* (1977a) and the data of Baker *et al.* (1974a) are compared in Fig. 6(a). There is essentially complete agreement in the angular dependence

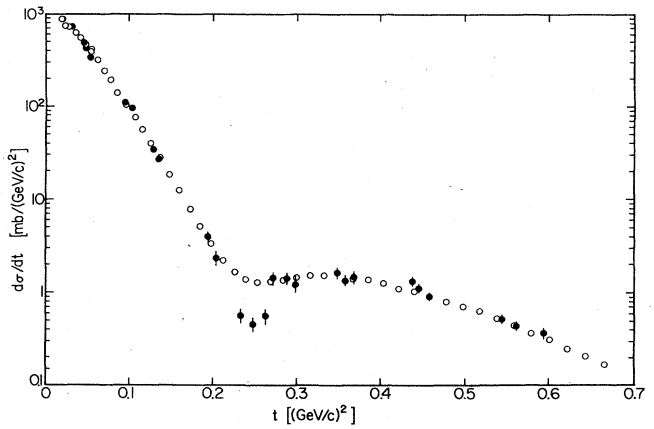

FIG. 5. Comparison of p-^{4}He data sets near 1.0 GeV: solid circles, Palevsky *et al.* (1967); and open circles, Baker *et al.* (1974a).

of the relative differential cross section except for an angular shift of 0.5° which is comparable to the uncertainty of the Saclay measurements. The Saclay data have been shifted 0.5° toward smaller angles to illustrate this point. A theoretical curve using the Glauber model is shown in Fig. 6(b) using the parameters given in Table I for the spin-independent, isospin-dependent nucleon–nucleon scattering amplitude $f_{pj}(t)$ and the distribution $\rho(r)$ for helium (N is a normalization factor)

$$\rho(r) = N\{\exp[-K_1^2 r^2] - C\exp[-K_2^2 r^2]\}, \tag{27a}$$

$$f_{pj}(t) = \frac{ik_0\sigma_{pj}}{4\pi}(1 - i\alpha_{pj})\exp(\beta_{pj}t/2)\,; \quad j = p,n\,. \tag{27b}$$

Here k_0 is the proton momentum in the center-of-mass system, σ_{pj} is the total cross section, α_{pj} is the ratio of real to imaginary parts of the scattering amplitude, and β_{pj} is the slope parameter. The Coulomb amplitude is included in the calculation. The parameters in $\rho(r)$ have been adjusted to reproduce the charge distribution of

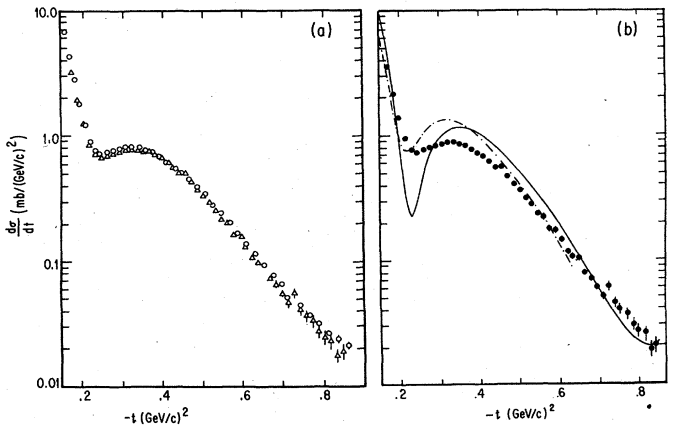

FIG. 6. (a) Elastic p-^{4}He scattering at 1.05 GeV: triangles, Geaga *et al.* (1977a); circles, Baker *et al.* (1974a). (b) The solid curve is a Glauber model calculation employing spin-independent, isospin-dependent nucleon–nucleon amplitudes. The dashed line is from the work of Auger *et al.* (1976). The data are from Geaga *et al.* (1976).

TABLE I. The values assigned to parameters describing the helium charge and matter distribution $\rho(r)$ and the nucleon-nucleon scattering amplitude $f_{pj}(t)(j=p,n)$. Parameters appearing in the table are defined in the text.

T_p	1.05 GeV	2.68 GeV
K_1^2	0.59	0.59
K_2^2	3.60	3.60
C	0.46	0.46
σ_{pp}	47.5 mb	42.7 mb
β_{pp}	5.75 (GeV/c)^2	6.5 (GeV/c)^2
α_{pp}	−0.1	−0.45
σ_{pn}	40.6 mb	42.7 mb
β_{pn}	5.75 (GeV/c)^2	6.5 (GeV/c)^2
α_{pn}	−0.2	−0.45

^{4}He. A Glauber-model calculation with spin–isospin-dependent nucleon–nucleon amplitudes (Auger *et al.*, 1976) employing essentially the same parameters for $\rho(r)$ and the same spin-independent parts of $f_{pj}(t)$ is also shown in Fig. 6. These two curves illustrate the importance of the spin dependence of the nucleon–nucleon amplitudes in the region of the minimum.

In the work reported by Geaga *et al.* (1977a), a study of the effect of the experimental uncertainty in t ($\sigma = 0.01$ GeV/c^2) in the measurement on the depth of the minimum was made. It was found that to fill in a minimum of the depth appearing in the BNL measurement (Palevsky, 1967) requires a fivefold increase of material between the target and wire proportional counters in the recoil arm.

With regard to the absolute scale of the cross section, particular care was taken to measure the absolute value of the beam flux. This was done by a method involving the counting of individual beam particles at low-flux levels with a scintillator telescope in order to calibrate the ^{11}C activity produced in graphite in the inclusive reaction $\alpha + {}^{12}\text{C} \rightarrow {}^{11}\text{C} + \text{anything}$. Self-absorption of ^{11}C activity in the graphite was accounted for by exposing graphite discs of two thicknesses. The beam was monitored by two-dimensional profile monitors during the activation measurement to ensure that the beam was well contained within the graphite disc and did not contain spatially separated satellite beams which might miss the graphite piece. The measurement method gave the absolute value of the cross section for production of ^{11}C activity and the result agreed very well with the energy dependence of previous measurements of the ^{11}C production cross section by alpha particles. Because of the large counting rates for elastic events experienced, it was possible to make a conservative cut in the azimuthal direction of the acceptance, which was constant in value over the horizontal aperture of the spectrometer. Monte Carlo calculations of the solid angle were in excellent agreement with a simple geometrical interpretation of the acceptance as would be expected under this circumstance. Efficiencies of the wire proportional counters (WPC's) were readily checked since each set of WPC's (preceding and following the bending magnets of the spectrometer) were redundant. As an internal check in the system, p–p scattering was measured at the same momentum. The measured cross section was found to agree within

the 15% variation of published values, which at this time is the quoted uncertainty reported by the experimenters.

Unfortunately there is disagreement on the absolute value of the cross section. In a new publication (Aslanides *et al.*, 1977), the group working at the Saturne facility at Saclay report a measurement of the absolute normalization of their data including the measurement at 1.05 GeV. They report a cross section 50% higher than the cross section obtained by Geaga *et al.* The latter has been reported to be in excellent agreement with the cross sections obtained with polarized beams [see Part B of this section (Klem *et al.*, 1977)]. Another Saclay group (Berger *et al.*, 1976) had obtained an absolute cross section in agreement with the measurement of Aslanides *et al.*, 1977, at 1.05 GeV, with a different spectrometer (discussed in Sec. VI in connection with large-angle scattering from ^{4}He).

Wallace (1977) has reported excellent agreement of the calculations of p-^{4}He elastic scattering at small angles using the high-energy expansion model (Wallace, 1977) discussed in Sec. II.A with the bevatron (Geaga *et al.*, 1977a), and ZGS results (Klem *et al.*, 1977), and poor agreement (50% discrepancy) with the cross section reported by Aslanides *et al.* (1977). Multiple-scattering calculations at small t depend essentially on single scattering and are very well determined by the nucleon–nucleon parameters.

However, it must be pointed out that there are many sources of error to deal with in obtaining an absolute cross section. The experimenters are urged to study their measurements carefully to attempt to resolve this issue.

The same magnetic spectrometer with a different recoil detector, a hodoscope-range telescope (Geaga *et al.*, 1977b) to detect recoil alpha particles, was used to measure p-^{4}He elastic scattering at 2.68 GeV (Nasser *et al.*, 1977). A gas-filled helium target was used in these measurements. The shape of the angular distribution (see Fig. 7) ($d\sigma/dt$ vs t) and the magnitude of $d\sigma/dt$ are almost identical to the results obtained at 1.05 GeV (Baker, 1974a). A Glauber-model calculation with spin-isospin dependent amplitudes at 1.05 GeV (Auger *et al.*, 1976) and a similar calculation at 2.68 GeV with spin-independent, isospin-dependent amplitudes (Nasser *et al.*, 1977) using the parameters listed in Table I are also shown in Fig. 7. Not unreasonably, a combination of the spin dependence and dependence on α (see Table I) are responsible for the relatively small differences observed experimentally and theoretically at 1 GeV and 2.68 GeV. As will be pointed out below, at lower energies, the experimental p-^{4}He distribution data and the corresponding Glauber calculations also agree qualitatively but vary considerably as a function of bombarding energy.

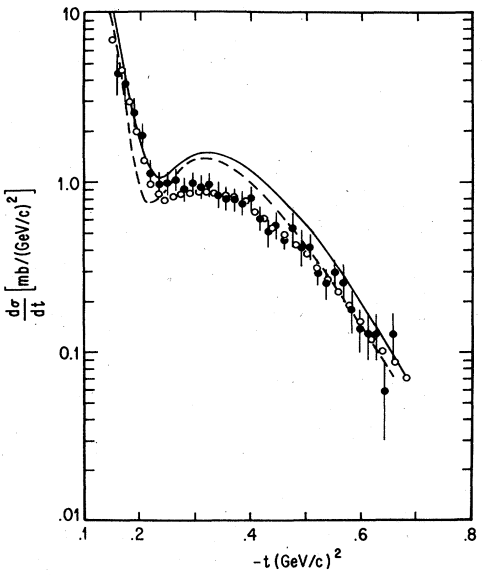

FIG. 7. Elastic p-^{4}He scattering: solid circles, 2.68 GeV (Nasser *et al.*, 1977); open circles, 1.05 GeV (Geaga *et al.*, 1977a). The solid curve is a Glauber model calculation at 2.68 GeV employing spin-independent, isospin-dependent nucleon–nucleon amplitudes. The dashed curve is a calculation at 1.05 GeV (Auger *et al.*, 1976).

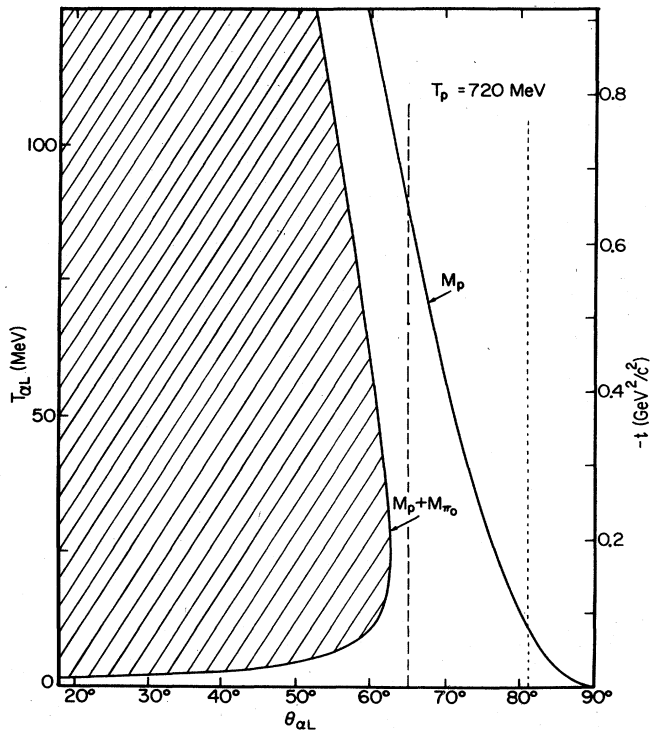

FIG. 8. Kinematics for $p + {}^4\text{He} \rightarrow {}^4\text{He} + \text{m.m.}$ at 0.72 GeV (Verbeck *et al.*, 1975). The solid curve at the right is for elastic scattering. In this case, the missing mass (m.m.) is equal to the mass of the proton (M_p). In the striped region, pion production processes occur. This area is bounded by single-pion production (m.m. $= M_p + M_\pi$). The dashed lines show the angular region investigated in the experiment.

Verbeck *et al.* (1975) have investigated the energy dependence of p-^{4}He elastic scattering at 0.58 GeV and 0.72 GeV. Fain *et al.* (1976) have recently measured p-^{4}He elastic scattering at 0.60 GeV. In this energy region, the ratio of the real to imaginary part of the p–p scattering amplitude, α_{pp}, passes through zero. The depth of the first minimum in p-^{4}He elastic scattering is sensitive to α_{pp} and α_{pn}. The quantity R, defined as the ratio of the cross sections at the second maximum and the first minimum, is found to vary significantly

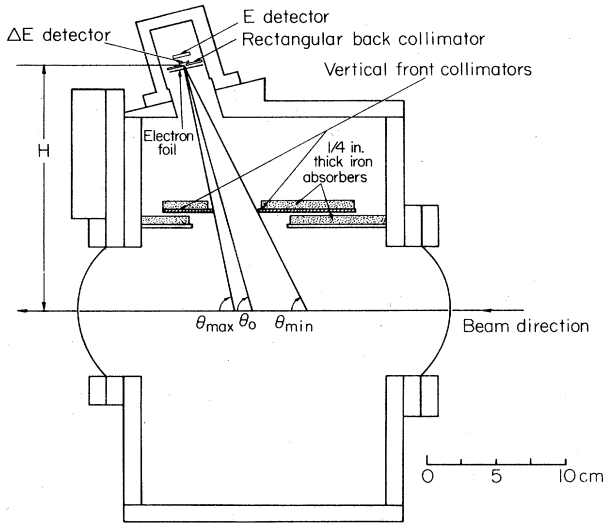

FIG. 9. The helium gas cell used to measure p-^{4}He elastic scattering at 0.72 GeV (Verbeck *et al.*, 1975).

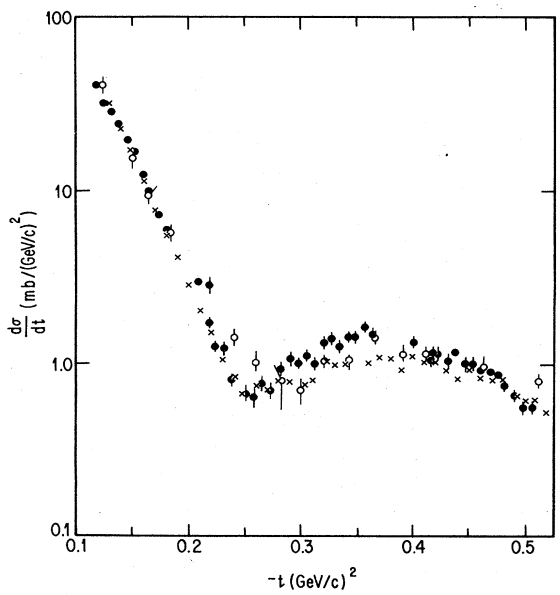

FIG. 10. Elastic p-^{4}He scattering near 0.6 GeV: open circles, Boschitz *et al.* (1972); solid circles, Fain *et al.* (1975); and crosses, Verbeck *et al.* (1975).

throughout this bombarding energy region.

Verbeck *et al.* and Fain *et al.* have applied a recoil technique, similar to the technique first used at 23.1 GeV for p-^{4}He scattering by Berthot *et al.* (1975). The technique makes use of the fact that the recoil α particle has no particle-bound excited states, and that the kinetic energy is a direct measure of t. The lowest possible inelastic threshold, pion production, kinematically constrains the α particle to move in a direction more forward than the angular region for elastic events. This is illustrated at 0.72 GeV in Fig. 8. The kinetic energy of the recoiling alpha particle $T_{\alpha L}$ in the laboratory system and t for elastic scattering are plotted against laboratory scattering angle $\theta_{\alpha L}$. Inelastic events are excluded in the range of $-t$ for elastic scattering up to 0.55 $(\mathrm{GeV}/c)^2$ by the angular collimation afforded by the apparatus (see Fig. 8). In the helium gas target cell, recoil α particles are detected by a counter telescope behind a double set of collimators. The front collimator, a vertical slit, defines the angular range $\theta_{\min}$ to $\theta_{\max}$ (corresponding to the dashed lines in Fig. 8) of allowed trajectories from the line source in the gas cell to the detector telescope. In this geometry, the differential cross section $d\sigma/dt$ is related to the background corrected spectrum dY/dT_α by

$$d\sigma/dt = (dY/dT_\alpha)\frac{\pi}{m_\alpha}\frac{H\sin\theta_\alpha}{nNa\cos(\theta_\alpha-\theta_0)}. \tag{28}$$

The area of the back collimator is a; the mass of the α particle, m_α; the helium gas density, n; and the number of beam particles, N. The recoil alpha particle scattering angle, θ_α, can be calculated from the measured T_α using kinematical relations for elastic scattering. The remaining geometrical quantities are defined in Fig. 9. Excellent ^{3}He–^{4}He separation is necessary since in the region of the minimum the ^{3}He yield exceeds the ^{4}He yield (Verbeck *et al.*, 1975). Since there is no redundancy in the measurement of $d\sigma/dt$ and because the distribution has little structure, a careful investigation of spurious sources of alpha particles in the T_α spectrum was made in the work of Verbeck *et al.* and found to be of a few percent. In addition there is a 5% (σ) absolute uncertainty in the scale of the differential cross sections in this work.

In Fig. 10 a comparison is made of the results at 0.58 GeV (Boschitz *et al.*, 1972), at 0.58 GeV (Verbeck *et al.*, 1975), and at 0.60 GeV (Fain *et al.*, 1976). There is fair agreement between the data set of Boschitz *et al.* (1972) when compared to either of the other data sets. However, a comparison of the data sets of Verbeck *et al.* and Fain *et al.*, which have smaller uncertainties, reveals a significant discrepancy at the secondary maximum.

Pursuing the question of the depth of the minimum at 1 GeV, it is convenient to remove some of the dependence on s. If $d\sigma/dt$ versus t is plotted, explicit dependence on beam momentum disappears in multiple-scattering formulations. Only the rather slowly varying effects associated with s dependence of the nucleon–nucleon amplitude cause differences. Some of the data which display the dependence of p-^{4}He elastic scattering on s near the first minimum are summarized in Fig. 11. The data at 0.58 GeV (Boschitz *et al.*, 1972) and the data at 0.60 GeV (Fain *et al.*, 1976) have not been included because the uncertainties are, respectively, larger than or comparable to the 0.58 GeV data set (Verbeck *et al.*, 1975) described above.

In 1967, Czyz and Lesniak (1967) showed that the Glauber model predicts that the slope before the first minimum will depend mainly on the t dependence of the form factor of helium. Czyz and Lesniak used the Glauber model with a Gaussian ground-state density

$$|\psi_0|^2 = \rho_0 \prod_{j=1}^{A} \exp(-r_j^2/R_H^2), \tag{29a}$$

and a spin-isospin-independent nucleon–nucleon scattering amplitude

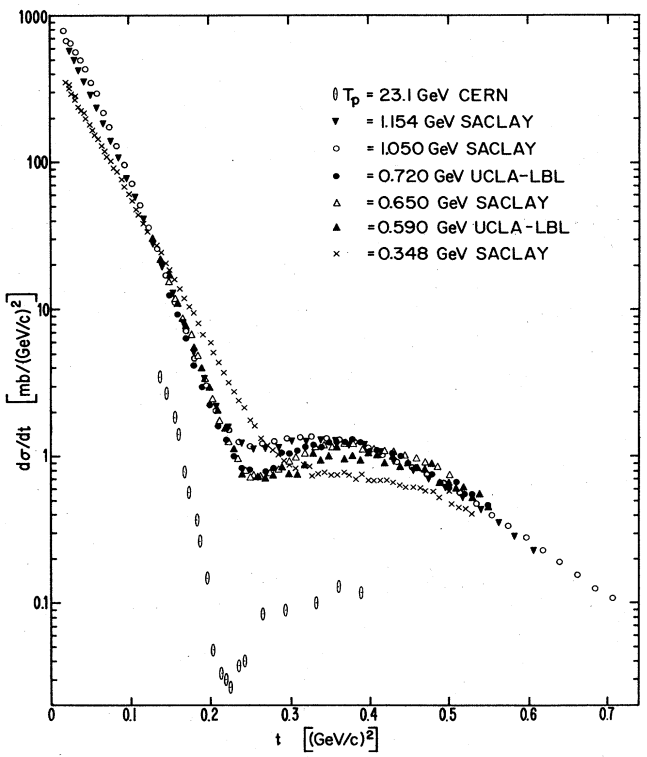

FIG. 11. The energy dependence of p-^{4}He elastic scattering: θ—23.1 GeV, Berthot *et al.* (1975); ∇—1.15 GeV, Aslanides *et al.* (1977); 0—1.05 GeV, Aslanides *et al* (1977); ●—0.72 GeV, Verbeck *et al.* (1975); Δ—0.65 GeV, Aslanides *et al.* (1977); ▲—0.59 GeV, Verbeck *et al.* (1975); x—0.35 GeV, Aslanides *et al.* (1977).

$$f(t) = i(\sigma_T/4\sqrt{\pi})(1 - i\alpha)\exp(bt/2)\,. \tag{29b}$$

The invariant nucleon–nucleon cross section is

$$(d\sigma/dt)_{NN} = |f(t)|^2\,. \tag{29c}$$

Here R_H is the radius of ^{4}He, and ρ_0 is the central nucleon density. Under these restrictive assumptions, they obtained an expression for the p-nucleus cross section in closed form, $d\sigma/dt = |F(t)|^2$, where

$$F(t) = \sqrt{\pi}\, i \times \exp[-(R_H^2 t/4A)] \sum_{m=1}^{A} \binom{A}{m} (-1)^{m+1} \left[\frac{\sigma(1-i\alpha)}{2\pi}\right]^m \times \left[\frac{1}{R_H^2 + 2b}\right]^{m-1} \frac{1}{2m} \exp[(R_H^2 + 2b)t/4m]\,. \tag{30}$$

Major features of the data shown in Fig. 11 are in agreement with the predictions of Eq. (30). As is easily seen, when the experimentally measured values of the nucleon–nucleon and charge distribution parameters are substituted for the variables appearing in Eq. (30), the slope of the p-^{4}He data before the first minimum is found to depend mainly on the t dependence of the form factor of helium and only weakly on the slope parameter b of the nucleon–nucleon scattering amplitude. This can be seen by examining the first term in Eq. (30). This term which represents single scattering, is the largest

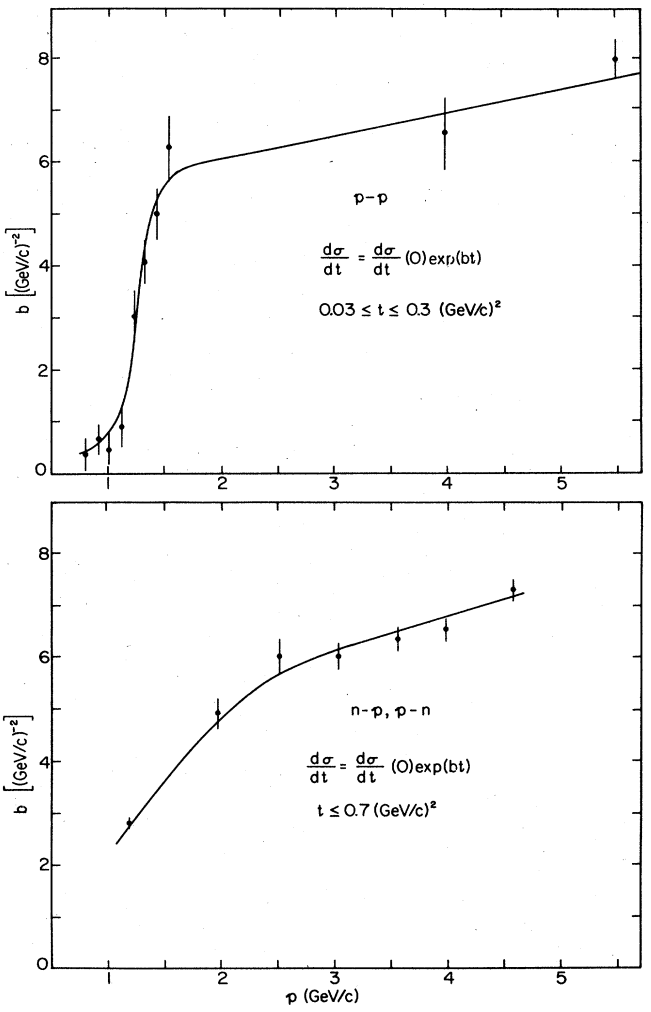

FIG. 12. Nucleon–nucleon slope parameters (Igo, 1975).

amplitude at small t.[1] The trend observed of the weak dependence of the slope of p-^{4}He scattering at small t on s is in good agreement with the prediction of Eq. (30). The nucleon–nucleon slope parameter (see Fig. 12) becomes larger with increasing s. This is reflected in the slow increase in steepness of the p-^{4}He data (compare the 1.15, 1.05, and 0.4 GeV data in Fig. 10). As can be seen in Eq. (30), the cross section near $t = 0$ depends sensitively on the average magnitude of the total cross section for nucleon–nucleon scattering. The momentum dependence of the latter is shown in Fig. 13. The total cross sections increase and then flatten out when the bombarding energy reaches 1 GeV ($cp = 1.7$ GeV/c).

The well-documented shallow minimum observed in p-^{4}He elastic scattering at 1 GeV is a very interesting phenomenon. In looking closely at the data (Fig. 14), the

[1]Succeeding terms on the right-hand side of Eq. (30) are the amplitudes for double, triple, and quadruple scattering. The series terminates with four terms because of the physically reasonable assumption of the Glauber theory that the nucleon-nucleon scattering amplitude is strongly peaked forward.

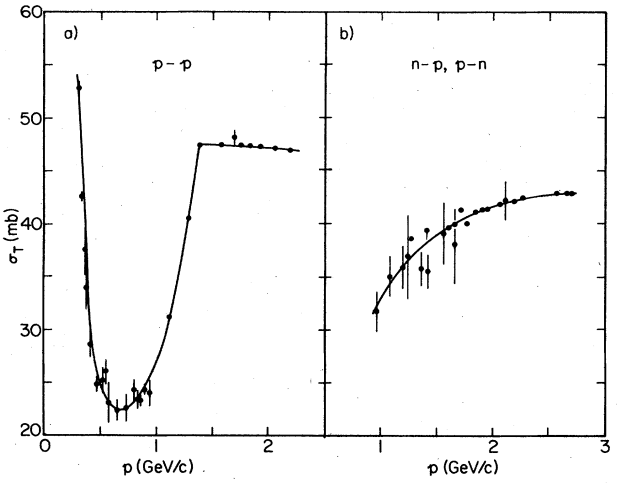

FIG. 13. Nucleon–nucleon total cross sections (Igo, 1975).

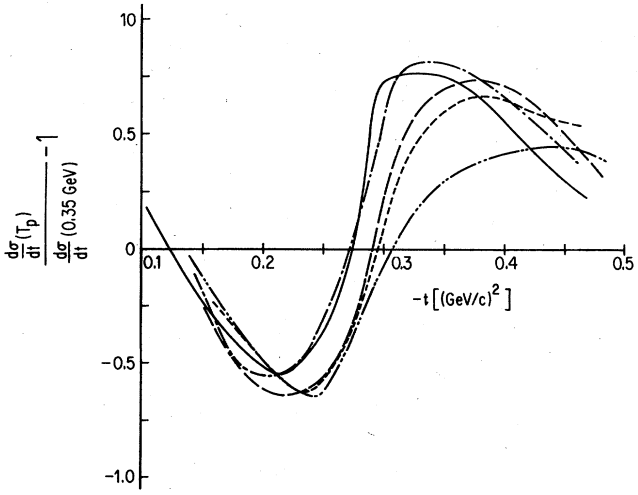

FIG. 15. The ratio of the differential cross sections at T_p and at 0.35 GeV minus one versus t: T_p=1.15 GeV (Aslanides *et al.*, 1977); 1.05 GeV (Baker *et al.*, 1974a); 0.72 GeV (Verbeck *et al.*, 1975); 0.65 GeV (Aslanides *et al.*, 1974); and 0.59 GeV (Verbeck *et al.*, 1975).

ratio R of the cross section at the second maximum and the first minimum is seen to vary systematically and to reach a maximum near 0.65 GeV. The dependence of the position of minimum on T_p is plotted in the same figure. These effects may be illustrated in another way. In Fig. 15, the difference between the smoothly varying 0.35 GeV cross section and the cross sections at the same t at 1.15, 1.05, 0.65, and 0.59 GeV normalized by the cross section at 0.35 GeV are plotted versus t. The minimum near 0.23 $(\text{GeV}/c)^2$ is associated with the depth of the first minimum, and the maximum at 0.33 $(\text{GeV}/c)^2$ is associated with the second maximum in the cross section.

The cross section has been calculated using the Glauber model with spin-independent nucleon–nucleon amplitudes (Igo, 1975). The object was to see if the momentum dependence of R could be reproduced *qualitatively*. It is well known from earlier calculations [example: Bassel and Wilkin (1967, 1968)] that the Glauber model utilizing spin-independent scattering amplitudes empirically adjusted to reproduce the small-angle behavior of p-p and p-n scattering and an empirical form factor for helium derived from electron scattering would predict larger R values than observed. In the calculations (Igo, 1975), spin-averaged nucleon–nucleon amplitudes of the form given by Eq. (29b) have been adopted using the empirical energy dependence of the slope parameter b illustrated in Fig. 12; of the total cross section σ_T (see Fig. 13) and of α_{pn} and α_{pp}, from Figs. 16 and 17. The charge form factors for helium of Frosch *et al.* (1967) have been used for both charge and mass form factors. The results are shown in Fig. 18. The behavior of R is qualitatively reproduced. The first minimum is shallow at 1.15 and 1.05 GeV, and also at 0.35 GeV. It is much deeper at 0.65 and 0.59 GeV. It is also evident that the spin dependence of the nucleon-nucleon amplitudes is needed in order to resolve the large quantitative discrepancies of the theoretical treatment at all five energies. The inverse of R, $d\sigma/d\Omega_{\text{min}}/d\sigma/d\Omega_{\text{max}}$, is shown in Fig. 19. The minimum is evident near 600 MeV. Figure 19 also shows the dependence of

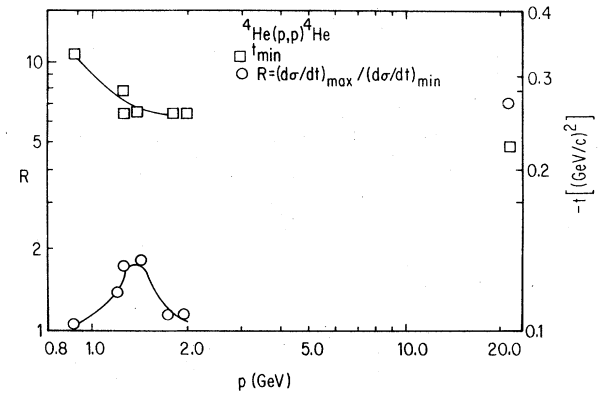

FIG. 14. The momentum dependence of R (circles), and the position of the minimum (squares) versus T_p.

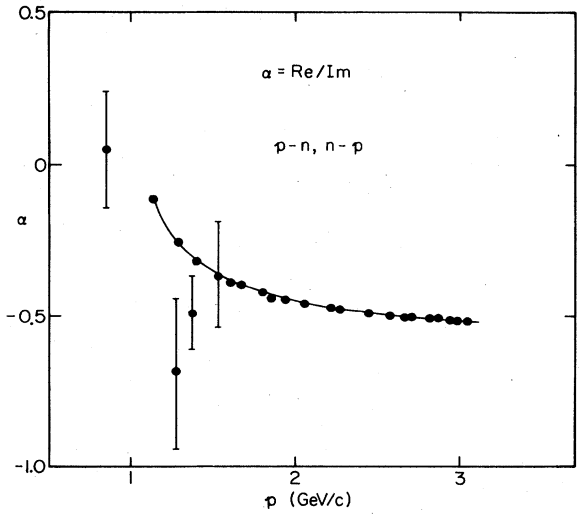

FIG. 16. The ratio α of the real to imaginary parts of the forward scattering amplitude for p-n scattering (Igo, 1975).

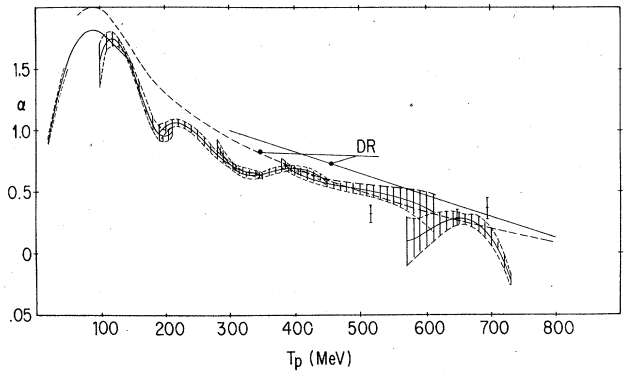

FIG. 17. The ratio α for p-p scattering. The hatched areas encompass acceptable values for α obtained from a series of spline fits to the p-p elastic and inelastic data (Bystricky *et al.*, 1975). The solid and dashed lines denoted by DR are predictions based on dispersion relations by Dutton and Van de Raay (1968), and Barashenkov and Toneev (1968), respectively. The experimental points are from the work of Vorobyov *et al.* (1972).

the real part of the scattering amplitude. It passes through zero near 600 MeV; the exact energy depends on the Coulomb amplitude.

A recent calculation (Auger, Gillespie, and Lombard, 1976) with spin dependence in the nucleon–nucleon amplitudes [see Figs. 6(b) and 7] includes a calculation of

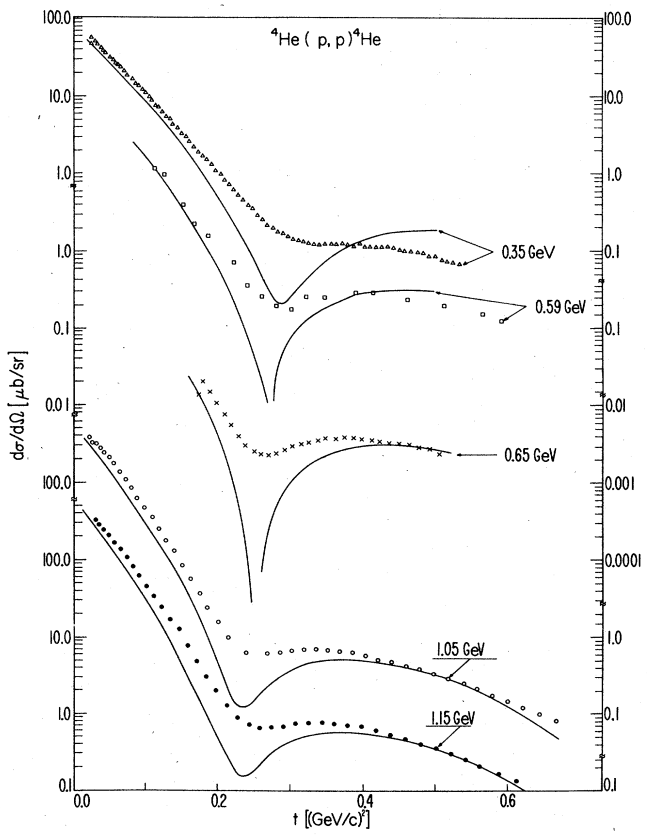

FIG. 18. Comparison of calculations using the Glauber approximation with spin-independent nucleon–nucleon amplitudes and p-^{4}He elastic scattering data.

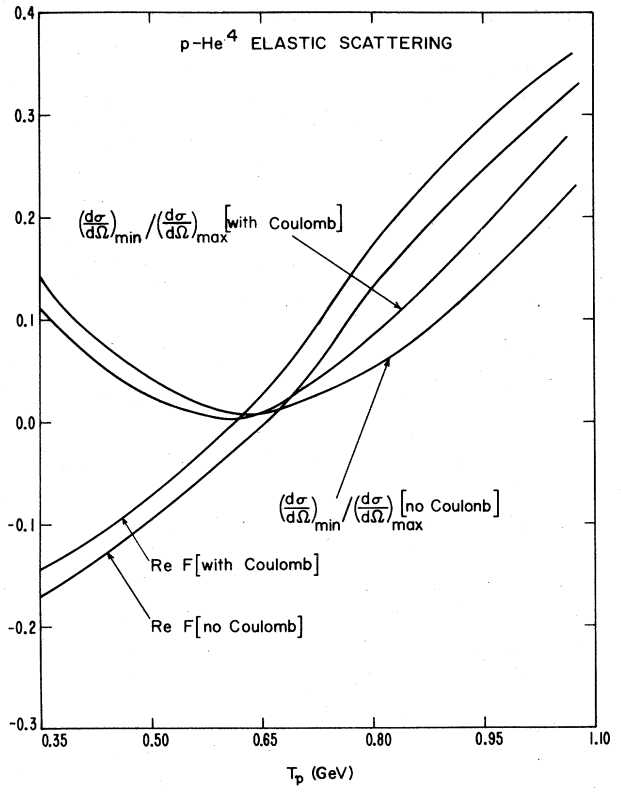

FIG. 19. The ratio of the calculated differential cross sections at the first minimum and the second maximum with and without the Coulomb amplitude versus energy, and the real part of the forward scattering amplitude with and without the Coulomb amplitude versus energy.

the differential cross section and polarization in the range $T_\alpha = 0.6 - 23.1$ GeV with the Glauber model. Corrections to the Glauber model due to target-nucleon overlap, charge exchange, and the Coulomb force are considered. With respect to spin effects, the most general representation of the nucleon–nucleon interaction consists of five amplitudes (Wolfenstein, 1956). Since the nucleon–nucleon data are not complete enough at these energies to determine these, only two amplitudes have been retained in the scattering matrix

$$M(t) \cong A(t) + C(t)(\underline{\sigma}_1 + \underline{\sigma}_2)\cdot\hat{\underline{n}}\,, \tag{31}$$

where $\hat{n}$ is the unit vector normal to the scattering place. The amplitudes A and C are parameterized in the form suggested by the optical theorem for diffractive scattering; $A(t)$ has the form given by Eq. (29b) and

$$C(t) = i\frac{\sigma_T}{4\pi}\sqrt{-t/4M}\,(1 - i\alpha_s)\exp(b_s t/2)\,. \tag{32}$$

Here α_s and b_s play roles in Eq. (31) equivalent to those that α and b play in Eq. (29b).

Obviously a more complete parameterization would require an expression for all five amplitudes together with complex values for slope parameters b and b_s. However, the lack of accurate experimental data, especially at very forward angles (namely in the angular domain relevant for application to nucleon-nucleus scat-

tering) does not warrant such refinements at present.

Distinct parameters have been measured for $A(t)$ for p–p and p–n scattering; but the spin-dependent parts are insufficiently defined; they were assumed the same for p–p and p–n scattering. The values of σ_T, α, and b were obtained from nucleon–nucleon data compilations (Benary *et al.*, 1975; Bystricky *et al.*, 1972). Differential cross section and polarization data for nucleon–nucleon scattering were fit by varying the parameters in Eqs. (29b) and (32). The helium density is represented by a form suggested by Bassel and Wilkin (1967) which has been used by a number of authors. This distribution reproduces the electron elastic scattering data on helium reasonably well.

The results are shown in Fig. 20. The theoretical differential corrections between 0.60 and 1.15 are much improved in the region of the first minimum compared to those using the spin-independent nucleon-nucleon parameters reported in Igo (1975). However, there is still a tendency to predict too large values of R, especially at 1.05 GeV and 1.15 GeV, and the positions of the minima are not improved compared to the calculated results reported in Igo (1975) (spin-independent case). The deviation from experiment at 1.05 GeV has already been shown quite clearly in Fig. 5. Another source of uncertainty is the parametric forms of the helium-4 form factor. One may critically question the theoretical assumptions which are implicit in extracting a form factor for helium from electron elastic scattering data.

The authors (Auger *et al.*, 1976) find that charge exchange effects do not affect the shape of the dip appreciably. There are other possibilities, however; isobaric resonances in intermediate states may lead to the observed energy dependence as well as dynamical two-body correlations in the ^{4}He wave function. It is possible that the omitted spin-dependent terms in Eq. (31) are responsible for the deviations from experiment.

The fits to the 23.1 GeV data are interesting in this regard. (At this energy, the spin-dependent effects in the nucleon-nucleon amplitudes are negligible.) The differential cross section (see Fig. 20) is readily reproduced by the Glauber model, as was pointed out earlier by Koefed-Hanson and Wilkin (1971). The fact that dynamical two-body correlations are not required at 23.1 GeV to obtain good fits implies a limitation on their contribution.

Lambert and Feshbach (1973) have shown that the two-body correlations will principally affect the height of the second maximum rather than the dip region, not an unexpected result. The presence of nuclear isobars (N^*) in intermediate state requires large longitudinal mass transfer and the necessity of an isospinflip transition in the nucleus. Despite this, a calculation by Ikeda (1972) suggests the importance of N^* configurations in ^{4}He. The s dependence of the dip between 1 GeV and 23.1 GeV may be a natural consequence of the production cross sections for various N^* (Wallace and Alexander, 1977).

As mentioned above, the minimum remains shallow between 1.05 and 2.68 GeV and the overall shape and magnitude is not changed. It will be interesting to study the transition from the shallow minimum seen at 2.68 GeV and the deeper minimum and reduction in the overall cross section seen at 23.1 GeV. Work in progress at the Bevatron at 5 GeV is directed to this question.

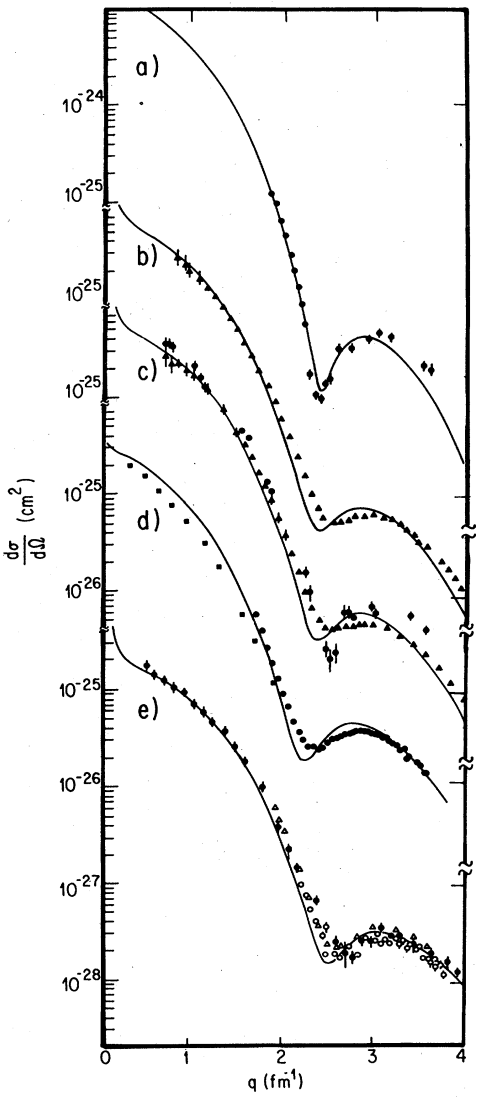

FIG. 20. Comparison of calculations using the Glauber model with spin-dependent nucleon–nucleon amplitudes (Auger *et al.*, 1976) with p-^{4}He elastic scattering data: (a) 23.1 GeV (Berthot *et al.*, 1975); (b) 1.15 GeV (Aslanides *et al.*, 1977); (c) near 1 GeV (circles, Palevsky *et al.*, 1967; triangles, Baker *et al.*, 1974a); (d) near 0.7 GeV (squares, McManigal *et al.*, 1965; circles, Verbeck *et al.*, 1975); and (e) near 0.6 GeV (closed circles, Aslanides *et al.*, 1977; open circles, Verbeck *et al.*, 1975; triangles, Boschitz *et al.*, 1972).

B. Polarization in p-^{4}He elastic scattering

Very little data existed, until recently, on polarization in p-^{4}He elastic scattering in the intermediate-energy region (see Fig. 21). A measurement at 0.56 GeV (Boschitz *et al.*, 1972) has been reported. The measurement was performed before the polarized proton beam at the ZGS (zero gradient synchrotron) accelerator at Argonne became available. An earlier measurement at the LBL 184 synchrocyclotron (McManigal *et al.*, 1965)

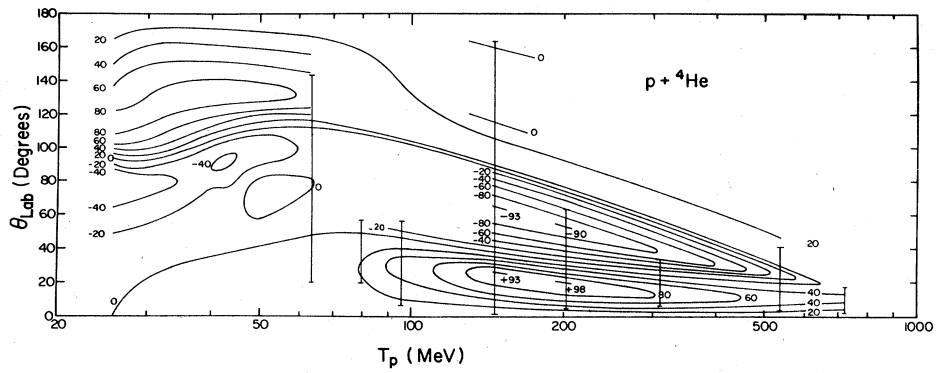

FIG. 21. The dependence of the polarization in p-^{4}He elastic scattering between 10 and 725 MeV. The contour diagram in the energy region 20–55 MeV is from a phase-shift analysis of p-^{4}He data (van Oers, 1977). The vertical lines correspond to energies where the experimental data exist, which have been used to construct the contour plot above 55 MeV: 63 MeV (Boschitz *et al.*, 1966); 70, 80 MeV (Perez-Mendez *et al.*, 1969); 147 MeV (Cormack *et al.*, 1959); 203 MeV (Gotow, 1954); 312 MeV (Chamberlain *et al.*, 1956); 540 MeV (Boschitz *et al.*, 1972); and 725 MeV (McManigal *et al.*, 1965).

over a smaller range of q is also available.

Recently data have become available (Klem *et al.*, 1977) at laboratory kinetic energies of 0.56, 0.80, 1.03, 1.3, and 1.7 GeV (see Fig. 22). The statistical accuracy of these data is improved because the intense ZGS beam (10^9 protons/pulse at 2 GeV/c, 70% polarized) was used. These measurements verify the magnitude of the polarization found in the earlier data (McManigal *et al.*, 1965; Boschitz *et al.*, 1972) at the first maximum at about 1.2 fm^{-1} and at the second peak, also positive, which occurs at 4 fm^{-1}. A very interesting behavior is noted in the region just before and at the q value where the minimum is observed in the differential cross section (see Fig. 22). At 1.03 GeV and above, the polarization is always positive; at 0.80 GeV, the polarization goes to zero in this region; and at 0.56 GeV, the polarization changes sign and is −0.35 at q = 1.24 fm^{-1}. This behavior is different from the polarization measured at lower energies and compiled by van Oers (1974b) (see Fig. 21). No such sharp structure has been reported at lower energies.

Young and Wong (1977a, b) have studied the energy dependence of the polarization using the Glauber model with a correction for the overlap of the nucleon–nucleon potentials, and the recoil of nucleons in individual collisions with the proton projectile (Wong and Young, 1975). They find, in agreement with Wallace (1975), that the corrections to the Glauber model, when all are considered, tend to cancel one another for small momentum transfers where the single scattering predominates. The appearance of the sharp negative polarization peak at 0.56 GeV is attributed by Young and Wong to the difference in the slope parameters b and b_s. (b_s is bigger than b.) This difference introduces a phase difference between the spin-dependent and -independent amplitudes (including single and double scattering in each case). The phase difference becomes $\pi/2$ (polarization zero) at the q value where the phase of $C(q)$ changes by π. At the larger value of q, $A(q)$ changes phase and the phase difference becomes $\pi/2$ once again. Experiment shows that these q values differ by 0.4 fm^{-1}. The effect is seen experimentally near 600 MeV where the effective value of α is known to be near zero. The observation of a sharp minimum requires that α_s is nearly zero. The amplitudes $A(t)$ and $C(t)$ are required to have distinctly different slope parameters at 0.56 GeV and almost equal ones near 1 GeV. This conclusion is in agreement with the analysis of nucleon–nucleon data by Franco (1968).

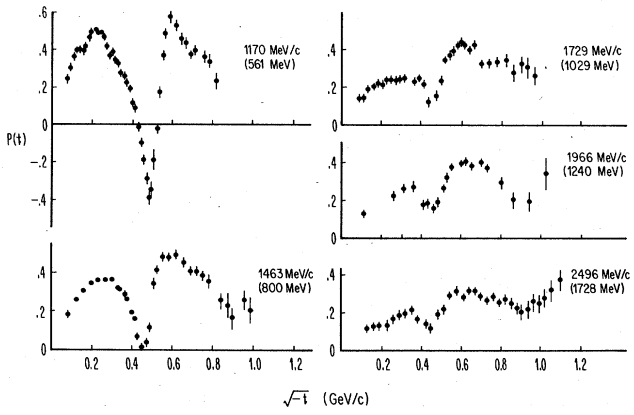

FIG. 22. The dependence of the polarization in p-^{4}He elastic scattering on bombarding energy between 0.56 and 1.7 GeV.

Figure 23 shows the polarization data of Boschitz *et al.* (1972) and of Klem *et al.* (1977) and the theoretical curve of Young and Wong at 0.56 GeV. A calculation by Auger *et al.* (1976), already referred to, and a calculation by Lykasov and Tarasov (1975), are also shown. Figure 24 shows the polarization data at 1.02 GeV (Klem *et al.*, 1977) and a theoretical fit obtained by Young and Wong (1976). The depth of the minimum and the height of the second maximum is sensitive to the double charge exchange contributions which effects the double scattering amplitude. Also shown are calculations (Kujawski, 1970; Lambert and Feshbach, 1973). The calculation of Lambert and Feshbach is of particular interest because it predicts that the effect of second-order correlations is small in the q region where polarization data exist.

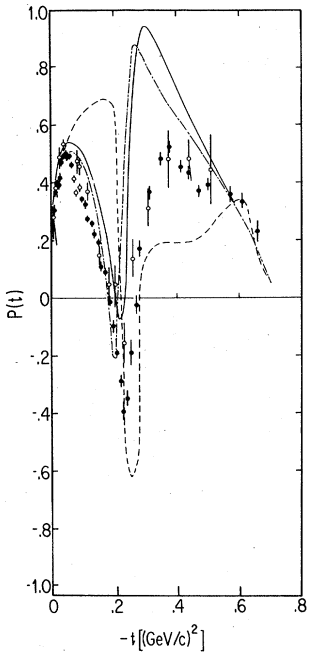

FIG. 23. The polarization in p-^{4}He elastic scattering near 0.55 GeV: open circles, Boschitz *et al.* (1972); closed circles, Klem *et al.* (1977). Predictions obtained using the Glauber model: long-dash-short-dash curve, Young and Wong (1976); solid curve, Auger *et al.* (1976); dashed curve, Lykasov and Terasov (1975).

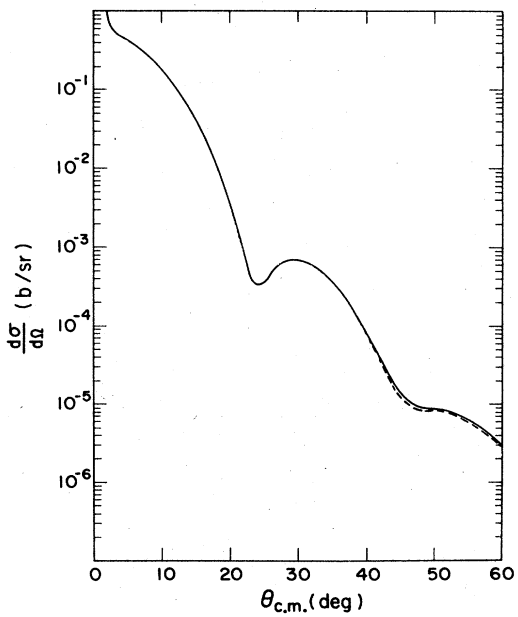

FIG. 25. Equivalent calculations of elastic p-^{4}He scattering at 1 GeV using the Dirac (dashed curve) and Klein–Gordon (solid curve) equations (Clark *et al.*, 1973).

C. Some recent results of phenomenological analyses of p-^{4}He elastic scattering

Using the Klein–Gordon equation, Palevsky *et al.* (1967) obtained good fits to the elastic scattering data at 1 GeV. The shape parameter of the optical potential for ^{12}C and ^{16}O was similar to those found below 100 MeV. The optical potential for ^{4}He, however, was characterized by a relatively small value of the diffuseness parameter, leading to a rapid falloff with increasing radial distance r at large r. This somewhat surprising result has been verified in recent analyses (Arnold *et al.*, 1976a; Ray and Coker, 1975). It is attributed to the importance of the second term in the Watson (1953) multiple-scattering matrix which depends on the potential quadratically. Attempts to represent elastic scattering from light nuclei with only a linear dependence lead to shapes which have small diffuseness parameters, to compensate for the higher-order term in the Watson series. The rms radius of the proton distribution is found to be comparable to the rms radius of the potential.

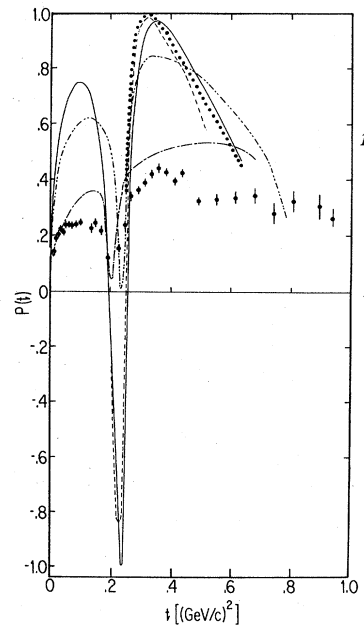

FIG. 24. The polarization in p-^{4}He elastic scattering near 1 GeV: solid circles, Klem *et al.* (1977). The dash-dot-dot curve is a prediction by Kujawski (1970). The solid, dashed, and dotted curves are theoretical predictions (Lambert and Feshbach, 1973) excluding dynamical correlations, including a short-range r_c correlation ($r_c = 0.4$), and including the dynamical correlation in the Reid soft-core potential, respectively. The long-dash-short-dash curve is a prediction obtained using the Glauber model (Young and Wong, 1976).

It was stated in Sec.II.C that phenomenological analyses are of interest because quantitatively better fits to the elastic scattering data are obtained (Arnold *et al.*, 1976a; Ray and Coker, 1976) than with the parameter-free models discussed above. In a recent analysis by Clark *et al.* (1973), the Klein–Gordon and Dirac equations have been used to study p-^{4}He scattering at 1 GeV. As long as the transformation character of the potential is that of a scalar U_s or that of the fourth component U_4 of a four vector with zero three-vector part, the two equations give equivalent acceptable fits to the data as illustrated in Fig. 25. The calculations for Fig. 25 were made at a time when the only existing data were from BNL (Palevsky *et al.*, 1967), so the curves shown would not represent currently accepted data. A quantitative idea of how the two types of fits would differ when compared to the data may be obtained by examining Fig. 26. In a recent study of the energy dependence in p-^{4}He scattering, the same group (Arnold, 1976a) has used the Klein-Gordon equation. A charge distribution for ^{4}He (Frosch *et al.*, 1960)

$$\rho(r) = \rho_0 \frac{1 + wr^2/c^2}{1 + \exp[(r-c)/z]} \tag{33}$$

with $c = 1.008$, $z = 0.32$ fm, and $w = 0.445$ was used, and

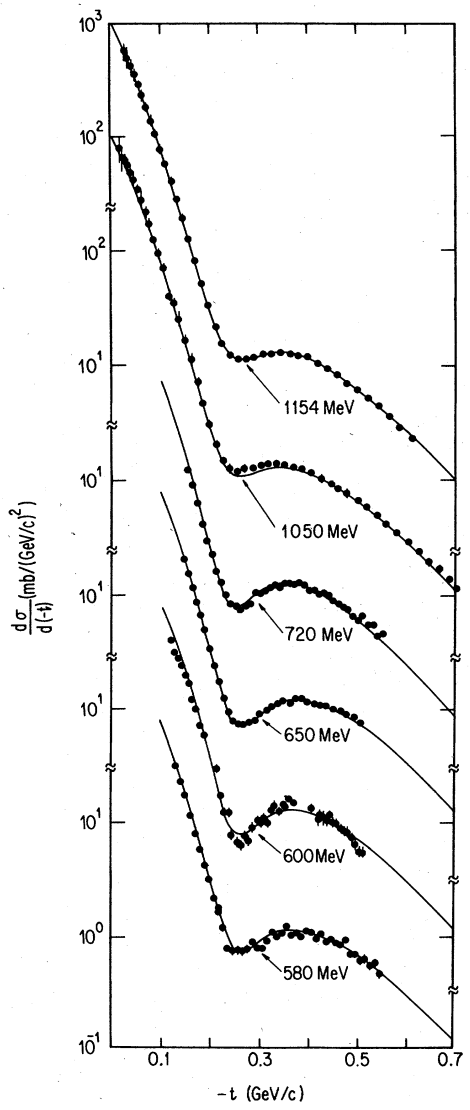

FIG. 26. Optical-model analysis of p-^{4}He elastic scattering data above 500 MeV using the Klein–Gordon equation (Arnold *et al.*, 1976b).

$$U_4 = (V + iW)\frac{1 + w'r^2/c'^2}{1 + \exp[(r - c')/z']} \tag{34}$$

with w' and c' set equal to w and c. The surface of the potential is less diffuse (using either U_4 or U_5, $z' = 0.28 - 0.30$ fm at 1.05 GeV) than the charge distribution ($z = 0.326$ fm) in agreement with calculations of Palevsky *et al.* (1967). Figures 26–28 show the results of a systematic analysis of p-^{4}He elastic scattering experiments above 500 MeV (Verbeck *et al.*, 1975; Baker *et al.*, 1974a; Aslanides *et al.*, 1975; Fain *et al.*, 1976; Boschitz *et al.*, 1972; Palevsky *et al.*, 1967) using Eqs. (31) and (32). In agreement with the reformulated optical model (Greenlees *et al.*, 1968, 1970), the volume integral per nucleon J_R/A and the rms radius of the real part of the optical potential are well determined and essentially in agreement with the analysis of van Oers *et al.* (1973) and van Oers *et al.* (1974) for heavier nuclei. The BNL data (Palevsky, 1967) and

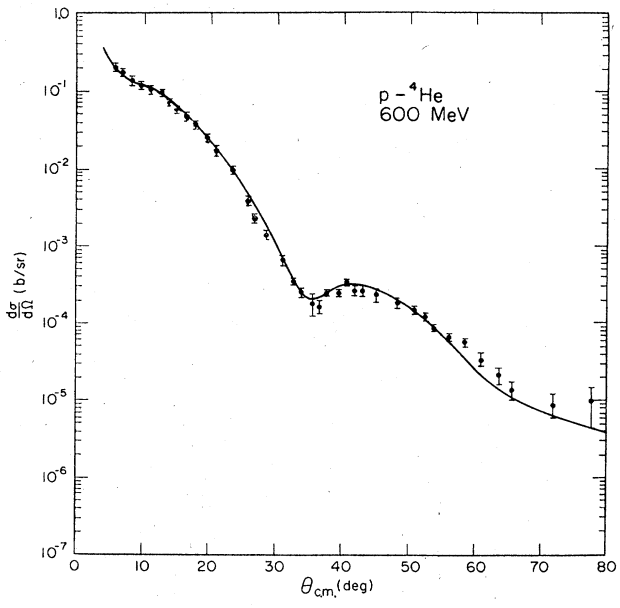

FIG. 27. Optical-model analysis of p-^{4}He elastic scattering data at 600 MeV using the Klein–Gordon equation (Arnold *et al.*, 1976b).

SREL (Space Radiation Effects Laboratory) data (Boschitz, 1972) have been excluded in the extraction of J_R/A because the large value of R in the former causes a disparate value of J_R/A and because, in the latter case, data of higher statistical accuracy (Verbeck, 1975) are used. The average of the rms radii from the analysis is 1.52 ± 0.06 fm, in agreement with the proton matter distribution 1.42 ± 0.05 fm (de Jager *et al.*, 1974). Figure 29 shows J_R/A plotted versus T_p. The values obtained in this energy region fall on an extrapolation of the straight line passing through the data below 500 MeV,

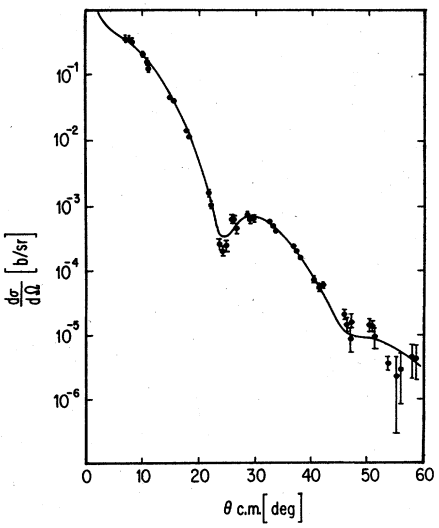

FIG. 28. Optical-model analysis of p-^{4}He elastic scattering data at 1000 MeV using the Klein–Gordon equation (Arnold *et al.*, 1976b).

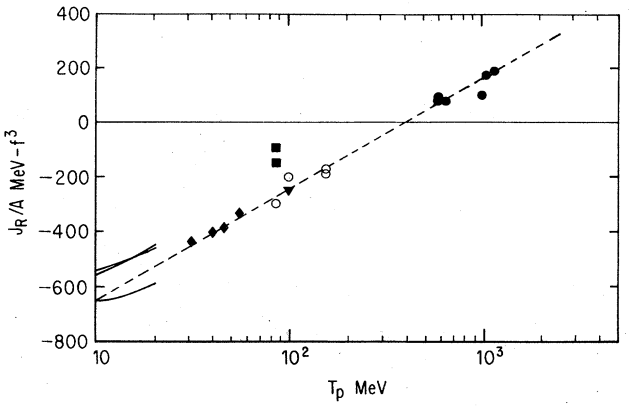

FIG. 29. The values of J_R/A for the real central optical potential from p-^{4}He elastic scattering versus T_p. The values above 500 MeV, solid circles, are from the work of Arnold *et al.*, (1976b). The values between 10 and 20 MeV, represented by solid curves, are from Satchler *et al.* (1968); the diamonds are from Thompson *et al.* (1970); the triangle is from Goldstein *et al.* (1969). The squares are from Votta (1974), and the open circles are from Comparat (1975). The dashed line is a fit to Eq. (35) for J_R/A obtained in the work of Arnold *et al.* (1976b).

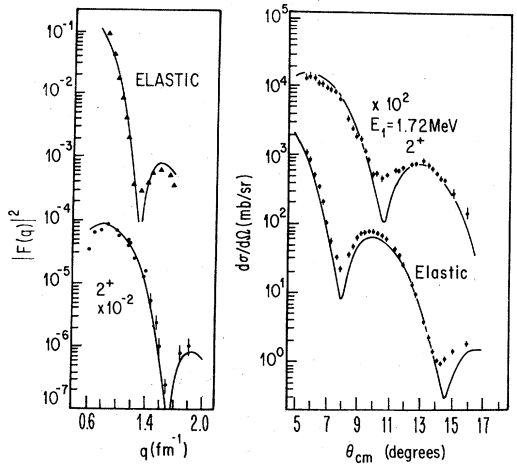

FIG. 30. (a) Form factors in elastic and inelastic scattering of electron on ^{28}Si (Alkhazov *et al.*, 1976a). (b) Differential cross sections at 1 GeV for elastic and inelastic proton scattering on ^{28}Si. The theoretical curves were calculated with Glauber model taking account of the excitation of collective degrees of freedom.

$$J_R/A = J_0/A + \beta \ln T_p \ . \tag{35}$$

This particular form depending on two fitted constants J_0 and β is in accord with an application (Passatore, 1967, 1968, 1975) of a dispersion relation derived by Feshbach (1958).

IV. ELASTIC AND INELASTIC SCATTERING, $A \geq 4$

The Glauber model provides a readily interpretable and qualitatively reliable way to calculate nuclear scattering and reaction processes with simple calculation methods in the intermediate-energy range. It has to be realized, though, that the model assumptions are rarely met rigorously in practical application. A recent example is the measurement and analysis using the Glauber model of elastic scattering and inelastic scattering on ^{28}Si, ^{32}S, and ^{34}S (Alkhazov *et al.*, 1976a). The object of the analysis was to show that the elastic scattering and inelastic excitation of the first excited states in ^{28}Si, ^{32}S, and ^{34}S could be fit consistently using the Glauber model. Spin–isospin-independent nucleon–nucleon amplitudes consistent with modern nucleon–nucleon analysis were employed. Unfortunately, the Coulomb aplitude was neglected. The excitation of collective degrees of freedom was described by the formalism of Starodubsky and Domchenkov (1972) and Starodubsky (1974). Form factors for ^{28}Si and ^{32}S were extracted from electron scattering data (Helm, 1956; Savitsky *et al.*, 1969; Horikawa, 1971). For ^{34}S, the mean nuclear density was extracted from the proton elastic and inelastic data, since the authors had no knowledge of the existence of electron scattering data. Correlations were neglected. Figure 30 shows the electron and proton elastic and inelastic data for ^{28}Si from this work. Satisfactorily consistent descriptions, on the whole, of both the form factors and cross sections for elastic and inelastic scattering are obtained when the same set of parameters is used for each nucleus.

Some discrepancies exist between theoretical curves and experimental values (for instance, elastic scattering of protons on ^{28}Si). Improved agreement could have been obtained by determining the parameters from the most consistent description of all experimental data, not of the form factors alone. The disagreement in the region of the diffraction minima is mainly due to neglect of proton-nucleus Coulomb effects as well as the Coulomb distortion of the electron wave, according to the authors.

Corrections to the Glauber model included in the high-energy expansion model (Wallace, 1975), or, in a different approach, by application of the KMT optical model (Kerman *et al.*, 1959; Feshbach, 1958; Feshbach, 1969; Feshbach and Hufner, 1970; Feshbach *et al.*, 1971; Lambert and Feshbach, 1973; Ullo and Feshbach, 1974; Boridy and Feshbach, 1974) to cite examples of frequency used approaches, must be examined in future analyses to assess the data more critically. In a recent analysis (Feshbach, 1977) using the KMT approach, comparison with elastic scattering of 1 GeV protons by ^{40}Ca, ^{48}Ni, and ^{208}Pb is considered. Excellent agreement is obtained using only the first term of the KMT optical potential. In addition it is found that variations in the strength of the Coulomb potential, the strength of the spin-orbit term, the ratio of the real to imaginary part of the zero-angle nucleon–nucleon scattering and pair correlations have identical effects. The authors conclude it is impossible, because of the absence of nucleon–nucleon data, to make any but qualitative statements regarding correlations and spin-orbit strengths from examination of the angular distributions (see Ericson, 1975). The polarizations are also calculated. At the present time, the experimental data, particularly the paucity of data on nucleon–nucleon scattering amplitudes, limit the application of these more quantitative methods. For this reason, we limit the discussion in Sec. IV to analyses based on the Glauber model (1959). It should be noted, however, that the paper of Boridy and Feshbach is quite relevant. Among other points report-

ed therein, the density-dependent Hartree-Fock densities are found to give better agreement than the Fermi model.

A. Measurements of the neutron mass distributions in calcium isotopes

Electron scattering experiments (Elton, 1966) show that the charge distributions for $A \geq 12$ can usually be described by Fermi functions with the density and diffuseness almost constant. In addition, the root-mean-square (rms) charge radius extracted from the data is found to be $r_{rms} = 1.02A^{1/3}$ fm.

A clear exception is found for the behavior of the charge distribution of the calcium isotopes (Frosch *et al.*, 1960). The rms charge radius of ^{48}Ca is 0.015 fm (0.5%) smaller than the radius of ^{40}Ca, whereas the $A^{1/3}$ rule predicts an 0.22 fm (6.3%) increase. If the matter radii of calcium isotopes follows the $A^{1/3}$ rule, then the rms radius of the neutron distribution of ^{48}Ca must exceed that of the proton distribution by 0.4 fm,

$$\Delta_{48} = (r_{\rm rms})_n - (r_{\rm rms})_p = 0.4 \text{ fm}. \tag{36}$$

Shell-model calculations (Elton and Swift, 1967; Batty and Greenlees, 1969) give values for Δ_{48} between 0.3 and 0.4 fm, but Hartree-Fock calculations (Vautherin and Brink, 1970; Lee and Cusson, 1971; Lombard, 1970) predict Δ_{48} is 0.1 – 0.2 fm.

Turning to experiment, optical-model analysis of the differential cross section data on the calcium isotopes for low-energy alpha particles (Fernandez and Blair, 1970), ^{16}O (Bertin and Tabor, 1971), and low-energy, polarised protons (Lombardi *et al.*, 1972) seem to support the $r_0 A^{1/3}$ dependence of the nuclear radii in these isotopes. Analysis of data on isobaric analog states (Nolen and Schiffer, 1969) implies a very small difference, $\Delta_{48} = 0.06$ fm. An optical-model analysis of 79 MeV alpha particle elastic scattering data from ^{40,48}Ca (Lerner *et al.*, 1975) also gives a small value, $\Delta_{48} = 0.05$ fm. The discrepancies may be more apparent than real since the theoretical analysis of low-energy elastic scattering data, sometimes, may be uncertain. On the other hand, proton elastic scattering in the GeV region can be handled theoretically with more confidence because the real part of the optical potential is nearly zero. Several optical-model analyses based on multiple-scattering theory have provided evidence that this is the case.

At 1.05 GeV, Alkhazov *et al.* (1976b) have investigated the even isotopes of calcium, ^{40}Ca, ^{42}Ca, ^{44}Ca, ^{48}Ca, and also ^{48}Ti, at Saclay. The charge distributions have been measured for all these nuclei (Frosch *et al.*, 1960). Angular distributions (protons) have been measured between 4° and 19° for all the targets with an angular resolution [(0.36° FWHM (full width at half maximum)], with a relative accuracy of 3% and with an absolute error of 10%. The absolute angle of scattering is measured with an uncertainty of 0.06°. A unique target-beam configuration is used. The target is small compared with the beam-spot size, and consequently the beam intensity is fairly constant over the target area (2 mm high by 6 mm wide). Under these circumstances, it can be shown that the counting rate depends only on the target mass and not on details of its shape or homogeneity. Another advantage is that the region of interaction, as determined by the target width, limits the horizontal angular acceptance. The contribution of this width to the angular uncertainty (0.32°) is 0.23°.

The Glauber model (see Sec. II) was used to calculate the elastic differential cross sections. Coulomb effects and center-of-mass correlations were accounted for. The spin-independent nucleon-nucleon amplitudes were parametrized in the usual way

$$f_{pj}(t) = \frac{ik_0\sigma_{pj}}{4\pi}(1 - i\alpha_{pj}) \exp(\beta_{pj}t/2); \quad j = p, n. \tag{27b}$$

The parameters were taken from computations of experimental data (Igo, 1975; Bystricky *et al.*, 1972) ($\sigma_{pp} = 4.75$ fm^2, $\sigma_{np} = 4.04$ fm^2, $\alpha_{pp} = -0.1$, $\alpha_{np} = -0.45$, $\beta_{pp} = 0.25$ fm^2, and $\beta_{np} = 0.17$ fm^2). Parabolic Fermi functions were used to characterize the charge distribution ρ_c and the neutron distribution ρ_n.

$$\rho_c(r) = C_c \frac{1 + W_c(r/R_c)^2}{1 + \exp[(r - R_c)/a_c]},$$
$$\rho_n(r) = C_n \frac{1 + W_n(r/R_n)^2}{1 + \exp[(r - R_n)/a_n]}, \tag{37}$$

where C_c and C_n are normalization constants. The charge distribution $\rho_c(r)$ obtained from electron scattering experiments is connected to the proton (point) distribution $\rho_p(r)$ by the following relation

$$\rho_c(\underline{r}) = \int_0^\infty \rho_{cp}(\underline{r}')\rho_p(\underline{r} - \underline{r}')\, d\underline{r}', \tag{38}$$

where the rms radius of the proton's charge distribution $\rho_{cp}(r)$ is 0.8 fm. The neutron distribution has been assumed to have the same shape. This leads to a straightforward relationship between the folded and point density radii:

$$\langle r_c^2 \rangle = \langle r_p^2 \rangle + 0.64 \text{ fm}^2,$$
$$\langle r_n^2 \rangle = \langle r_n^2 \rangle + 0.64 \text{ fm}^2. \tag{39}$$

Parameters for the neutron matter densities were obtained using a least-squares fitting routine. The absolute normalization was left as a free variable. The magnitude of the parameter W_n has a weak influence on the calculated cross section; it was therefore set equal to W_c. Data out to 16° were included. There was a systematic disagreement (the theory underestimated the experimental measurements) beyond 16°. The authors chose to ignore the lack of fit on the basis that the Glauber model should not apply at large angles. The normalization factor was found to be 0.95. This is within the stated uncertainty in the absolute normalization. The calculated cross sections and the data are displayed in Fig. 31. One set of curves corresponds to equal neutron and proton distribution. In this case, the fit gets progressively worse with increasing isotope number. Theoretical curves are also presented for the case where the neutron distribution is allowed to be optimized independently to obtain the best fit; then the fits are much improved. An independent assessment of the relative charge densities of ^{40}Ca and ^{48}Ca has been made

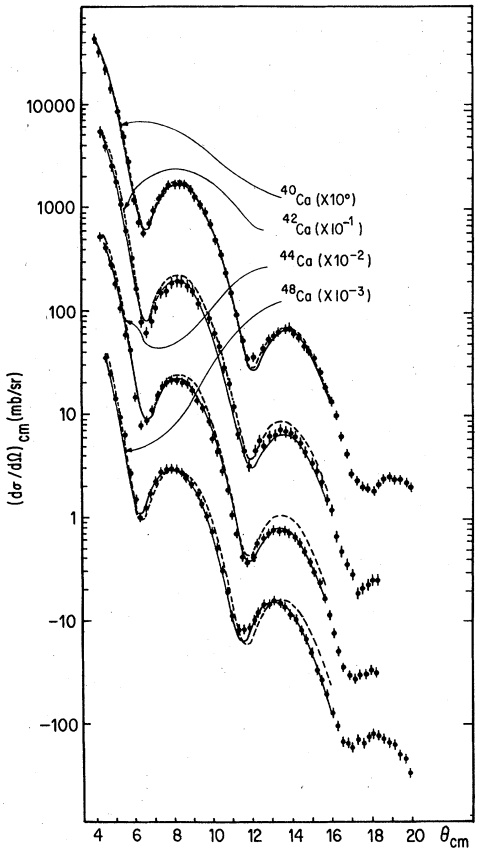

FIG. 31. Experimental angular distributions for 1.044 GeV proton elastic scattering on ^{40}Ca, ^{42}Ca, ^{44}Ca, ^{48}Ca, and ^{48}Ti (Alkhazov *et al.*, 1976b). The dashed curve refers to a calculation where the neutron distribution was taken to be identical to the previously known charge distribution. The solid curve represents a set of calculations where the neutron distribution parameters have been adjusted to give the best fit to the angular distributions.

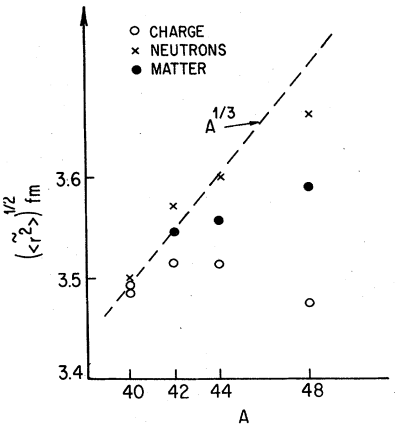

FIG. 32. The rms proton (open circles), neutron (crosses), and nuclear matter (closed circles) densities as a function of the mass number A (Alkhazov *et al.*, 1976b). Charge radii values are from Frosch *et al.* (1960). The dashed line corresponds to the $A^{1/3}$ rule. The quantity $\langle \tilde{r}^2 \rangle^{1/2}$ is the rms radius of the folded density distribution and is related to the rms radius of the point density distribution, $\langle r^2 \rangle^{1/2}$ by $\langle \tilde{r}^2 \rangle = \langle r^2 \rangle + 0.64$ fm^2.

by Bertozzi *et al.* (1972). There is good agreement with the parameters obtained in a previous experiment (Alkhazov *et al.*, 1972) in which ^{40}Ca and ^{48}Ca were studied.

The principal result concerns the quantity $\Delta n = \langle r^2 \rangle^{1/2}_{n,^{48}Ca} - \langle r^2 \rangle^{1/2}_{n,^{40}Ca}$; Δn is quite stable at the value 0.16 fm. For instance, analysis of electron scattering data at 205 MeV and 500 MeV yields different parameters for the charge form factor (Frosch, 1968). Use of these two sets makes small but noticeable differences in the rms radius for the same isotope. However, Δn is virtually unchanged. Further, there are uncertainties in the nucleon–nucleon interaction obtained from very recent experimental data (Bystricky *et al.*, 1972; Chaumeaux *et al.*, 1976; Hendrik and Lautraup, 1975). Again Δn is virtually unchanged. In contrast to the small variation of the radius of the charge densities, the neutron rms radii increase approximately proportional to $A^{1/3}$ (Fig. 32). The corresponding rms radius of the matter distribution exhibits some deviation from the $A^{1/3}$ dependence.

A recent measurement of the neutron radii of the calcium isotopes from pion total cross section has been reported (Jacobson *et al.*, 1977). This is a very promising method, because near 200 MeV the cross section is dominated by the isospin = 3/2 resonance. Thus the cross-section measurement with negative pions will primarily sample the diffuse edge of the neutron distribution; and, with positive pions, the protons. In this connection a particularly beautiful measurement of the π^+ differential elastic cross sections on ^{40}Ca and ^{48}Ca exists (Boschitz, 1977). The first two maxima for π^+ plus ^{40}Ca and ^{48}Ca occur at the same angles (52° and 82° in the laboratory system), while for π^-, the first and second maxima of the ^{40}Ca distributions are shifted to larger angles by 4° and 10°, respectively, as compared with the ^{48}Ca spectra.

It will be very instructive to interpret these new results quantitatively. Together with the electron and proton scattering results at intermediate energies, there is a promise of very qualitative answers to the question of the neutron behavior.

B. Model-independent analysis of calcium elastic scattering data

Brissaud and Brussel (1976a) have used a nearly model-independent analysis similar to the one by Lombard and Wilkin (Sec.II.D) to extract the mass distribution of ^{40}Ca. The scattering is described by the Glauber multiple-scattering theory in the optical limit. Nucleon-nucleon scattering amplitudes, the center-of-mass correction, and the charge distribution were obtained as described in Sec.II.D. The experimental data on ^{40}Ca discussed earlier in this section were used. Gaussian terms in the density distribution were fixed in width to 1.3 fm. This was justified on the basis that the Hartree-Fock wave function (Campi and Spring, 1974) has oscillations of this order. The positions of the Gaussians were chosen with regular spacing Δr_j in the range $\Delta r = 0.3 - 0.8$ fm or, alternatively, with random spacings adjusted between 0.3 and 0.7 fm in different calculations.

Figure 33 shows the envelope of different trial densities for different spacings. The curve labeled "T" is ob-

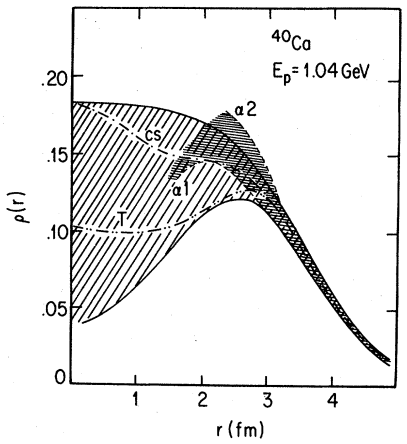

FIG. 33. Envelope of trial densities (Brissaud and Brussel, 1976a). The curves T and CS are obtained using a typical density distribution and a density distribution derived from a Hartree-Fock calculation, respectively. The region bounded by the curves marked α_1 and α_2 was obtained in the analysis of 166-MeV alpha particle data. The hatched region extending to $r=0$ is obtained in the analysis of 1.04-GeV proton-elastic scattering from ^{40}Ca.

tained with 12 Gaussians and an equivalent spacing $\Delta r_j = 0.4$ fm. A typical Hartree-Fock density (Fernandez and Blair, 1970) is also shown. One sees that the best defined part of the nuclear density distribution is near the surface, at $r \geq 3$ fm. The authors point out that the envelope near the surface of the nucleus is nearly the same as the one obtained in their analysis of 166-MeV α-particle elastic scattering data (Brissaud and Brussel, 1976b). In agreement with the conclusion reached by Lombard and Wilkin (1975) (Sec. II.D), the best-defined moments lie between 2 and 3. The rms radius is 3.49 ±0.03 fm. The uncertainty in the rms radius is about the same as obtained in the 166 MeV α-particle analysis and from a model-independent analysis of electron scattering data (Sick, 1974).

Brissaud and Brussel conclude, from their analysis of existing 1 GeV proton elastic scattering data on ^{40}Ca, that no new information about the mass distribution emerges not already available from the 166 MeV α-particle analysis. Obviously, analysis of a larger sampling of elastic scattering data will be necessary before a definitive conclusion can be reached concerning this matter.

C. Attempts to extract nuclear correlation structure information from (p,p) and (p,p′) scattering near 1 GeV

For $A \geq 12$, high-resolution elastic and inelastic scattering data have recently become available (Bertini *et al.*, 1973; Alkhazov *et al.*, 1972; Alkhazov *et al.*, 1973). A theoretical analysis of the elastic and inelastic data by Ahmad (1975) using the Glauber model is summarized here. Ahmad has tested the effects of long-range collective correlations, or short-range correlations, and of the coupling between the elastic and inelastic amplitudes. There have been closely parallel developments by Auger and Lombard (1973), Brissaud *et al.* (1974), Alexander and Rinat (1974), Starodubsky and Domchenkov (1972), Saudinos and Wilkin (1974), Viollier (1975), Starodubsky (1974), and Manaenkov (1975).

To keep the main ideas of the analysis of Ahmad uncluttered, the difference between the proton and neutron amplitides, the center-of-mass constraint, and the effects of the Coulomb force will be ignored. These effects are included explicitly in the quantitive comparisons made with the data at the end of this section.

Following the general development of the Glauber model in Sec. II, the nuclear phase-shift function must be specified. In this case, the target wave function is written as

$$\psi_i = \phi_0(\underline{\xi}_1, \cdots \underline{\xi}_A)\psi_i^{\text{coll}}, \quad i=0,4, \tag{40}$$

where ϕ_0 and ψ_i^{coll} describe, respectively, the intrinsic and collective states of the target nuclei (in this case ^{12}C, ^{58}Ni, ^{40,48}Ca, and ^{208}Pb). Thus the nuclear phase shift is

$$S_{f0}(\underline{b}) = \langle \psi_f^{\text{coll}} | e^{i\chi(\underline{b})} | \psi_0^{\text{coll}} \rangle, \tag{41}$$

where the phase-shift operator $\chi(\underline{b})$ is

$$\chi(\underline{b}) = -i \ln \left[\left\langle \phi_0 \middle| \prod_{j=1}^{A} \{1 - \Gamma(\underline{b} - \underline{s}_j)\} \middle| \phi_0 \right\rangle \right]. \tag{42}$$

Note that the long-range correlation due to collective effects has been separated out in going from Eq. (41) to Eq. (42). Using an expansion similar to Eq. (8), the operator $\chi(\underline{b})$ is expanded in a power series, $\chi(\underline{b}) = \hat{\chi}_0(\underline{b}) + \hat{\chi}_1(\underline{b}) + \cdots$. The result, up to second order, is:

$$\hat{\chi}_0(\underline{b}) = iA \int \Gamma(\underline{b} - \underline{s})\rho(\underline{\xi}) d\underline{\xi}, \tag{43a}$$

$$\hat{\chi}_1(\underline{b}) = -\frac{iA}{2} \int\int [(A-1)\rho_2(\xi_1, \xi_2) - A\rho(\underline{\xi}_1)\rho(\underline{\xi}_2)]\Gamma(\underline{b} - \underline{s}_1)\Gamma(\underline{b} - \underline{s}_2) d\underline{\xi}_1 d\underline{\xi}_2, \tag{43b}$$

where $\rho(\underline{\xi})$ and $p_2(\underline{\xi}, \underline{\xi}')$ are respectively the one- and two-body density operators which depend on the collective coordinates.

Here $\chi(\underline{b})$, defined through Eq. (42), should be distinguished from the similarly defined optical phase function Eq. (8). In the latter, the intrinsic-state wave function ϕ_0 in Eq. (42) is replaced by the ground-state wave function χ_0, and $\rho(\underline{\xi})$ and $\rho_2(\underline{\xi}, \underline{\xi}')$ are the one- and two-body ground-state densities. Although $\chi_{\text{opt}}(\underline{b})$ describes only the elastic scattering, it is still interesting to compare it with $\chi(\underline{b})$. Because of $\rho_2(\underline{\xi}, \underline{\xi}')$, $\hat{\chi}_1(\underline{b})$ describes the pair correlation present in the intrinsic state ϕ_i. To fix ideas, ϕ_i is considered built of single-particle states generated in a deformed well. Then $\rho_2(\underline{\xi}, \underline{\xi}')$ would be different from the product of two single-particle densities because of (1) center-of-mass corrections, (2) Pauli correlations, and (3) other dynamical short-range correlations. To order $1/A$, $\hat{\chi}_1(\underline{b})$ would be zero in the absence of correlations 1–3. It therefore follows that for small deformations, $\hat{\chi}_1(\underline{b})$ would not be very different in a nondeformed state. Summarizing, for collective nuclear states in nuclei, the long-range correlation responsible for collective behavior stands separated from

the rest of the correlations and is mainly described in the first term $\hat{\chi}_0(\underline{b})$ which only weakly depends on correlations 1–3. In contrast, the second term in Eq. (8) describes all correlations including those arising from the collective nature of the target.

It is convenient to express $\chi(\underline{b})$ in a momentum-transfer representation

$$\chi(\underline{b}) = \frac{A}{2\pi\hbar} \int d^2q e^{-i\underline{q}\cdot\underline{b}} f(\underline{q}) F(\underline{q}) , \tag{44}$$

where $f(\underline{q})$ is defined in Eq. (3c), and

$$F(\underline{q}) = \int e^{i\underline{q}\cdot\underline{r}} \rho(\underline{r}) d\underline{r} . \tag{45}$$

Within the framework of the collective model, the rotational and vibrational nuclei are described by the Tassie hydrodynamical model (Tassie, 1956). The density operator is then of the form

$$\rho(\underline{r}) = \rho_i(r) + \sum_{LM} \rho_L(r)[b_{LM} Y_{LM}(\Omega) + b^+_{LM} Y^*_{LM}(\Omega)] , \tag{46}$$

where $\rho_i(r)$ is the ground-state density, b^+_{LM} and b_{LM} are one-phonon creation and annihilation operators respectively, $Y_{LM}(\Omega)$ is a spherical harmonic, and

$$\rho_L(r) = N_L r^{L-1} d\rho_0/dr . \tag{47}$$

here N_L is the transition strength parameter. Effects of terms higher-order in the deformation have been discussed by Friar (1973) using a generalization of the Tassie model by Lane and Pandlebury (1969) and are found to be quite small. Substitution of Eqs. (44), (45), and (46) into (43) results in the following expression

$$\hat{\chi}_0(\underline{b}) = \hat{\chi}_{00}(\underline{b}) + \sum_{LM} g_{LM}(\underline{b})[A_{LM} + A^+_{LM}] , \tag{48}$$

where

$$\hat{\chi}_{00}(\underline{b}) = \frac{A}{k} \int_0^\infty q dq J_0(qb) f(q) F_0(q) q dq , \tag{49}$$

and

$$g_{LM}(\underline{b}) = (-1)^M \delta\{L + M - 2n\} \frac{A}{k} \left(\frac{2L+1}{4\pi}\right)^{1/2} \times \frac{[(L-M)!(L+M)!]}{[(L-M)!!(L+M!!)]} \int_0^\infty q dq f(q) F_L(q) J(qb) . \tag{50}$$

For convenience, the operators $A_{LM} = b_{LM}\exp(iM_\phi b)$, $A^+_{LM} = b^+_{LM}\exp(-iM_\phi b)$ have been defined in terms of the azimuthal angle ϕ_b of **b**. They satisfy the same commutation rules as b_{LM} and b^+_{LM}.

Neglecting higher-order terms,

$$S_{fo}(\underline{b}) = \langle \psi^{\rm coll}_f | \exp\left\{ i\left[\chi_{00} + \sum_{LM} g_{LM}(A_{LM} + A^+_{LM})\right]\right\} | \psi^{\rm coll}_0 \rangle . \tag{51}$$

Following the approach of Bassichis *et al.* (1971), $S_{fi}(\underline{b})$ may be evaluated. For elastic scattering,

$$S_{00}(\underline{b}) = \exp i\left\{\chi_{00} + \frac{i}{2}\sum_{LM} g^2_{LM}\right\} , \tag{52}$$

and the contribution to the scattering amplitude $F_{00}(q)$ is

$$F_{00}(q) = ik \int_0^\infty b db J_0(qb) \left[1 - \exp\left[i\left\{\chi_{00}(\underline{b}) + \frac{i}{2}\sum_{LM} g^2_{LM}(\underline{b})\right\}\right]\right] \tag{53}$$

With $i/2\sum_{LM} g^2_{LM}$ set equal to zero, the optical limit result is recovered. The additional phase change of the exponential term which results when $i/2\sum_{LM} g^2_{LM}$ is nonzero alters the elastic cross section. It describes the effect of coupling the elastic with the one-phonon inelastic channels in which the target nucleus makes an initial transition to an excited state and then decays back to the ground state. This term was included in the calculation of Starodubsky and Domchenkov (1972). Since the term is second order in $f(q)$, Ahmad also considers the correction to the phase $\psi_1(b)$ due to the short-range, two-body correlations which are of the same order. For describing inelastic scattering from the ground state $|00\rangle$ to a one-phonon state $\psi^{\rm coll}_f = b^+_{L_f M_f}|00\rangle$, $S_{fo}(\underline{b})$ is

$$S_{L_f M_f, 00}(\underline{b}) = \langle 00 | A_{L_f M_f} \exp\left\{ i\left[\chi_{00} - M_\phi b + \sum_{LM} g_{LM}(A_{LM} + A^+_{LM})\right]\right\} |00\rangle . \tag{54}$$

By the method of Bassichis *et al.*,

$$S_{L_f M_f, 00}(\underline{b}) = i g_{L_f M_f}(\underline{b}) \exp\left[i\left\{\chi_{00}(\underline{b}) + \frac{i}{2}\sum_{LM} g^2_{LM}(\underline{b}) - M_f \phi_b\right\}\right] . \tag{55}$$

The scattering amplitude

$$F_{L_f M_f, 00} = -\frac{ik}{2\pi} \int_0^\infty d^2b e^{i\underline{q}\cdot\underline{b}} S_{L_f M_f}(\underline{b}) \tag{56}$$

$$\left(\frac{d\sigma}{d\Omega}\right)_{L_f} = \sum_{M_f = -L_f}^{L_f} \left| k_0 \int_0^\infty b db J_{M_f}(qb) g_{L_f M_f}(\underline{b}) \times \exp\left[i\left\{\chi_{00}(\underline{b}) + \frac{i}{2}\sum_{LM} g^2_{LM}(\underline{b})\right\}\right]\right|^2 ,$$

$$L_f + M_f = \text{even} . \tag{57}$$

Equation (57) can be compared with the cross section expressions for inelastic scattering obtained by Alexander and Rinat (1974) and Saudinos and Wilkin (1974). These authors do not include the coupling term $i/2\sum_{LM} g^2_{LM}(\underline{b})$ in the nuclear phase function.

In the work of Saudinos and Wilkin (1974) and Alexander and Rinat (1974), the A-body transition density is taken as the product of single-particle densities in which $A-1$ nucleons remain in the ground state, i.e., the transition strength is assumed to be carried only by the remaining nucleon. Because of the collective character of the low-lying states, which are strongly excited in inelastic proton scattering, they may be more adequately described in the approach of Ahmad (1974), Friar (1973), and Starodubsky (1974). This point has already been made by Saudinos and Wilkin (1974).

To obtain an approximate expression for $\hat{\chi}_1(\underline{b})$, the two-

body density operator is parameterized, following Glauber's approach for a spherical nucleus, as:

$$\rho_2(\underline{r},\underline{r}') = [A/(A-1)]\rho(r)\rho(r')g(|\underline{r}-\underline{r}'|), \quad (58)$$

where $g(r)$ is a short-range correlation function assumed to be independent of the collective coordinates for small deformations. It has the behavior

$$g(r)\begin{cases}=0, & r=0\\ =1, & r=\pm\infty\end{cases}. \quad (59)$$

Making the zero-range approximation for the nucleon–nucleon profile function (which is a very good one at 1 GeV if the point matter densities are replaced by the measured charge densities), and assuming the correlation length l_c is much less than the nuclear radius

$$\hat{\chi}_1(b) \approx -i\left[\frac{2\pi A f(0)}{k_0}\right]^2 l_c \int_{-\infty}^{\infty} dz[\hat{\rho}(\underline{b},z)]^2, \quad (60)$$

where

$$l_c = -\int_0^{\infty}[g(r)-1]dr. \quad (61)$$

Substituting Eq. (46) into Eq. (60) shows that the contribution of the deformation term in Eq. (60) is of higher order than 2, and is therefore neglected. Thus the two-body correlation correction term to be added to the nuclear phase function in Eq. (53) (for elastic scattering) and Eq. (57) (for inelastic scattering) is

$$\hat{\chi}_{\rm corr}(\underline{b}) = -i\left[\frac{2\pi A f(0)}{k_0}\right]^2 l_c \int_{-\infty}^{\infty} dz\rho_0^2(\underline{b},z). \quad (62)$$

A similar expression would have been obtained for the correction to the elastic phase in Eq. (8). The two differ in the interpretation of the correlation length. In the latter case, l_c would include, additionally, the effects of long-range correlations.

Coulomb scattering is included in the Ahmad formulation following the approach of Glauber and Matthiae (1970) in which the distorted nuclear charge distribution is replaced by a spherically symmetric charge distribution. This adds terms to the phase functions for both elastic and inelastic scattering. The effects are, of course, expected to be much more visible in the elastic calculations and the experimental data support this contention. The difference in the density distribution of protons and neutrons, and the corresponding difference in the corresponding elementary amplitudes, has been included in the formulation. The transition densities for protons and neutrons have been assumed to be the same.

The results of scattering on ^{12}C, ^{58}Ni, and ^{208}Pb have been compared with experiment. The inputs needed in the calculation are the p-N scattering amplitudes and the ground-state transition nuclear densities. The proton densities were determined from charge densities measured in electron scattering. At 1 GeV, this can be done simply by dividing the form factor of the measured nuclear charge distribution by the proton charge distribution. For the parameters describing the elementary nucleon–nucleon amplitudes $f_{pj}(t)$

$$f_{pj}(q) = \frac{ik_0\sigma_{pj}}{4\pi}(1-i\alpha_{pj})\exp-\left[\frac{1}{2}\beta_{pj}t\right], \quad (j=p,n), \quad (27b)$$

Ahmad has used $\sigma_{pp}=47.5$mb, $\sigma_{pn}=40.4$mb, $\alpha_{pp}=-0.05$, and $\alpha_{pn}=-0.5$. The value of β_{pp} determined from low momentum-transfer pp data is 4.7 $(\mathrm{GeV}/c)^{-2}$. Ahmad has assumed that β_{pn} and β_{pp} are equal to 4.7 $(\mathrm{GeV}/c)^{-2}$. Values of β_{pp} and β_{pn} obtained from a nucleon–nucleon compilation (Igo, 1975) are 5.9 and 4.5 $(\mathrm{GeV}/c)^{-2}$, respectively. The latter is less certain because data for $t<0.7$ $(\mathrm{GeV}/c)^2$ were used; for pp scattering, the data were taken obtained from a smaller t range, $0.03<t<0.3$ $(\mathrm{GeV}/c)^{-2}$ (see Fig. 14). The value selected by Ahmad for α_{pp}, -0.5, is consistent with a new analysis by Bystricky *et al.* (1972) using small-angle data on the polarization and differential cross section.

TABLE II. The values of the parameters appearing in the inelastic charge form factors for the excitation of the 2^+ and 3^- states in ^{12}C. The corresponding $B(EL)$ (electric multipole transition rate) values are 37.1 fm^4 and 576.4 fm^6.

	B_L	C_L (fm^2)	β_L (fm^2)
$L=2$	0.24 fm^2	0.13	0.63
$L=3$	0.13 fm^3	0.0	0.77

For the analysis of the ^{12}C data, the ground-state proton density was obtained from the charge density of Sick and McCarthy (1970). To calculate inelastic scattering to a one-phonon level and to study the effect on the elastic cross section of coupling with inelastic channels, the transition density was calculated from the ground-state density according to Eq. (46). However, in the case of the collective excitations in ^{12}C, this procedure does not yield an acceptable fit to the inelastic electron scattering, particularly at large momentum transfer, and the transition form factor was modified phenomenologically to fit inelastic electron scattering data, an approach known as the modified Tassie model (Gul'karov, 1973). Alternatively, it is possible to use directly the experimental charge form factor, implicitly assuming that the modified Tassie model applies.

The parameterization of the inelastic charge form factors used is due to Saudinos and Wilkin (1974) and is given by $F_{in}^L(q) = B_L q^L(1-C_L q^2)\exp[-\beta_L q^2]$. The values of the parameters used in the results presented in Figs. 35 and 37 are given in Table II.

Figure 34 shows the elastic scattering data for ^{12}C.

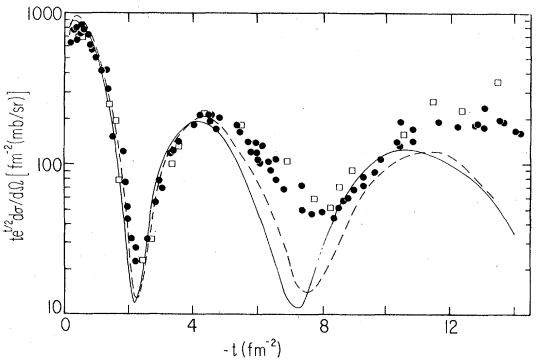

FIG. 34. Elastic p-^{12}C scattering at 1 GeV: squares, Alkhazov *et al.* (1972); circles, Bertini *et al.* (1973); solid line, Saudinos and Wilkin (1974); dashed line, Ahmad (1975). The differential cross section $d\sigma/d\Omega$ multiplied by $t^{5/2}$ has been plotted on the ordinate.

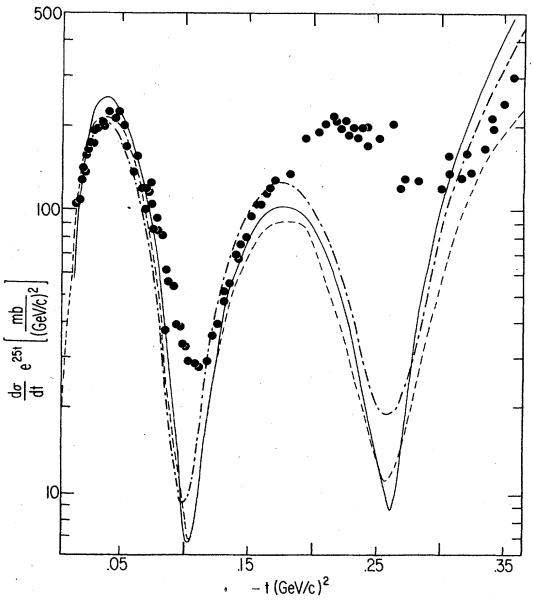

FIG. 35. The cross section for the excitation of the 2^+ (4.43 MeV) level in ^{12}C multiplied by e^{25t} (Bertini *et al.*, 1973). The solid curve is from Saudinos and Wilkin (1974). The dot-dashed curve and the dashed curve, from Ahmad (1975), are with and without coupling and correlation corrections, respectively.

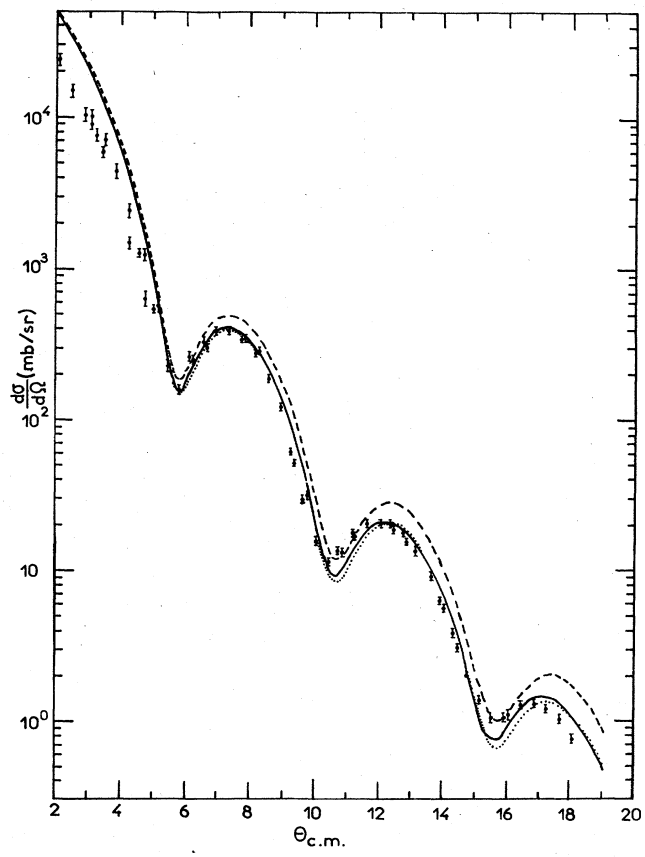

FIG. 36. Elastic differential cross section for ^{58}Ni at 1.05 GeV (Ahmad, 1975). The solid, dotted, and dashed curves are calculated without coupling or correlation, with coupling to the low-lying 2^+ and 3^- levels, and with coupling and correlation.

The predictions of Ahmad neglecting coupling and short-range correlations agree rather well with experiment in the region of the secondary maximum. Also plotted is a calculation by Saudinos and Wilkin (1974) using the optical limit of Glauber theory, where only the center-of-mass constraint is kept. Both calculations provide a reasonable fit to the data out of 4.5 fm^{-2}. Other calculations for this state by Starodubsky and Domchenkov (1972) and by Friar (1973) done earlier, employed less accurate ground-state charge distributions which fit only the low momentum transfer elastic electron data. These authors predict higher cross sections in the region of the second maximim in disagreement with the data. The 2^+ inelastic angular distribution without correlations and coupling (Fig. 34) agrees well up to $-t=0.16$ (GeV/c)^2, but beyond this the fit is poor. A calculation by Saudinos and Wilkin (1974), using the same inelastic form factor, is also shown. They obtain about 20% higher values at the first maximum. This is due to the use of a different elastic phase [see Eq. (57)]. The 2^+ inelastic angular distribution (Fig. 35) with coupling and correlations agree quite well in the vicinity of the first maximum and again near the second and third maxima, but the predicted diffraction structure is too deep. The long-range correlations (LRC), which are responsible for coupling between elastic and inelastic scattering and the short-range correlations (SRC), described by $g(r)$, almost cancel one another at the second maximum. If the problem had not been formulated to separate the LRC and SRC, the conclusion would be reached that the correlation effects were of negligible importance in this momentum-transfer region. In fact, the combined effects of SRC and LRC are responsible for the improvement in the fit near the second maximum.

Regrettably, when the calculations are made for another element, ^{58}Ni, the fits are worsened when the LRC coupling and SRC coupling length obtained from the ^{12}C analysis are used. In Fig. 36, the fit to the elastic data is seen to worsen when the effects of both the coupling and the correlation using the same correlation length as obtained for ^{12}C are used. The effect on the inelastic (2^+) cross section (not shown) is to degrade the fit near the first maximum and to improve the fit near the second maximum. However, the inelastic spectrum is based on a transition form factor obtained from electron data obtained over a limited momentum-transfer range ($t \leq 0.01$ GeV/c)^2. The effect of the LRC and SRC in heavier element data follows the same pattern as in ^{58}Ni. Therefore the evidence for LRC and SRC effects from the study of elastic and inelastic scattering, while encouraging for carbon, cannot be applied in a consistent fashion to heavier elements. Furthermore, a serious discrepancy exists in the prediction of the model for the 3^- state in ^{12}C where a secondary maximum predicted by the model is not seen experimentally (see Fig. 37). Further, the predicted cross section is much larger than expected. This result has been noted previously (Saudinos and Wilkin, 1974) in other calculations based on the Glauber model. For this reason, another measurement in the 1 GeV region of the 3^- excitation in ^{12}C is highly desirable. It also appears that the theoretical model will have to be improved to achieve quantitative agreement with the data for light and heavy targets.

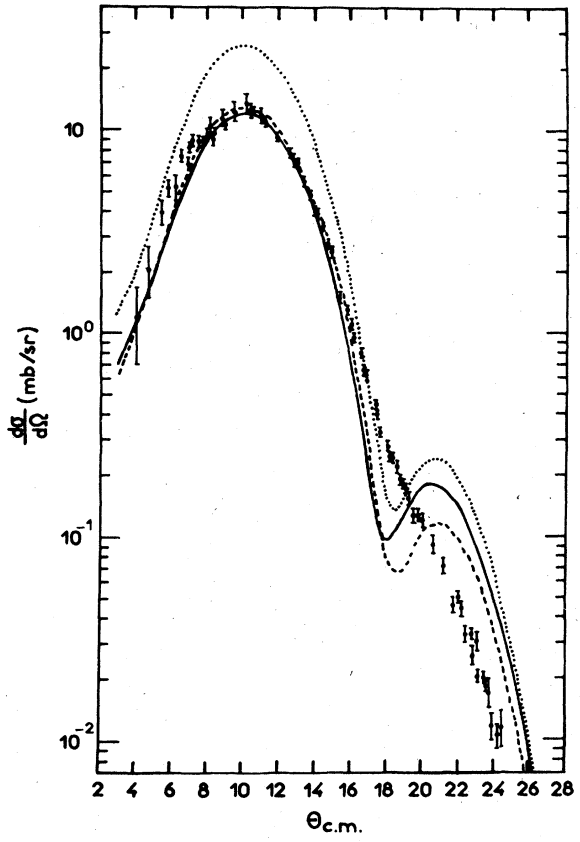

FIG. 37. Inelastic differential cross sections for 1.04 GeV protons on ^{12}C for populating the 3^- (9.62 MeV) level (Ahmad, 1975). The dotted, dashed, and solid curves are calculated without correlation, without correlation but normalized to the experimental value at the maximum, and normalized to the experimental value at the maximum including both coupling and correlation, respectively.

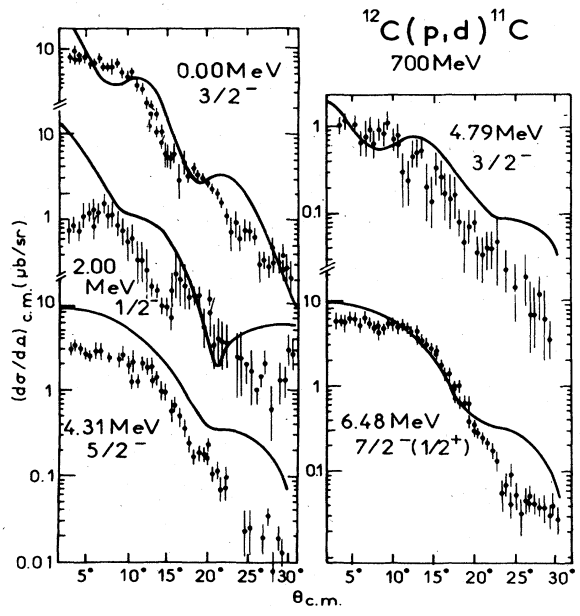

FIG. 38. Angular distributions for the lowest five states of ^{11}C excited by the ^{12}C $(p,d)^{11}C$ reaction at 700 MeV (Baker *et al.*, 1974b). The solid curves are DWBA fits.

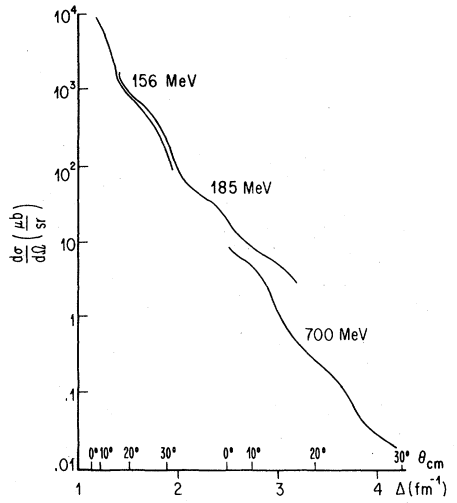

FIG. 39. The $^{12}C(p,d)^{11}C$(G.S.) experimental cross sections at three energies vs Δ.

V. NEUTRON PICKUP REACTION

In 1974 Baker *et al.* (1974b) measured the angular distributions for five states populated by $^{12}C(p,d)^{11}C$ reaction at $T = 700$ MeV. All earlier measurements were at bombarding energies less than 200 MeV. The energy resolution at 700 MeV was 350 keV. These data, measured between 2.5° and 25° (lab), are shown in Fig. 38. There is a normalization uncertainty of ±7% in the absolute scale of the cross section. Kislinger (1977) has pointed out that the $^{12}C(p,d)^{11}C(g.s.)$ angular distribution obtained by Baker *et al.* (1974b) at 700 MeV, by Kallne and Hagberg (1971) at 85 MeV, and by Bachelier *et al.* (1969) at 156 MeV depend, at least approximately, only on the variable $\Delta = |\underline{d} - 11/12\underline{p}|$ (see Fig. 39). Here $\underline{p}$ and $\underline{d}$ are the momenta of the incoming proton and outgoing deuteron. In the specific case of large-angle $p-d$ scattering, the variable Δ is discussed in Sec.VI.B. Briefly for now, it is the component of the picked-up neutron's momentum distribution in ^{12}C which is sampled at a particular scattering and ϕ_{cm} (see Fig. 39) in the (p,d) reaction according to the Chew–Goldberger model (1964).

There are several interesting features which distinguish the pickup reaction at 700 MeV from the same reaction below 200 MeV. A striking result is the relative importance of the cross section for high-spin states. For the $5/2^-$ level at 4.31 MeV and the $7/2^-$ level at 6.48 MeV, the relative yields are much smaller at 156 MeV (Bachelier *et al.*, 1969). This feature is also apparent in the comparison of 700 MeV and 45 MeV data (Baker *et al.*, 1974b) in Fig. 40. A second striking feature is the magnitude of the cross sections. Between 2° and 26° in the laboratory system, the cross sections range over three orders of magnitude, from 9 μb/sr down to 8 nb/sr. The cross section at small angles is three orders of magnitude smaller than at low energies, where it is typically 10 mb/sr. A third feature, less well established, is the dependence of the pickup cross section on the mass of the target at 700 MeV. A preliminary inves-

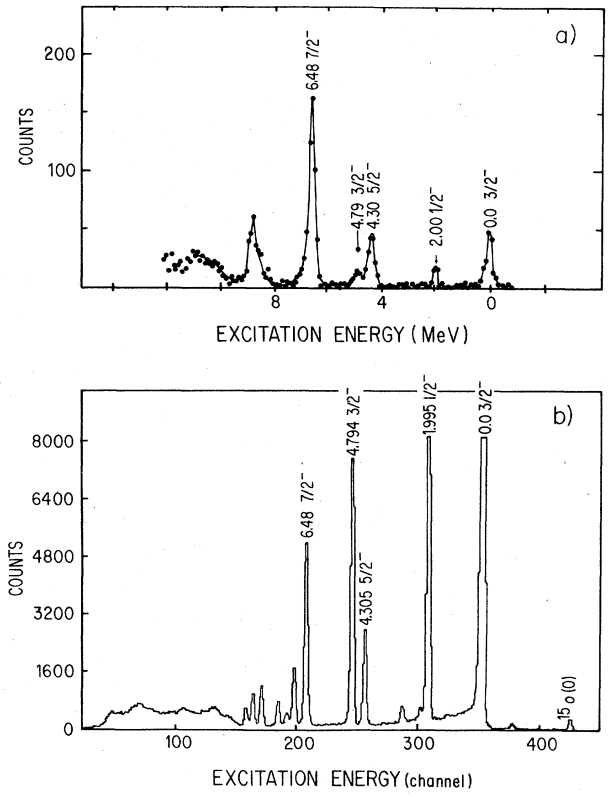

FIG. 40. Experimental spectra for the $^{12}C(p,d)^{11}C$ reaction (Baker *et al.*, 1974b): (a) at $T_p = 700$ MeV, $\theta_{lab} = 12.5°$; (b) at $T_p = 45$ MeV, $\theta_{lab} = 22.5°$.

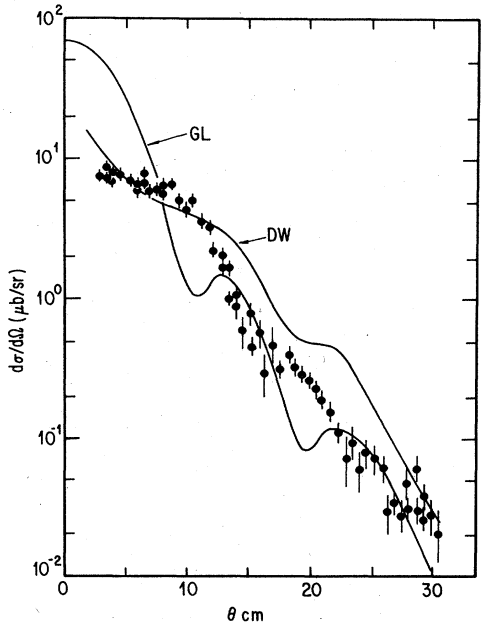

FIG. 41. The $^{12}C(p,d)^{11}C$(G.S.) reaction at 700 MeV (Baker *et al.*, 1974b). The curve marked DW is a finite-range DWBA calculation by Rost and Shepard (1975); the curve marked GL is a Glauber-model calculation by Tekou (1976).

tigation of the (p,d) reaction on calcium isotopes suggests that the cross section is considerably reduced from the results obtained with carbon (Beurtey, 1975).

To analyze the data, Baker *et al.* employed the distorted-wave Born approximation (DWBA) code (Kunz, 1971) and included first- and second-order excitations. All feedback effects were ignored, and all processes leading to excitation of the inelastic states in ^{11}C were ignored. The zero-range approximation was employed, and the D-state contribution was unfortunately neglected. The transfer form factor at this level of approximation is

$$\langle p^{12}C_I | V | d^{11}C_J \rangle_j = D n_j^{1/2} \gamma_{Ij}^J \theta_j^*(\underline{r}_n) \delta(\underline{r}_{np}) . \tag{63}$$

Here θ_j is the wave function of the transferred neutron; n_j the number of such neutrons in the ^{12}C state considered; and γ_{Ij}^J a structure factor (Clegg, 1962). The constant D incorporates all the information about the deuteron wave function. The value of D ($\approx$60 MeV-fm$^{3/2}$) required at 700 MeV to fit the data differs by a factor of 2 from the value obtained at low energies. Since the constant of D at 120 MeV – fm$^{3/2}$ at lower energies is well established, it is clear that some features of the calculations must be examined more closely. Nevertheless, several interesting conclusions result from the analysis. Figure 38 shows the results obtained. The three orders-of-magnitude decrease in the cross section is reproduced. A serious discrepancy in the shapes of the cross section is revealed, particularly at forward angles, in the case of the $3/2^-$ ground state and $1/2^-$ excitation. An important feature of the calculation is that the two-step amplitude was approximately equal to the one-step amplitude for excitations where the one-step and two-step processes were both allowed. At 45 MeV, the authors report that the one-step process is an order of magnitude larger than the two-step in the same cases.

A finite-range DWBA calculation (Austern *et al.*, 1964; DeVries, 1973) for the excitation of the $3/2^-$ ground state of ^{11}C has been reported recently by Rost and Shepard (1975). An improved fit at small angles results (see Fig. 41). Entering into the finite-range calculation is the quantity $V_{np}\phi_d$, where V_{np} is the operator representing the proton interaction, and ϕ_d is the deuteron wave function

$$[V_{np}\phi_d]_M = \tilde{D}_0(r)[Y^0(\hat{r})\chi_1^1]_M^1 + \tilde{D}_2(r)[Y^2(\hat{r})\chi_1^1]_M^1 . \tag{64}$$

Using a Reid soft-core potential which contains central (c), tensor (T), and spin-orbit (LS) terms

$$V_{np} = V_c(r) + V_T(r)S_{pn} + V_{LS}(r)\mathbf{L}\cdot\mathbf{S} \tag{65}$$

gives

$$\tilde{D}_0(r) = V_c u(r) + \sqrt{8}\, V_T(r) S_{pn} w(r) + V_{LS}(r)\mathbf{L}\cdot\mathbf{S} ,$$
$$\tilde{D}_2(r) = (V_c - 2V_T - 3V_{LS})w(r) + \sqrt{8}\, V_T u(r) . \tag{66}$$

Here $u(r)$ and $w(r)$ are S and D radial functions of the deuteron, respectively. In Fig. 42 a plot of $D_L(\Delta)$ versus component Δ is presented where

$$D_L(\Delta) = 4\pi \int_0^\infty r^2 dr j_L(\Delta r)\tilde{D}_L(r) . \tag{67}$$

In the plane-wave Born Approximation (PWBA), the cross section is proportional to $\sum_L |D_L(\Delta)|^2$. The momentum components, which are important in the PWBA calculation at 700 MeV on ^{12}C, range from 2.3 to 3.0

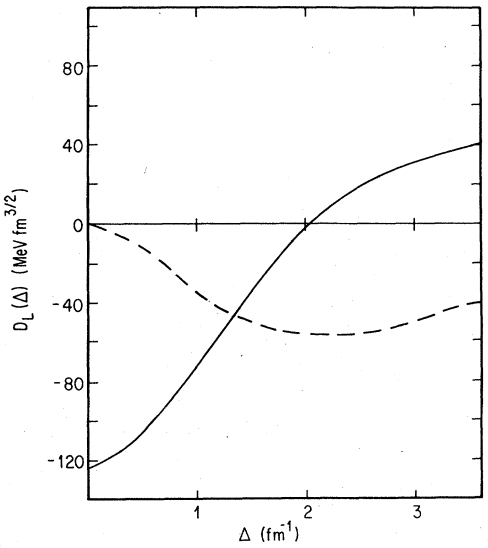

FIG. 42. The momentum components $D_L(\Delta)$ of the deuteron wave function used in a $^{12}C(p,d)^{11}C$(G.S.) calculation (Rost and Shepard, 1975). The solid curve is the S wave; the dashed curve is the D wave.

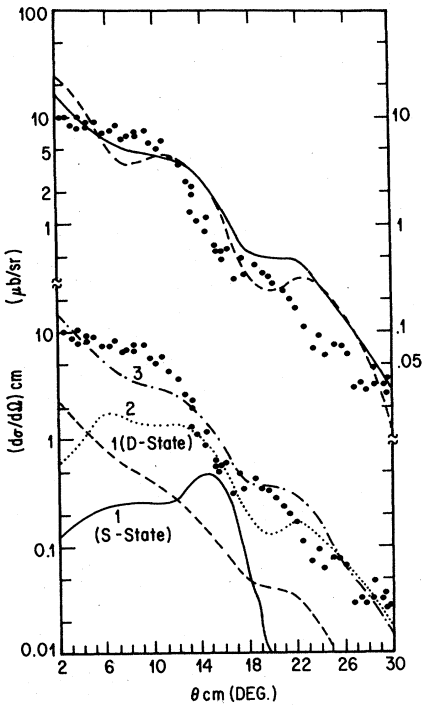

FIG. 43. The $^{12}C(p,d)^{11}C$(G.S.) reaction at 700 MeV (Rost and Shepard, 1975). Lower curves show S-state $l=1$ and D-state $l=1,2,3$ contributions to the finite-range cross section. The upper solid curve is the sum of the $l=2,3$ contributions. For comparison the renormalized zero-range DWBA results are given by the upper dashed curve.

fm^{-1}. Figure 39 shows that the D-wave amplitude predominates between 2.3 to 3.0 fm^{-1}. Note that in the calculation of Baker *et al.* (1974b), the D wave was ignored and the cross section calculated (zero-range approximation) was proportional to $|D_0^0|^2$, which is a factor of four larger than $\sum_L |D_L(\Delta)|^2$ in the range $\Delta = 2.3 - 3$ fm^{-1}. This accounts for the anomalous value of D (see above) which was extracted in the analysis of Baker *et al.* (1974b).

The momentum component, Δ, is related to the momenta k_{p_o} and k_{d_f} of the incident proton and outgoing deuteron by the relation

$$\underline{\Delta} = \left[\underline{k}_{p_o} - \frac{\underline{k}_{df}}{2}\right]. \tag{68}$$

In PWBA, Δ is the momentum of the picked-up neutron in the rest frame of the target when the relative momentum of the proton and neutron in the deuteron is zero after the collision.

In both zero- and finite-range DWBA calculations (Baker, 1974b; Rost and Shepard, 1975), the neutron radial wave function is generated from the potential parameters of Elton and Swift (1967) which are determined from electron scattering data and bound-state energies. Baker *et al.* (1974a) had successfully calculated optical potentials to describe 1 GeV proton scattering, using the KMT approach (Kerman *et al.*, 1959). Measured nucleon–nucleon scattering phase shifts and an electron scattering density distribution were used as input. Finally the data were refitted to a Woods–Saxon shape. Only a rough estimate of the deuteron optical potential could be made because of the paucity of deuteron elastic scattering data. These authors chose to make a rough estimate, in the spirit of the adiabatic model of Johnson and Soper (1970), by summing neutron and proton optical potentials at half the deuteron's kinetic energy. This is a weak point in the calculations since the criterion of applicability of the Johnson–Soper model is not met for high-energy transfer reaction (Baker *et al.*, 1974b). Further, an extrapolation is necessary since the energy dependence of the proton and neutron optical parameters has not been measured very close to half-energy (300 MeV).

Since the fits are quite sensitive to the optical potentials, it is important to measure elastic deuteron scattering at 700 MeV. The only existing data on deuteron elastic scattering ($T_d = 650$ MeV) on ^{12}C (Dutton *et al.*, 1965) cover a limited angular range ($4° \leq \theta_{lab} \leq 12°$) and are of poor statistical accuracy. An analysis of these data using the Glauber model has recently been made by Chadha and Varma (1976).

In the calculation of Rost and Shepard, the ^{11}C ground-state wave function is described as a $p_{3/2}$ hole coupled to the ground state of ^{12}C with a spectroscopic factor of 3 (Clegg, 1962; Cohen and Kurath, 1967). The results of the finite-range DWBA calculation for each l transfer with parameters described above are shown in Fig. 43. For the D state $l=1$, 2, and 3 transfers are allowed. The S and D $l=1$ amplitudes were ignored in generating the upper curve in Fig. 43, which is the incoherent sum of the $l=2$ and $l=3$ contributions. The authors point out that the $l=3$, D-wave contribution dominates.

The DWBA calculations described above treat the deuteron, which results in the pickup reaction, as an entity. A more general treatment is desirable. The proton and the neutron, the latter released by an interaction from a bound orbit, may propagate through nuclear material

in a continuum state, subsequently falling into the deuteron ground state at the end of a multiple-scattering sequence. An analysis in which this effect has been studied has been made by Tekou (1976) using the Glauber model. He has analyzed the data discussed above for the $3/2^-$ (G.S.) and the $5/2^-$ (4.37 MeV) states in ^{12}C. Instead of obtaining the phase of the distorted proton (deuteron) wave function at the point $\underline{r}$ where the transfer takes place from an optical potential, the phase function appearing in the Glauber approximation is set equal to the sum of the elementary distortion phases introduced by the collisions that the proton suffers before a neutron is released from a bound state and in the collisions suffered by the proton and the released neutron before they finally scatter into the ground-state configuration of the deuteron.

It is interesting to compare the results of the DWBA calculation of Rost and Shepard and the Glauber-model calculation of Tekou for the ground state of ^{11}C. These are shown together with the data in Fig. 41. The DWBA result is seen to be in better agreement at small angles where the approximations involved in the Glauber model calculations should be the most valid. Both calculations use the Reid soft-core potential. Tekou uses a harmonic-oscillator wave function for the picked-up neutron. As mentioned above, Rost and Shepard use a neutron radial wave function generated from the potential parameter of Elton and Swift (1967), which are determined from electron scattering data and bound-state energies. Tekou has also used a Woods-Saxon potential well which reproduces the binding energy of the picked-up neutron and finds minor differences at small angles. In the calculation of Rost and Shepard, two-step processes are ignored. In the calculations of Tekou, two-step processes are accounted for. However, both calculations must be considered only as estimates because of the uncertainty associated with the deuteron optical potential. As mentioned before, the calculation could be improved by using the deuteron elastic scattering data of Dutton *et al.* (1965). Elastic deuteron data of better quality is highly desirable. No investigation of the effect on the (p,d) cross section at forward angles associated with the uncertainty in the knowledge of the deuteron wave was reported by either author.

Schaeffer (1974) has investigated the influence of N^* (nucleon isobar) components in ^{12}C on the pickup reaction. Schaeffer estimated that the probability of ^{12}C being in an N^* plus ^{11}C configuration ϕ_{N^*} is typically 10^{-4} for each of several possible configurations. For large momentum transfers the N^* configurations may dominate. This is because an N^* with high spin may be coupled with an orbital angular momentum larger than $l=1$ in a component of the ground-state configuration; and because higher angular momentum components will tend to have a larger fraction of high-momentum components. Since ϕ_{N^*} is the product of three bound-state functions, its momentum dependence is approximately

$$|\phi_{N^*}(Q)|^2 \cong (c/A^2)\exp[-1/2(Q^2/k_F^2)] \tag{69}$$

with C of the order of 10^{-2}; A, the atomic weight; and k_F, the Fermi momentum. The nucleon momentum distribution will be

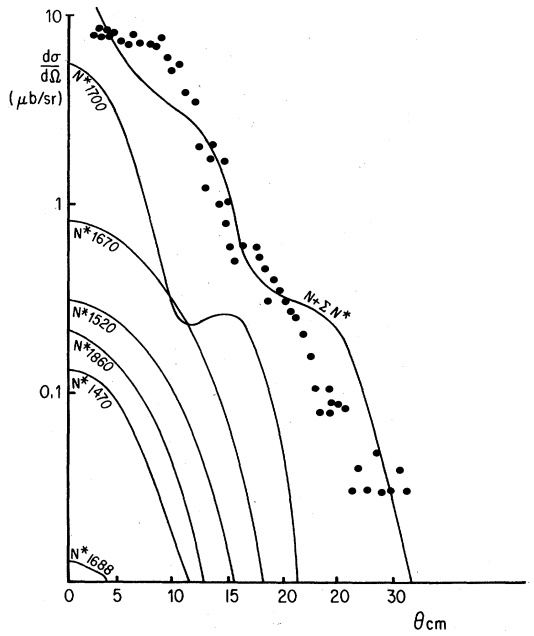

FIG. 44. Comparison of nucleon transfer and N^* transfer cross sections for the $^{12}C(p,d)^{11}C$(G.S.) reaction at 700 MeV with the data of Baker *et al.* (1974b). The N^* components are labeled. The curve labeled $N+\Sigma N^*$ is the sum of the N^* and nucleon components.

$$|\phi_N(Q)|^2 \cong \exp[-3/2(Q^2/k_F^2)]\,. \tag{70}$$

The N^* components will become important in the pickup reaction when momentum of the picked-up particle is of the order

$$|\underline{Q}| = k_F[\ln(A^2/C)]^{1/2}. \tag{71}$$

At 700 MeV, the N^* contributions begin to show up for the transition to the ^{11}C ground state. They are compared with the nucleon transfer contributions in Fig. 44 and are non-negligible compared to them. The situation would be more favorable at a higher bombarding energy. At 3 GeV, for instance, the baryon resonance contribution will be comparable to the nucleon contributions. It is seen that N^* contributions enhance the cross section preferentially near 0°. Kisslinger (1977) has written a comprehensive review of experimental tests of isobar components in nuclei.

Finally, it is interesting to understand the reduced magnitude of the (p,d) cross section on ^{40}Ca (Beurtey, 1975). The transition amplitude (Schaeffer, 1974) is

$$T_{pd} = \langle \chi_d^{(-)}\psi_D\psi_{A-1}|U|\psi_p^{(+)}\psi_A\rangle \approx (\Delta^2+\epsilon^2)F_D(\Delta)\tilde{F}_N(Q)\,, \tag{72}$$

with $\underline{Q} = \underline{d} - [(A-1)/A]\underline{p}$, and ϵ is the laboratory energy per nucleon. Here U is the interaction between the two baryons in the deuteron; $\chi_d^{(-)}$ and $\chi_p^{(+)}$, outgoing and incoming deuteron and proton waves with momenta $\underline{d}$ and $\underline{p}$, respectively; and ψ_{A-1}, and ψ_A, and ψ_D, wave functions of the residual, the initial, and the deuteron states, respectively. The deuteron vertex $F_D(\underline{\Delta})$ is the reasonably well known form factor of the deuteron. Thus for a transparent nucleus, one would measure the form factor $\tilde{F}_N(Q)$ of the picked-up baryon. However, nuclear ab-

sorption is known to be large and one has access only to the tail of the wave function in coordinate space. In this case there may be a large mismatch between the transferred linear momentum Q and angular momentum transfer l_{tr} in the vertex function. As a consequence, the angular distribution changes drastically; in fact, it tends to become structureless. In addition, there is no longer a clear correspondence between the scattering angle and the momentum transfer $\underline{Q}$. Nevertheless, the cross sections increase considerably when the magnitude of l_{tr} approaches $QR/\hbar$ (R is the strong absorption radius). At 700 MeV, Q is ~0.42 GeV/c at forward angles. For ^{12}C, R is 3.4 fm and $QR = 1.44$ GeV/c fm or $l_{tr} \approx 7.5$. There is a mismatch of ~6.5 units for a $p_{3/2}$ transition. In the ^{40}Ca$(p,d)^{39}$Ca, most levels near the ground state are $l = 2, 0$. For ^{40}Ca, l_{tr} turns out to be 11, and the mismatch is even larger. In the case of ^{208}Pb, l_{tr} is 19.

A measurement of the differential cross section of the ^{4}He$(p,d)^3$He pickup reaction has been measured at 770 MeV (Bauer *et al.*, 1977). As discussed at the beginning of this section, the plane-wave Born approximation for the pickup of an S-wave neutron in ^{4}He is proportional to $\sum_L |D_L(\underline{\Delta})|^2 \psi_0^2(\mathbf{P})$, where ψ_0 describes the state of the transferred neutron in ^{4}He at a momentum $\mathbf{P}$ defined by kinematics. Bauer *et al.* point out that $\sum_L |D_L(\underline{\Delta})|^2$ is almost constant between 2 and 3.5 fm^{-1} which the reaction is sensitive to in the angular range studied (see Fig. 45), and it is possible to use the zero-range DWBA-code DWUCK (a distorted-wave program written by P. D. Kunz at the University of Colorado) with $D^2 = D_0^2 + D_2^2 = 0.36 \times 10^4$ MeV^2 fm^3. The neutron form factor was evaluated as the overlap of the internal wave functions of ^{3}He and ^{4}He and has the following form

$$\phi(\underline{r}, \ldots, \underline{r}_A) = N \prod_{i=1}^{A} \exp[-r_i^2/2R^2](1 - B \exp[-r_i^2/R^2\gamma^2]) \prod_{j<i} (1 - C \exp[-r_{ij}^2/a^2]) . \quad (73)$$

The parameters of the ^{3}He and ^{4}He wave functions were adjusted to fit the electron scattering data for three cases: (1) single Gaussian with correlations ($B = 0$); (2) double Gaussian without correlations ($C = 0$); and (3) B and $C \neq 0$. Table III lists the parameters of the wave functions for the three cases. The optical parameters were chosen using the method of Baker *et al.* (1974b) described in this section. The results are presented in Fig. 45. Case III was calculated with and without a standard low-energy LS term. Including the LS term has the effect of filling in of the dip in the angular distribution. The closest approximation to a fit was obtained using Case I parameters in Table 3. As in the ^{12}C(p,d) reaction, the DWBA fails to fit the data at small angles; in this case, both in shape and magnitude. The authors also included the transfer of an N^*[1440 MeV($J^\pi = 1/2^+$), 1525 MeV($3/2^-$), 1550 MeV($1/2^-$), 1670 MeV($5/2^-$), 1688 MeV($5/2^+$), and 1700 MeV($1/2^-$)]. These contributions are found to be small and cannot affect the cross section significantly.

Summarizing, the neutron pickup reaction at intermediate energies presents a challenge to both multiple-scattering and DWBA formulations of the theory of neutron pickup. There are problems with both the shape and magnitude of the observed cross section on ^{12}C and ^{4}He. In the near future, data on other light nuclei including closed-shell nuclei besides helium will become available at a number of energies from Saclay, TRIUMF (Tri-University Meson Facility), Indiana, and Los Alamos. It is expected that there will be a corresponding theoretical effort to resolve the current discrepancies between theory and experiment.

VI. PARTICLE PRODUCTION AND ELASTIC SCATTERING NEAR 180°

Particle production near 180°, when the momentum of the backward particle is comparable to the incident momentum, and large-angle elastic scattering will be reviewed in this section. An example of the latter is the elastic scattering of protons from deuterium at bombarding energies above 100 MeV (van Oers, 1974b). Recently Berger *et al.* (1976) have completed a measurement of the energy variation of backward p-^{4}He elastic scattering between 300 MeV and 840 MeV. The inclusive cross sections for production of $z = 1$ particles at 800 MeV have been measured at 180° (Frankel *et al.*, 1976).

Elastic scattering and particle production near 180° are potentially of great interest because the cross sections may depend sensitively on the high momentum components of the nuclear wave function. Gurvitz *et al.* (1975a, b) and Chen (1974) have suggested that large-angle elastic scattering proceeds through a multiple-scattering mechanism in which only one nucleon-nucleon

TABLE III. Parameters of the wave functions defined by Eq. (73) and used in the calculations I, II, III in Fig. 45.

	^{4}He					^{3}He				
	R (fm)	C	a (fm)	D	γ	R (fm)	C	a (fm)	D	γ
I	1.156	1	0.842	0		1.402	1	0.697	0	0.189
II	1.295	0		1.729	0.263	1.454	0		1.793	0.220
III	1.280	1	0.349	1	0.307	1.449	1	0.200	1	

collision entails a large momentum transfer. Amado and Woloshyn (1976) have fitted the 180° inclusive proton production data of Frankel *et al.* (1976) by a mechanism involving a low-Q nucleon-nucleon collision with a nucleon with a large backward momentum in the nucleus.

A. Inclusive production of $z = 1$ particles

Inclusive production has been measured at 600 and 800 MeV on a series of nuclear targets by Frankel *et al.* (1976). At 600 MeV, Be, C, Cu, and Ta targets were investigated; and at 800 MeV, the targets were Ag, Ta, and Pt. The experimental apparatus used at LAMPF (The Clinton P. Anderson Meson Physics Facility) is shown in Fig. 46. The beam, passing through the bending magnet, impinges on a target before the shielding wall. Secondary particles produced at 180° passed back through the magnet and into a scintillation counter telescope composed of two scintillator triplets separated by 1.8 m. The magnet acted as an analyzing spectrometer with a momentum resolution of ~5% and an acceptance of ~0.04 *msr*. The $z = 1$ particles were identified by energy loss in the plastic scintillators and by time of flight.

Figure 47 shows the differential cross section $d\sigma/d^3p$ versus $p^2/2m_p$ for the production of protons. It is of interest that the data can be represented by a straight line in Fig. 46 which is of the functional form

$$d\sigma/d^3p = B_p \exp(-\eta_p p^2/2m_p) . \tag{74}$$

The production of deuterons and tritons can also be fit with straight lines on the same kind of plot. All data are characterized by small differences in the η parameter for different values of A for the same reaction product (proton, deuteron, or triton).

Another interesting feature is the large numbers of deuterons and tritons of the same momentum (see Fig. 48) as the protons. At the highest value of $p^2/2m_p \simeq 0.5$ GeV, where $p \simeq 1$ GeV/c, the numbers of tritons and of deuterons each exceed protons by a factor of 200. This feature can be understood qualitatively in terms of a pickup mechanism. In a pickup mechanism, the momentum/nucleon is the important quantity. When the magnitudes of the cross sections for deuterons and tritons with the same momentum/nucleon (p) are compared with the production cross section for protons of momentum p, the proton production cross section is ~10^3 times larger than the deuteron production and ~10^6 times larger than the triton production cross section.

Amado and Woloshyn (1976) have made an analysis of the backward production of protons using a simple direct process, a single scattering. The mechanism they have calculated is illustrated in Fig. 49. The struck nucleon must be moving backward with high virtual mo-

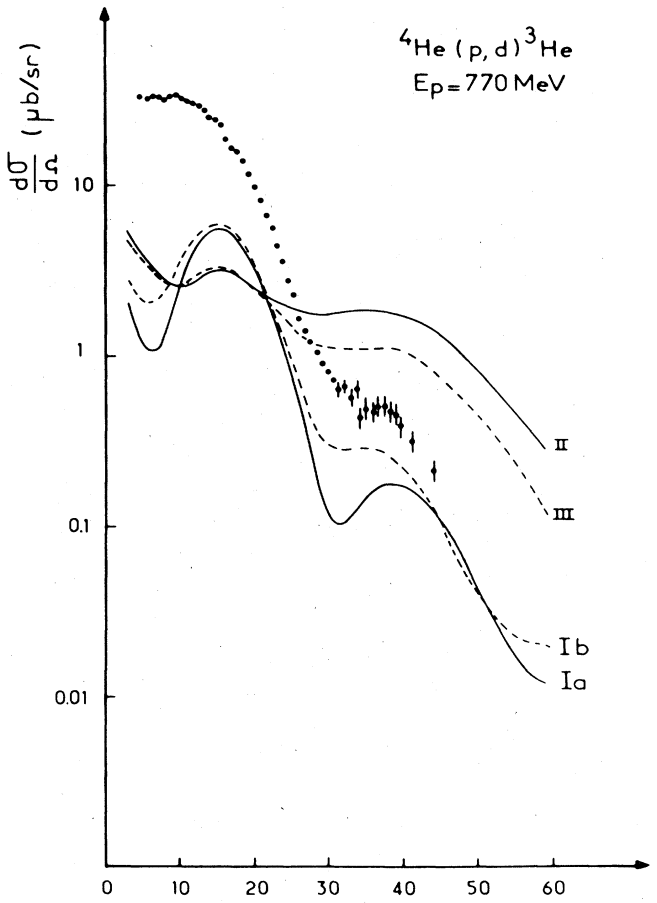

FIG. 45. The ^{4}He$(p,d)^3$He differential cross section. Gaussian with correlations, curve Ia (without LS contribution); curve Ib (with LS contribution); double Gaussian without correlations, curve II; double Gaussian with correlations, curve III.

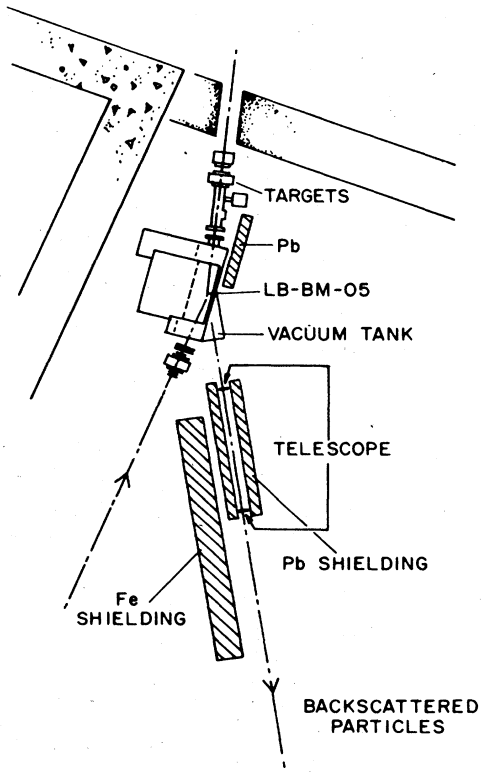

FIG. 46. The experimental layout for 180° production of protons, deuterons, and tritons (Frankel *et al.*, 1976).

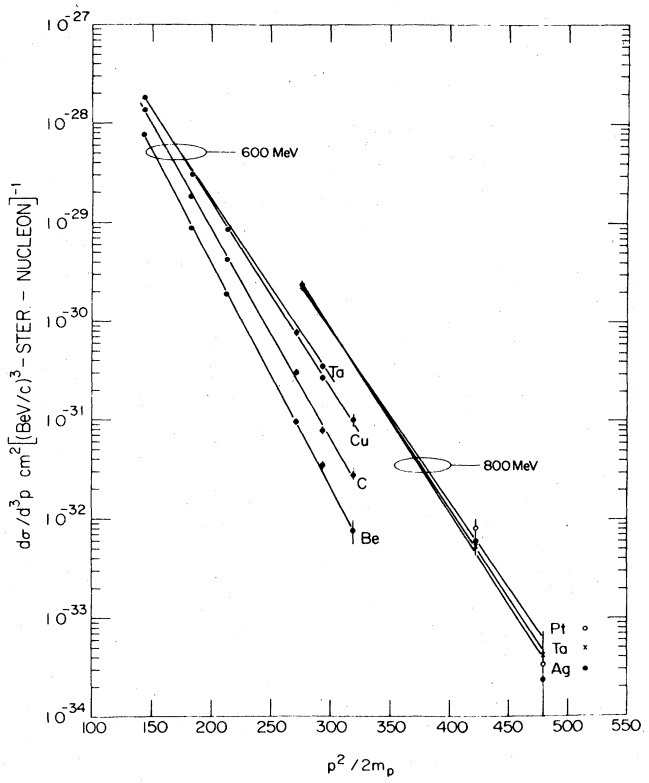

FIG. 47. The differential cross sections for 180° production of protons at $T_p = 600$ and 800 MeV (Frankel *et al.*, 1976).

mentum at the collision time, and on the basis of this simple model, the rapid falloff in cross section with increasing momentum is a manifestation of the single-particle momentum distribution in the nucleus. The off-shell nucleon-nucleon scattering amplitude to describe the scattering from $\underline{p}$ to $\underline{p}'$ is approximated by the on-shell scattering amplitude M. Further it is assumed

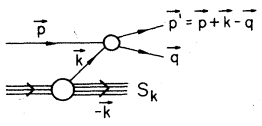

FIG. 49. Single scattering mechanism for proton inclusive scattering (Amado and Woloshyn, 1976). The incident proton with momentum $\boldsymbol{p}_0$ strikes a nucleon of virtual momentum $\boldsymbol{k}$. The residual nucleus recoils with momentum $\boldsymbol{k}$ and in the states S_k. After the collision the observed proton has momentum $\boldsymbol{p}$ and the unobserved nucleon has momentum $\boldsymbol{p}'$.

that the nuclear excitation is small so that to a good approximation the sum over excited states can be done by closure. Then the cross section is given by the expression

$$\frac{d\sigma}{dp^3} = \frac{M^4}{k_0 E(\underline{p})} \frac{1}{2(2\pi)^5} \int \frac{d^3k}{E(\underline{k}) E(\underline{k}_0 + \underline{k} - \underline{p})} \eta_p(k) \sum |M_{pp}|^2 + \eta_n(k) \sum |M_{pn}|^2 \delta[E(\underline{k}_0) + M - E(\underline{p}) - E(\underline{k}_0 + \underline{k} - \underline{p}) - \bar{\epsilon}], \tag{75}$$

where $E(k_0) = (k_0^2 + m^2)^{1/2}$, $|M|^2$ is summed over spins, $\bar{\epsilon}$ is the average nucleon interaction energy, and $\eta_p(k)[\eta_n(k)]$ is the proton [neutron] momentum distribution in the target ground state. After a trivial angular integration, an integration over k remains, $k_{\min}$ is of the order of 0.7–1.4 GeV/c in the experiment, and therefore the k integral in Eq. (75) will be dominated by wave numbers near $k_{\min}$. The cross section will be approximately proportional to $\eta(k_{\min})$. In order to tie down $\eta(k)$, quasi-elastic (e, e') scattering, dependent on lower momentum components, as well as the backward production data are fit. A finite-temperature, Fermi-gas distribution

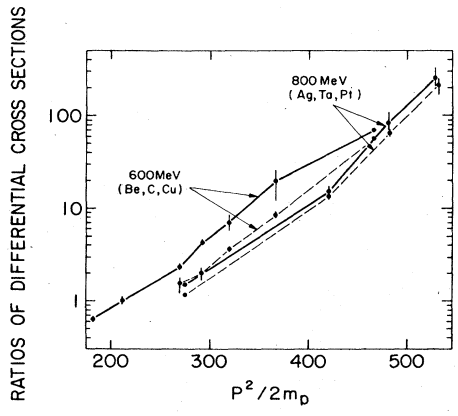

FIG. 48. Ratios of differential cross sections for the production of deuterons and tritons relative to protons for light (Be, C, Cu) and heavy (Ag, Ta, Pt) targets (Frankel *et al.*, 1976). The ratios are calculated for the same momentum.

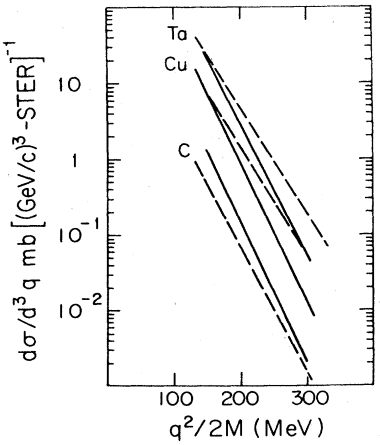

FIG. 50. Comparison of calculated (dashed lines) and experimental (solid lines) inclusive proton spectra for 600 MeV protons incident on C, Cu, and Ta (Amado and Woloshyn, 1976).

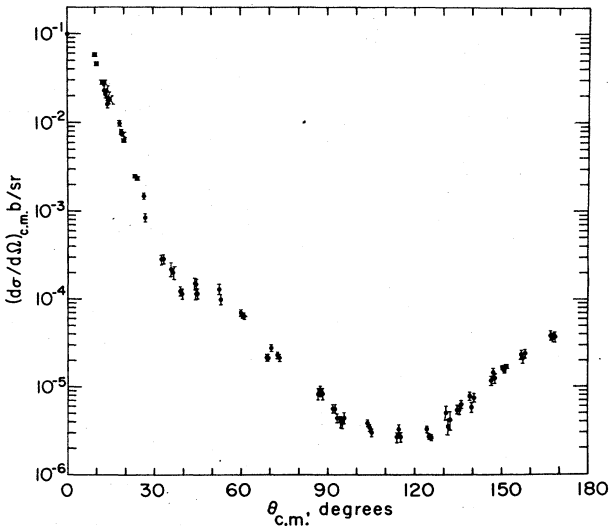

FIG. 51. Elastic 1 GeV proton-deuteron scattering (Bennett *et al.*, 1967).

was found to be unsatisfactory since the Gaussian fall-off does not provide the high momentum components required. A form for the probability density that fits (e, e') quasielastic data and backward production data at 800 MeV is

$$\eta(k) = N\{(\xi k)/[\sinh(\xi k)]\}\ , \tag{76}$$

where N is a normalization factor and ξ is a scale factor. Once having specified an analytical form for $\eta(k)$, the parameters of $\eta(k)$[Eq. (76)] are fixed by the (e, e') experiment. The differential cross section is calculated with no free parameters. The A dependence, magnitude,

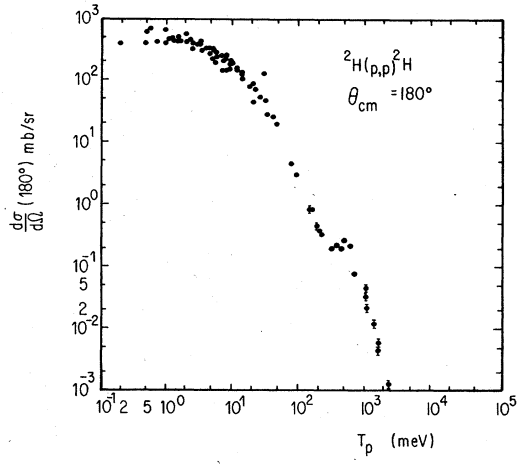

FIG. 52. N-d elastic scattering 180° excitation function (van Oers, 1974). The open circles are n-d results (Seagrave, 1970 van Oers, 1977). The solid dots are p-d results: 145, 181, 216 MeV (Igo *et al.*, 1972); 146 MeV (Postma and Wilson, 1961); 155 MeV (Kuroda *et al.*, 1966); 185 MeV (Gugelot *et al.*, 1974); 198 MeV (Adelberger and Brown, 1972); 425 MeV (Booth *et al.*, 1971). 660 MeV (Leksin, 1957); 1 GeV (Bennett *et al.*, 1967); 1.0, 1.3, 1.5 GeV (Coleman *et al.*, 1967); 1.0, 1.5, 2.08, 2.49 GeV (Dubal *et al.*, 1974); 1.18 GeV (Banaigs *et al.*, 1970). The solid squares and p-d results at 316, 364, 470, and 590 MeV (Alder *et al.*, 1972).

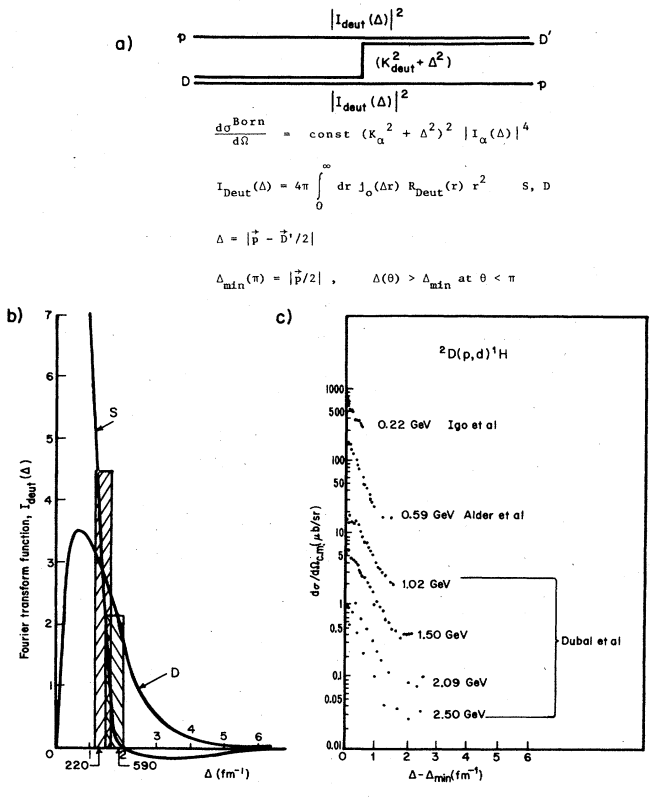

FIG. 53. (a) The neutron pickup reaction. (b) The Fourier transform function I_{deut} for S and D waves in the deuteron. (c) The differential cross section near 180° versus proton bombarding energy: Igo *et al.* (1972), Alder *et al.* (1972), and Dubal *et al.* (1974).

and slope of the cross sections (see Fig. 50) predicted by such a simple model is quite interesting.

B. Large-angle elastic scattering

Proton-deuteron elastic scattering has been investigated over a broad energy range. Most of the recent activity has centered on backward scattering. At all proton bombarding energies investigated (up to 2.5 GeV), the backward cross section is peaked at 180°. An example of this behavior (Bennett, 1967) is shown in Fig. 51. The behavior of the backward peak in the differential cross section as a function of energy has been compiled by van Oers (1974) and by Dubal and Pedrisat (1974). The appearance of a second maximum in the 180° excitation function (see the square symbols in Fig. 52) has created a great deal of theoretical interest. Remler (1972), Blankenbecler *et al.* (1959), Craigie and Wilkin (1969), Barry (1972), Tezuka and Yamazaki (1975), Kerman and Kisslinger (1969), Nasser *et al.* (1974), and Morioda and Ueda (1976) have used theoretical models which emphasize various aspects of the problem and the dependence of the cross section on the invariant total energy squared s, and the momentum transfer squared u, variables. Chen (1974) has shown that the Glauber model may be extended to explain 180° elastic scattering. One of the nucleon–nucleon collisions provides the large momentum transfer required

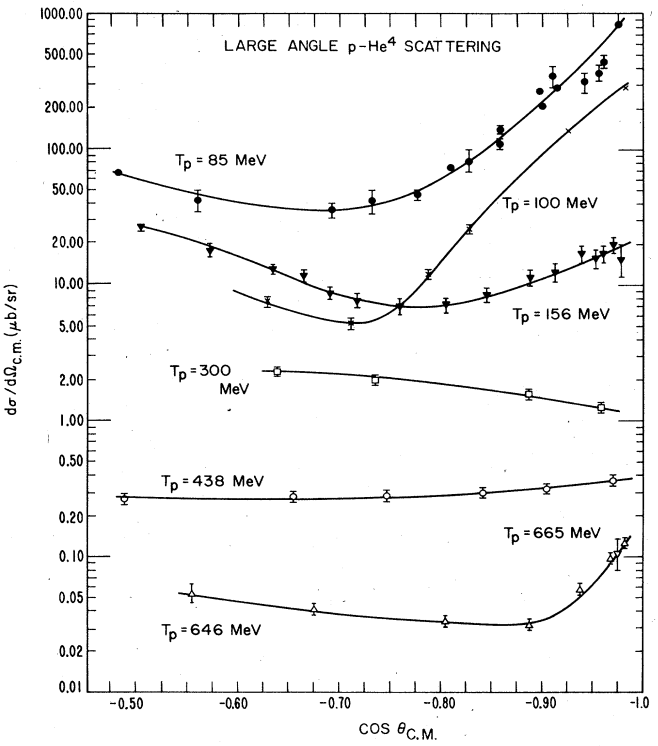

FIG. 54. The differential cross section for p-^{4}He elastic scattering in the backward direction at $T_p = 85$ MeV (solid circles), $T_p = 100$ MeV (crosses), $T_p = 156$ MeV (inverted solid triangles), $T_p = 300$ MeV (squares), $T_p = 438$ MeV (open circles), $T_p = 646$ MeV (triangles), and $T_p = 665$ MeV (inverted triangle). The single point at 665 MeV is from Komarov *et al.* (1970). References for the remainder of the data are given in the caption of Figure 55.

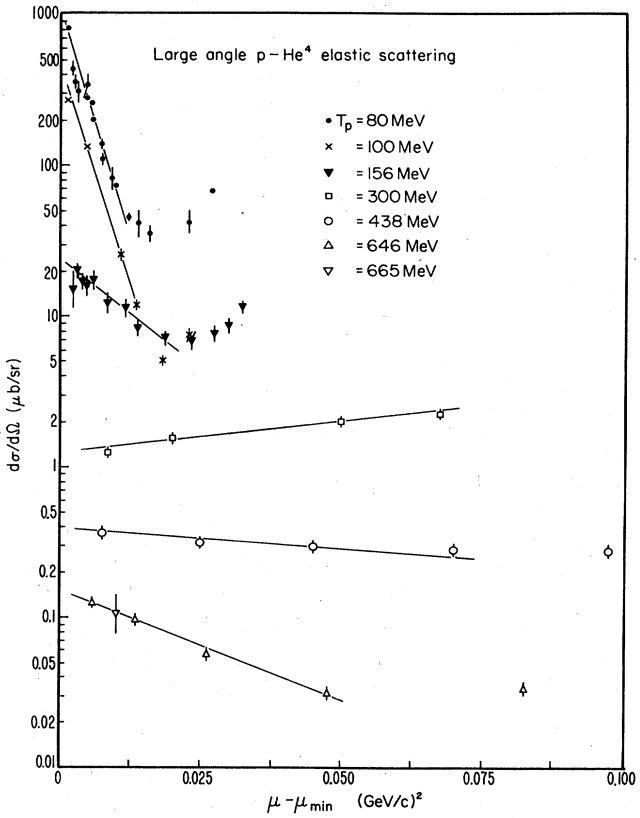

FIG. 55. Large-angle proton helium data illustrate the behavior of the backward peak with increasing incident energy: the data at 85 MeV are from Votta *et al.* (1974); at 100 MeV Golstein *et al.* (1969); and at 156 MeV, Comparat *et al.* (1975). The remainder of the data are from Berger *et al.* (1976). The quantity $d\sigma/d\Omega$ is plotted against the invariant four-momentum transfer, u-u_{min}.

for 180° scattering. Gurvitz *et al.* (1975a, b) have emphasized the importance of the single scattering term in the Glauber model to explain the backward peaking observed in elastic scattering.

The Chew-Goldberger neutron pickup model (1964) adapted to handle relativistic kinematics (Kerman and Kisslinger, 1969), explains many of the features of $p-d$ elastic scattering at large angles (but not by itself the peak at 220 MeV in the excitation function). As shown in Fig. 53, the Born cross section depends on the square of the Fourier transform function, $I_{deut}(\Delta)$, of the deuteron wave function at each vertex and on the propagator; K_{deut} is the binding energy of the deuteron. $I_{deut}(\Delta)$ for S and D components is shown in part (b) of Fig. 53. The momentum components Δ in the deuteron wave function, on which the backward scattering at 220 MeV and 590 MeV depend, are illustrated. In part (c), the cross section plotted against Δ-Δ_{min} for several bombarding energies shows the typical peaking at Δ_{min}. The minimum value of Δ, Δ_{min} occurs at $\theta = 180°$.

Recently large-angle p-^{4}He elastic scattering has been studied above 150 MeV bombarding energy by Berger *et al.* (1976). An interesting feature of the data, shown in Fig. 54, is the appearance of a backward peak in the differential cross section as the equivalent proton energy (α-particle beams were used in the experiment) is raised from 300 MeV to 650 MeV. In Fig. 55, the differential cross section is plotted against $u - u_{min}$ where u is the usual crossed four-momentum transfer variable involving in this case the momentum transfer squared difference of the proton in the initial state and the alpha particle in the final state. To describe large-angle scattering of protons by ^{4}He in the framework of multiple-scattering theory, Gurvitz *et al.* (1975a) have used a noneikonal model taking into account recoil, rescattering from the same nucleon, and a realistic representation of the nucleon–nucleon interaction. A backward rise in the nucleon–nucleon cross section, according to this model, results in a backward peaking in the p-^{4}He elastic scattering.

The predictions of Gurvitz *et al.* (1975a) and a Glauber-model calculation (Dymarz and Malecky, 1976) are compared in Fig. 56 with data obtained at equivalent proton energies of 438 MeV, 648 MeV, and 1.05 GeV. At these energies there are data over an extended range of four-momentum transfer including backward angles. In the work of Dymarz and Malecky (1976), the optical potential limit to the Glauber multiple-scattering series was evaluated. For this calculation, the ^{4}He wave function including a short-range correlation was used. The scattering cross section was obtained by solving the Schrödinger wave equation with this optical

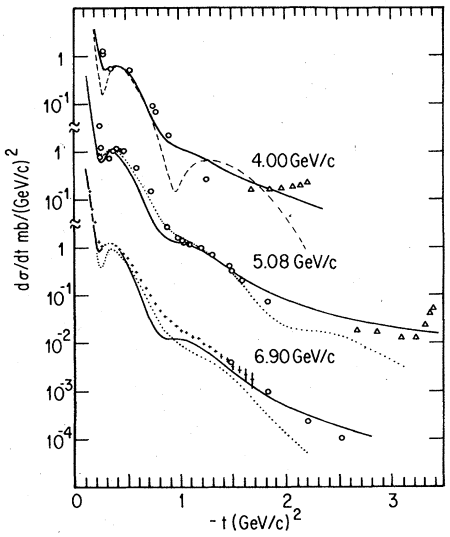

FIG. 56. The quantity $d\sigma/dt$ plotted versus t (Berger *et al.*, 1976). The dotted and solid curves are taken from Gurvitz *et al.* (1975b) and Dymarz and Malecki (1976), respectively. The dashed line is a simple Glauber-model calculation. The experimental data are from (circles) Berger *et al.* (1975), from (triangles) Berger *et al.* (1976), and from (crosses) Baker *et al.* (1974a).

potential. The fit of Gurvitz *et al.* (1975a) up to $t=-1.7$ $(\mathrm{GeV}/c)^2$ at 648 MeV is in good agreement with the data while at 1.05 GeV, the fit is less satisfactory. On the other hand the calculation of Dymarz and Malecky (1976) is in reasonable agreement with the data at all three energies for momentum transfers extending up to the backward rise.

It is not surprising that neither calculation predicts the sharp backward rise near 180° seen in the data. A triton exchange mechanism has been suggested by Kopelovich and Potashnikova (1971) to explain the backward cross section measured earlier at 660 MeV (Komarov *et al.*, 1970). This earlier back-angle measurement is in good agreement with the data of Berger *et al.* (1976) obtained at almost the same equivalent proton energy. The model of Kopelovich and Potashnikova (1971) predicts a rise in the backward direction, but the slope is a factor of two lower than the measurement at 648 MeV. Recently Lesniak, Lesniak, and Tekou (1976) have included important absorption corrections to the tribaryon exchange model. Their prediction is in better agreement with the data, especially at 648 MeV.

VII. CONCLUSIONS

Four topics in the area of nucleon-nucleus scattering at intermediate energies have been discussed in Secs. II–VI: proton elastic scattering from helium at forward angles, elastic and inelastic scattering for nuclei with $A \geq 4$, the neutron pickup reaction, and particle production and elastic scattering near 180°. Closely associated theoretical topics have been discussed in Sec. I.

A. p-^{4}He scattering

The topic of p-^{4}He has been actively pursued since the close of the last review article in this field (Saudinos and Wilkin, 1974). The energy dependence of the parameter R has been investigated over the range of 0.3 to 4.9 GeV and at 23.1 GeV bombarding energy. The maximum near 0.8 GeV and the very large value at 23.1 GeV are directly related to the energy dependence of the nucleon–nucleon amplitudes including the t dependence of α, and to the presence of a Δ intermediate state in the multiple-scattering amplitude. There is evidence from differential cross section and polarization measurements that triple scattering is non-negligible. Polarization data have become available between 0.54 and 1.7 GeV. The polarization data at 0.54 GeV provide new information about the relative phases of the spin-dependent and spin-independent parts of the averaged nucleon–nucleon amplitude. Proton-proton scattering amplitudes are under extensive investigation in this energy range at the present time. The neutron–proton problem is unfortunately less well in hand. A significant advance in the understanding of the p-^{4}He problem can be expected in the next few years when the proton–proton amplitudes have been established experimentally and the neutron–proton to a lesser extent.

B. Elastic and inelastic scattering $A \geq 4$

The existence during the past few years of elastic data and data on the inelastic excitation of low-lying collective states at 1 GeV on a range of light to heavy nuclei has stimulated a number of theoretical studies. One of the more comprehensive of these was discussed in Sec. III (Ahmad, 1975). The effect of correlations was investigated in this work. A method was described for separating out the effects of long-range correlations. In ^{12}C, the effects of short-range and long-range correlations tend to cancel one another in certain angular regions and in another region, near the second maximum in the elastic scattering angular distribution, are responsible for an improved fit. Regrettably, when the calculations are made for another element, ^{58}Ni, the fits to the elastic data are worsened when the correlation lengths obtained from the ^{12}C analysis are used. The improvement in the fit to the inelastic data (2^+) is marginal. The fits obtained for nuclei heavier than ^{58}Ni follow the same pattern. The evidence for correlation effects, while encouraging for carbon, cannot be applied in a consistent fashion to heavier elements. A serious discrepancy between the model prediction and the data for the inelastic excitation of the 3^- state in ^{12}C was noted where a predicted secondary maximum is not seen experimentally.

Elastic measurements on isotopes of elements, particularly calcium, were described. An analysis of data obtained on ^{40,42,44,48}Ca showed that proton elastic data at intermediate energies are sensitive to neutron mass distributions and insensitive to uncertainties in the charge distribution resulting from two electron scattering experiments. The principal result concerns the 40–48 difference in the rms radius of the neutron distribution which was found to be 0.16 fm. The rms difference is also insensitive to differences in the nucleon-nucleon

parameters obtained from two recent analyses of nucleon–nucleon data. The neutron rms increases as $A^{1/3}$ in contrast to the proton rms radius which is constant from 40–48. The corresponding rms radius of the matter distribution exhibits some deviation from the $A^{1/3}$ dependence.

In the near future, there will be a substantial increase in the data available, resulting from measurements at 0.8 GeV at the HRS of the differential cross section and asymmetry for elastic and inelastic scattering. The differential cross-section data for a number of nuclei will extend to significantly larger momentum transfer than the existing data. The combination of differential cross section extending to larger t values and asymmetry data will provide more constraints on the neutron distribution. In less than two years, the improved Saturne accelerator at Saclay, with extended high-resolution facilities, and a high-resolution spectrometer at TRIUMF will provide data over a broad range of energies (and projectiles at Saclay). During the next five years, it will be possible to test predictions of fine details in the mass distribution predicted by Hartree–Fock calculations, and substantial progress on the understanding of correlations in nuclei can be expected.

C. The neutron pickup reaction

Measurements of $^{12}C(p,d)^{11}C$ to several excited states and $^4He(p,d)^3He$ at 700 MeV have been analyzed using the DWBA with finite range and using the Glauber multiple-scattering model. The principal results of the analysis are that neither model predicts the scattering at small angles very well, particularly in the case of ^4He. The average slope of the theoretical calculations agrees with the data, but both models predict oscillations in the angular distribution for $^{12}C(p,d)^{11}C$ which are not observed. The amplitudes for nucleon isobar pickup are found to be too small at 700 MeV to account for the discrepancies noted above.

During the next few years, the (p,d) reaction will be studied extensively. Most of the data will be on light targets ($A \leq 40$) since it has been established that the cross sections for heavier targets are very small. Nevertheless the (p,d) reaction is of great interest because it provides a method of obtaining large momentum transfers at forward angles where single scattering, in the language of the Glauber model, dominates. Care must be taken into account for two-step processes since they are relatively much more important than at low bombarding energies.

D. Particle production and elastic scattering near 180°

Recently, a measurement of protons, deuterons, and tritons produced at 180° when 0.8 GeV protons impinge on nuclei has been made. If the particle distributions are characterized in terms of a variable η_p, determined by the kinematics at large angles, they fall on a straight line which has a slope that is nearly constant for all nuclear targets involved. More recently, data obtained at large angles over a broad range of different energies and with different projectiles when plotted as a function of this same kinematical variable display strikingly similar slopes. Although the relation of η_p to nuclear properties (the momentum distribution of nucleons and clusters in nuclei) is very obscure, the ability to correlate many kinds of reaction data suggest that the variable η_p has some more general significance which is not yet understood. Several experimental tests are underway to try to evaluate the mechanism of particle prediction at large angles including asymmetry measurements at large angles with a polarized beam and a search for coincidences between forward fast particles and the backward produced particles.

Large-angle elastic scattering has been measured recently in the proton–deuteron and the proton–helium systems. The proton–deuteron backward elastic scattering is characterized by a peak at 180° at all energies at intermediate energies. The differential cross section at backward angles decreases with increasing energy as predicted by the Chew–Goldberger model. Centered at 0.4 GeV, a very interesting effect is observed: the cross section does not decrease over several hundred MeV of bombarding energy. This region has recently been studied in detail using n-d elastic scattering at large angles (Bonner *et al.*, 1977). This secondary peak or shoulder is probably associated with a resonance transfer of a nucleon plus a pion or a nucleon isobar. Further theoretical studies and measurements with polarized deuteron beams are expected to elucidate the mechanism. Large-angle p-^4He scattering peaks at 180° near 100 MeV, and is flat or decreases between 200 and 500 MeV. Above 500 MeV, the cross section peaks at 180°. The peak becomes increasingly narrower in angular width as the energy is increased up to 1-GeV proton bombarding energy. The backward peak above 500 MeV has been analyzed with a triton pickup mechanism. Nuclear absorption is found to be extremely important in this reaction. A recent measurement (Whitten *et al.*, 1977) of p-^4He elastic scattering at the HRS (high-resolution spectrometer) (0.8 GeV) over a large angular range ($\theta_{lab} = 13° - 165.5°$) has shown that there is additional structure besides the 180° rise. Starting at 110°, a relatively deep dip followed by a maximum and another equally deep dip are found, before the rise discussed above toward 180° occurs. The triton pickup model does not predict this behavior. Measurements of the polarization in elastic scattering in this angular region and theoretical analysis of polarization and differential cross section data, including both multiple scattering and pickup amplitudes, will be available in the near future to attempt to understand these interesting phenomena.

ACKNOWLEDGMENTS

I wish to thank B. Blonsky and R. Bohn for assistance with the preparation of the manuscript, and A. Wang for the final proofreading.

REFERENCES

Adelberger, R. E., and C. N. Brown, 1972 Phys. Rev. D **5**, 2139.
Ahmad, I., 1975, Nucl. Phys. A **247**, 418.
Alder, J. C., W. Dollhopf, C. Lunke, C. F. Perdrisat, W. K. Roberts, P. Kitching, G. Moss, W. C. Olsen, and J. R. Priest, 1972, Phys. Rev. C 6, 2010.

Alexander, Y., and A. S. Rinat, 1974, Ann. Phys. (N.Y.) **82**, 301.
Alkhazov, G. D., G. M. Amalsky, S. L. Belostotsky, A. A. Vorobyov, O. A. Domchenkow, Yu. V. Dotsenko, and V. E. Starodubsky, 1972 Phys. Lett. B **42**, 121.
Alkhazov, G. D., S. L. Belostotsky, O. A. Domchenkov, Yu. V. Dotsenko, N. P. Kuropatkin, M. A. Shuvaev, and A. A. Vorobyov, 1975 Phys. Lett. B **57**, 47.
Alkhazov, G. D., S. L. Belostotsky, A. A. Vorobyov, V. T. Grachev, O. A. Domchenkov, Yu. V. Dotsenko, N. P. Kuropatkin, V. E. Starodubsky, and M. A. Shuvaev, 1976a, Sov. J. Nucl. Phys. **22**, 469.
Alkhazov, G. D., T. Bauer, R. Beurtey, A. Bouchard, G. Bruge, A. Chaumeaux, P. Couvert, G. Cvijanovich, H. H. Duhm, J. M. Fontaine, D. Garreta, A. V. Kulikov, D. Legrand, J. C. Lugol, L. Saudinos, J. Thirion, and A. A. Vorobyov, 1976b, Nucl. Phys. A **274**, 443.
Amado, R. D., and R. M. Woloshyn, 1976, Phys. Rev. Lett. **36**, 1435.
Arnold, L. G., B. C. Clark, and R. L. Mercer, 1976a, Phys. Rev. C **14**, 1878.
Arnold, L. G., B. C. Clark, and R. L. Mercer, 1976b, Ohio State Univ. TR No. 201.
Aslanides, E., T. Bauer, R. Bertini, R. Beurtey, A. Boudard, F. Brochard, G. Bruge, A. Chaumeaux, H. Catz, J. M. Fontaine, R. Frascaria, D. Garreta, P. Gorodetzky, J. Guyot, F. Hibou, D. Legrand, M. Matoba, Y. Terrien, J. Thirion, and E. Lambert, 1977, Phys. Lett. B **68**, 221.
Auger, J. P., and R. J. Lombard, 1973, Phys. Lett. B **45**, 115.
Auger, J. P., J. Gillespie, and R. J. Lombard, 1976, Nucl. Phys. A **262**, 372.
Austern, N., R. M. Drisko, E. C. Halbert, and G. R. Satchler, 1964, Phys. Rev. B **3**, 133.
Bachelier, D., M. Bernas, I. Brissaud, C. Détraz, P. Radvanyi, 1969, Nucl. Phys. A **126**, 60.
Baker, S. D., R. Beurtey, G. Bruge, A. Chaumeaux, J. M. Durand, J. C. Faivre, J. M. Fontaine, D. Garreta, D. Legrand, J. Saudinos, J. Thirion, R. Bertini, F. Brochard, and F. Hibou, 1974a, Phys. Rev. Lett. **32**, 839.
Baker, S. D., R. Bertini, R. Beurtey, F. Brochard, G. Bruge, H. Catz, A. Chaumeaux, G. Cvijanovich, J. M. Durand, J. C. Faivre, J. M. Fontaine, D. Garreta, F. Hibou, D. Legrand, J. C. Lugol, J. Saudinos, and J. Thirion, 1974b, Phys. Lett. B **52**, 57.
Banaigs, J., J. Berger, J. Duflo, L. Goldzahl, H. Cottereau, and F. Lefebvres, 1970, Nucl. Phys. B **23**, 596.
Barashenkov, V. S., and V. D. Toneev, 1968, Preprint JINR P2–3850, Dubna.
Barry, G. W., 1972, Ann. Phys. (N.Y.) **73**, 482.
Bassel, R. H., and C. Wilkin, 1967, Phys. Rev. Lett. **18**, 871.
Bassel, R. H., and C. Wilkin, 1968, Phys. Rev. **174**, 1179.
Bassichis, W. H., H. Feshbach, and J. F. Reading, 1971, Ann. Phys. (N.Y.) **68**, 462.
Batty, G. J., and C. W. Greenlees, 1969, Nucl. Phys. A **133**, 673.
Bauer, T., A. Boudard, H. Catz, A. Chaumeaux, P. Couvert, M. Garcon, J. Guyot, D. Legrand, J. C. Lugol, M. Matoba, B. Mayer, J. P. Tabet, and Y. Terrien, 1977, Phys. Lett. B **67**, 265.
Benary, O., L. R. Price, and G. Alexander, 1970, UCRL–20000 NN.
Bennett, G. W., J. L. Friedes, H. Palevsky, R. J. Sutter, G. J. Igo, W. D. Simpson, G. C. Phillips, R. L. Stearns, and D. M. Corley, 1967, Phys. Rev. Lett. **19**, 387.
Berger, J., J. Duflo, J. Goldzahl, J. Oostens, F. Plouin, M. Van Den Bossche, L. Vullai, G. Bizard, C. LeBrun, F. L. Fabri, P. Picozza, and L. Satta, 1975, contribution to the VIth International Conference on High Energy Physics and Nuclear Structure, Santa Fe and Los Alamos, New Mexico, June 9–14 (unpublished).
Berger, J., J. Duflo, L. Goldzahl, F. Plouin, J. Oostens, M. Van Den Bossche, L. Vu Hai, G. Bizard, C. LeBrun, F. L. Fabbri, P. Picozza, and L. Satta, 1976, Phys. Rev. Lett. **37**, 1195.
Berthot, J., G. Douhet, J. Gardès, L. Mèritet, M. Querrou, A. Têtefort, F. Vazeille, J. P. Burg, M. Chemarin, M. Chevallier, B. Ille, M. Lambert, J. P. Marin, J. P. Gerber, and C. Voltolini, 1975, contribution to the VIth International Conference on High-Energy Physics and Nuclear Structure, Santa Fe and Los Alamos, New Mexico, June 9–14 (unpublished).
Bertin, M. C., and S. L. Tabor, 1971, Nucl. Phys. A **167**, 206.
Bertini, R., R. Beurtey, F. Brochard, G. Bruge, H. Catz, A. Chaumeaux, J. M. Durant, J. C. Faivre, J. M. Fontaine, D. Garreta, C. Gustafsson, D. Hendrie, F. Hibou, D. Legrand, J. Saudinos, and J. Thirion, 1973, Phys. Lett. B **45**, 119.
Bertozzi, W., J. Friar, J. Heisenberg, and J. W. Negele, 1972, Phys. Lett. B **41**, 408.
Beurtey, R., 1975, private communication.
Blankenbecler, R., M. L. Goldberg, and F. R. Halpern, 1959, Nucl. Phys. **12**, 629.
Bonner, B. E., C. L. Hollas, C. R. Newsom, P. J. Riley, and G. Glass, 1977, Phys. Rev. Lett. **39**, 1253.
Booth, N. E., C. Dolnick, R. J. Esterling, J. Parry, J. Scheid, and D. Sherden, 1971, Phys. Rev. D **4**, 1261.
Boridy, E., and H. Feshbach, 1974, Phys. Lett. B **50**, 433.
Boschitz, E. T., M. Chabre, H. E. Conzett, E. Shield, and R. J. Slobodrian, 1966, in *Proceedings of the Second International Conference of Polarization Phenomena of Nucleons*, edited by P. Huber and H. Schopper (Birkhäuser Verlag, Basel and Stuttgart), p. 328.
Boschitz, E. T., 1977, in *Proceedings of the VIIth International Conference on High Energy Physics and Nuclear Structure*, Zurich, Aug.–Sept., to be published.
Boschitz, E. T., W. K. Roberts, J. S. Vincent, M. Blecher, K. Gotow, P. C. Gugelot, C. F. Perdrisat, L. W. Swenson, and J. R. Priest, 1972, Phys. Rev. C **6**, 457.
Brissaud, I., L. Bimbot, Y. Le Bornec, B. Tatischeff, and N. Willis, 1974, Phys. Lett. B **48**, 319.
Brissaud, I., and M. K. Brussel, 1976a, submitted to Nucl. Phys.
Brissaud, I., and M. K. Brussel, 1976b, preprint.
Bystricky, J., F. Lehar, and Z. Janout, 1972, CEA–N–1547 (E), Saclay, France.
Campi, X., and D. Spring, 1974, Nucl. Phys. A **194**, 401.
Chadha, K. A., and V. S. Varma, 1976, Phys. Rev. C **13**, 715.
Chamberlain, O., E. Segrè, R. D. Tripp, C. Wiegand, and T. Ypsilantis, 1956, Phys. Rev. **102**, 1659.
Chaumeaux, A., V. Layly, and R. Schaeffer, 1976, to be published.
Chen, T. W., 1974, Nuovo Cim. Lett. **11**, 315.
Chew, G. F., and H. L. Goldberger, 1950, Phys. Rev. **77**, 470.
Ciofi degli Atti, C., 1974, in *Proceedings of the Topical Meeting on High-Energy Collisions Involving Nuclei*, Trieste, September 1974, edited by G. Bellini, L. Bertocchi, and P. G. Rancoita (Editrice Compositori, Bologna), p. 41.
Clark, B. C., R. L. Mercer, D. G. Ravenhall, and A. M. Saperstein, 1973, Phys. Rev. C **7**, 466.
Clegg, A. B., 1962, Nucl. Phys. **38**, 353.
Cohen, S., and D. Kurath, 1967, Nucl. Phys. A **101**, 1.
Coleman, E., R. M. Heinz, O. E. Overseth, and D. E. Pellet, 1967, Phys. Rev. **164**, 1655.
Comparat, V., R. Frascaria, N. Fujiwara, N. Marty, M. Morlet, P. G. Roos, and A. Willis, 1975, Phys. Rev. C **12**, 251.
Cormack, A. M., J. N. Palmieri, N. F. Ramsey, and R. Wilson, 1959, Phys. Rev. **115**, 599.
Craigie, N. S., and C. Wilkin, 1969, Nucl. Phys. B **14**, 477.
Czyz, W., and L. Lesniak, 1967, Phys. Lett. B **24**, 227.
de Jager, C. W., H. de Vries, and C. de Vries, 1974, Atomic Data and Nuclear Data Tables **14**, 1.
DeVries, R. M., 1973, Phys. Rev. C **8**, 951.
Dubal, L., C. K. Hargrove, E. P. Hincks, R. J. McKee, H. Mes, A. C. Thompson, L. Bird, C. H. Halliwell, R. W. Morrison, J. Walters, J. B. McCaslin, and A. R. Smith, 1974,

Phys. Rev. D **9**, 597.
Dubal, L., and C. F. Perdrisat, 1974, Nuovo Cimento Lett. **11**, 265, and references therein.
Dutton, L. M. C., J. D. Jafar, H. B. Van der Raay, D. G. Ryan, J. A. Stiegelmair, R. K. Tandon, and J. F. Reading, 1965, Phys. Lett. **16**, 331.
Dutton, L. M. C., and H. B. Van der Raay, 1968, Phys. Lett. B **26**, 679.
Dymarz, R., and A. Malecki, 1976, Frascati Internal Report, LNF 76/23 (unpublished).
Elton, L. B. R., 1966, *Introductory Nuclear Theory*, 2nd edition (Saunders, Philadelphia).
Elton, L. B. R., and A. Swift, 1967, Nucl. Phys. A **94**, 52.
Fain, J., J. Gardes, A. LeFort, L. Meritet, J. F. Pauty, G. Peynet, M. Querrou, F. Vazeille, and B. Ille, 1976, Nucl. Phys. A **262**, 413.
Fernandez, B., and J. S. Blair, 1970, Phys. Rev. C **1**, 523.
Feshbach, H., 1958, Ann. Phys. (N.Y.) **5**, 357.
Feshbach, H., 1969, *In Honor of Philip M. Morse*, edited by H. Feshbach and K. U. Ingard (MIT, Cambridge, Mass.), p. 190.
Feshbach, H., 1977, private communication.
Feshbach, H., and J. Hufner, 1970, Ann. Phys. (N.Y.) **56**, 268.
Feshbach, H., A. Gal, and J. Hufner, 1971, Ann. Phys. (N.Y.) **66**, 20.
Franco, V., 1968, Phys. Rev. Lett. **21**, 1360.
Frankel, S., W. Frati, O. Van Dyck, R. Werbeck, and V. Highland, 1976, Phys. Rev. Lett. **36**, 642.
Friar, J. L., and J. W. Negele, 1972, Nucl. Phys. A **212**, 93.
Friar, J. L., 1973, Particles and Nuclei **5**, 45.
Friederich, J., and F. Lenz, 1972, Nucl. Phys. A **183**, 523.
Frosch, R. F., J. S. McCarthy, R. E. Rand, and M. R. Yearian, 1967, Phys. Rev. **160**, 874.
Frosch, R. F., R. Hofstadter, J. S. McCarthy, G. K. Noldeke, K. J. van Oostrum, M. R. Yearian, B. C. Clark, R. Herman, and D. G. Ravenhall, 1968, Phys. Rev. **174**, 1380.
Geaga, J. V., M. M. Gazzaly, G. J. Igo, J. B. McClelland, M. A. Nasser, A. Sagle, H. Spinka, J. B. Carroll, V. Perez-Mendez, and E. T. B. Whipple, 1977a, Phys. Rev. Lett. **38**, 1265.
Geaga, J. V., G. J. Igo, J. B. McClelland, M. A. Nasser, S. Sander, H. Spinka, D. A. Treadway, J. B. Carroll, D. Fredrickson, V. Perez-Mendez, and E. T. B. Whipple, 1977b, Nucl. Instrum. Meth. **141**, 263.
Gillespie, J., G. Gustafsson, and R. J. Lombard, 1974, Report No. IPNO/TH 74-30, Institut de Physique Nucléaire, Orsay, France.
Glauber, R. J., 1959, in *Lectures in Theoretical Physics*, edited by W. E. Brittin (Interscience, New York), Vol. 1, p. 315.
Glauber, R. J., and G. Matthiae, 1970, Nucl. Phys. B **21**, 135.
Goldberger, M. L., and K. M. Watson, 1964, *Collision Theory* (Wiley, New York).
Goldstein, N. P., A. Held, and D. G. Stairs, 1969, Can. J. Phys. **48**, 2629.
K. Gotow, University of Rochester, Report NYO–2532, unpublished.
Greenlees, G. W., G. J. Pyle, and Y. C. Tang, 1968, Phys. Rev. **171**, 1115.
Greenlees, G. W., W. J. Makofske, and G. J. Pyle, 1970, Phys. Rev. C **1**, 1145.
Gugelot, P. C., J. Källne, and P. U. Renberg, 1974, Phys. Scr. **10**, 252.
Gul'karov, I. S., 1973, Sov. J. Nucl. Phys. **16**, 386.
Gurvitz, S., Y. Alexander, and A. Rinat, 1975a, Phys. Lett. B **59**, 22.
Gurvitz, S., Y. Alexander, and A. Rinat, 1975b, Report WIS-75/119 Ph, Weizmann Institute, Rehovot, Israel.
Harrington, D. R., 1975, Nucl. Phys. B **87**, 413.
Helm, R. H., 1956, Phys. Rev. **104**, 1466.
Hendrik, R. E., and B. Lautrup, 1975, Phys. Rev. D **11**, 529.
Horikawa, Y., Y. Torizuka, A. Nakada, S. Mitsunobu, Y. Korma, and M. Kimura, 1971, Phys. Lett. B **36**, 9.
Igo, G. J., C. Fong, S. L. Verbeck, M. Goitein, D. L. Hendrie, J. C. Carroll, B. McDonald, A. Stetz, and M. Makino, 1972, Nucl. Phys. A **195**, 33.
Igo, G., 1975, in *High-Energy Physics and Nuclear Structure*, edited by D. E. Nagle, R. L. Burman, B. G. Storms, A. S. Goldhaber, and C. K. Hargrove (American Institute of Physics, New York), p. 63.
Ikeda, M., 1972, Phys. Rev. C **6**, 1608.
Jakobson, M. J., G. R. Burleson, J. R. Calarco, M. D. Cooper, D. C. Hagerman, I. Halpern, R. H. Jeppeson, K. F. Johnson, L. D. Knutson, R. E. Marrs, H. E. Meyer, and R. P. Redwine, 1977, Phys. Rev. Lett. **38**, 1201.
Johnson, R. C., and P. G. R. Soper, 1970, Phys. Rev. C **1**, 976.
Källne, J., and E. Hagberg, 1971, Phys. Scr. **4**, 151.
Kerman, A. K., H. McManus, and R. M. Thaler, 1959, Ann. Phys. (N.Y.) **8**, 551.
Kerman, A. K., and L. S. Kisslinger, 1969, Phys. Rev. **180**, 1483.
Kisslinger, L. S., 1977, Preprint entitled "Experimental Tests of Isobar Components of Nuclei," Carnegie Mellon University.
Klem, R., G. Igo, R. Talaga, A. Wriekat, H. Courant, K. Einsweiler, T. Joyce, H. Kagan, Y. Makdisi, M. Marshak, B. Mossberg, E. Peterson, K. Rudnick, and T. Walsh, 1977, Phys. Rev. Lett. **38**, 1272.
Kofoed-Hansen, O., and C. Wilkin, 1971, Ann. Phys. (N.Y.) **63**, 309.
Komarov, V., G. Kosarev, and O. Savchenko, 1970, Sov. J. Nucl. Phys. **11**, 339.
Kopelvich, B., and I. Potashnikova, 1971, Sov. J. Nucl. Phys. **13**, 592.
Kujawski, E., 1970, Phys. Rev. C **1**, 1651.
Kunz, P., 1971, unpublished.
Kuroda, K., A. Michalowicz, and M. Poulet, 1966, Nucl. Phys. **88**, 33.
Lambert, E., and H. Feshbach, 1973, Ann. Phys. (N.Y.) **76**, 80.
Lane, A. M., and E. D. Pendlebury, 1969, Nucl. Phys. **15**, 39.
Lee, H. C., and R. Y. Cusson, 1971, Nucl. Phys. A **170**, 439.
Leksin, G. A., 1957, Sov. Phys.–JETP **5**, 371.
Lerner, G. M., J. C. Hiebert, L. L. Rudledge, Jr., C. Papanicolas, and A. M. Bernstein, 1975, Phys. Rev. C **12**, 778.
Lésniak, H., L. Lésniak, and A. Takou, 1976, Nucl. Phys. A **267**, 413.
Lombard, R. J., 1970, Phys. Lett. B **32**, 652.
Lombard, R. J., and C. Wilkin, 1975, Report No. IPNO/TH 75-5, Institut de Physique Nucléaire, Orsay, France.
Lombardi, J. C., R. N. Boyd, R. Arking, and A. B. Robbins, 1972, Nucl. Phys. **188**, 103.
Lykasov, G. I., and A. V. Tarasov, 1975, Sov. J. Nucl. Phys. **20**, 263.
Manaenkov, S. I., 1975, Sov. J. Nucl. Phys. **21**, 51.
McManigal, P. G., R. F. Eandi, S. N. Kaplan, B. T. Moyer, 1965, Phys. Rev. B **137**, 620.
Morioka, S., and T. Ueda, 1976, "Structure in the Backward Proton-Dueteron Scattering in the 40–1000 MeV Region," in *Proceedings of the VIIth International Conference on Few Body Problems in Nuclear and Particle Physics*, edited by A. Mitra (New Delhi, India).
Nasser, M. A., G. J. Igo, and V. Perez-Mendez, 1974, Nucl. Phys. A **229**, 113.
Nasser, M. A., M. M. Gazzaly, J. V. Geaga, B. Hoistad, G. Igo, J. B. McClelland, A. L. Sagle, H. Spinka, J. B. Carroll, V. Perez-Mendez, and E. T. B. Whipple, 1977, submitted to Physics Letters.
Nolen, J. A., Jr., and J. P. Schiffer, 1969, Ann. Rev. Nucl. Sci. **19**, 1560.
Palevsky, H., J. L. Friedes, R. J. Sutter, G. W. Bennett, G. J. Igo, W. D. Simpson, G. C. Phillips, D. M. Corley, N. S. Wall, R. L. Stearns, and B. Gottschalk, 1967, Phys. Rev. Lett. **18**, 1200.

Passatore, G., 1967, Nucl. Phys. A **95**, 694.
Passatore, G., 1968, Nucl. Phys. A **110**, 91.
Passatore, G., 1975, Nucl. Phys. A **248**, 509.
Perez-Mendez, V., J. M. Sperinde, and A. W. Stetz, 1969, Phys. Lett. B **28**, 648.
Postma, H., and R. Wilson, 1961, Phys. Rev. **121**, 1229.
Ray, L., and W. R. Coker, 1977, Phys. Rev. C 16, 340.
Remler, E. A., 1972, Nucl. Phys. B **42**, 69.
Rost, E., and J. R. Shepard, 1975, Phys. Lett. B **59**, 413.
Rule, D. W., and Y. Hahn, 1975a Phys. Rev. Lett. **34**, 332.
Rule, D. W., and Y. Hahn, 1975b, Phys. Rev. C **12**, 1607.
Rule, D. W., and Y. Hahn, 1975c, Phys. Rev. C **12**, 1616.
Satchler, G. R., L. W. Owen, A. J. Elwyn, G. L. Morgan, and R. L. Walter, 1968, Nucl. Phys. A **112**, 1.
Saudinos, J., and C. Wilkin, 1974, Annu. Rev. Nucl. Sci. **24**, 341.
Savitskii, G. A., N. G. Afanas'ev, I. S. Gul'karov, V. D. Kovalev, A. S. Mellaenko, V. M. Khvastunov, N. G. Shevchenko, 1969, Sov. J. Nucl. Phys. **8**, 376.
Schaeffer, R., 1974, Summer Study on Reactions with Relativistic Heavy Ions, Lawrence Berkeley Laboratory, unpublished.
Seagrave, J. D., 1970, in *The Three-Body Problem in Nuclear and Particle Physics*, edited by J. S. C. McKee and P. M. Rolph (North-Holland, Amsterdam), p. 41.
Sick, I., and J. S. McCarthy, 1970, Nucl. Phys. A **150**, 631.
Sick, I., 1974, Nucl. Phys. A **218**, 509.
Sparrow, D. A., 1975, Ann. Phys. (N.Y.) **91**, 157.
Starodubsky, V. E., and O. A. Domchenkov, 1972, Phys. Lett. B **42**, 319.
Starodubsky, V. E., 1974, Nucl. Phys. A **219**, 525.
Tassie, L. J., 1956, Aust. J. Phys. **9**, 407.
Tekou, A., 1976, CEN Saclay Report CEA-N-1861.
Tezuka, H., and M. Yamazaki, 1975, contributions to the VIth International Conference on High Energy Physics and Nuclear Structure, Santa Fe, New Mexico, June 9–14 (unpublished).
Thompson, G. E., M. B. Epstein, and T. Sawada, 1970, Nucl. Phys. A **142**, 571.
Ullo, J., and H. Feshbach, 1974, Ann. Phys. (N.Y.) **82**, 156.
van Oers, W. T. H., and H. Haw, 1973, Phys. Lett. B **45**, 227.
van Oers, W. T. H., H. Haw, N. E. Davison, A. Ingemarsson, B. Hagerström, and G. Tibell, 1974, Phys. Rev. C **10**, 307.
van Oers, W. T. H., 1975, in *Few Body Problems in Nuclear and Particle Physics* (Université Laval, Quebec) p. 307.
van Oers, W. T. H., 1977, private communication and permission to publish the p-^4He contour diagram and the 180° elastic p-d cross section diagram appearing in this article.
Vautherin, D., and D. M. Brink, 1970, Phys. Lett. B **32**, 149.
Verbeck, S. L., J. C. Fong, G. Igo, C. A. Whitten, Jr., D. L. Hendrie, Y. Terrien, V. Perez-Mendez, and G. W. Hoffmann, 1975, Phys. Lett. B **59**, 339.
Viollier, R. D., 1975, Ann. Phys. (N.Y.) **93**, 335.
Vorobyov, A. A., A. S. Denisov, Yu. K. Zalite, G. A. Korelev, V. A. Korolev, G. G. Kovshevny, Ye. M. Maev, V. I. Medvedev, G. L. Sokolov, G. Ye. Solyakin, E. M. Spiridenkov, I. I. Tkach, V. A. Shegelsky, 1972, Phys. Lett. B **41**, 639.
Votta, L. G., P. G. Roos, N. S. Chant, and R. Woodsy, III, 1974, Phys. Rev. C **10**, 520.
Wallace, S. J., 1975, Phys. Rev. C **12**, 179.
Wallace, S. J., and Y. Alexander, 1977, Phys. Rev. Lett. **38**, 1269.
Wallace, S. J., 1977, Preprint No. ORO 5126–11, University of Maryland.
Watson, K. M., 1953, Phys. Rev. **89**, 575.
Weber, H. J., 1976, Fortschr. Phys. **24**, 1.
Whitten, Jr., C. A., T. S. Bauer, J. C. Fong, G. Igo, R. Ridge, G. W. Hoffmann, N. Hintz, M. Oothoudt, G. Blanpied, R. Liljestrand, and T. Kozlowski, 1977, Abstract J32, VIIth International Conference on High Energy Physics and Nuclear Structure, Zurich, Switzerland (unpublished).
Wolfenstein, L., 1956, Annu. Rev. Nucl. Sci. **6**, 43.
Wong, C. W., and S. K. Young, 1975, Phys. Rev. C **12**, 1301.
Young, S. K., and C. W. Wong, 1977a, Bull. Am. Phys. Soc. **22**, 82.
Young, S. K., and C. W. Wong, 1977b, Phys. Rev., to be published.